

Anthropogenic CO₂, air-sea CO₂ fluxes and acidification in the Southern Ocean: results from a time-series analysis at station OISO-KERFIX (51°S-68°E).

Nicolas Metzl¹, Claire Lo Monaco¹, Coraline Leseurre^{1,2}, Céline Ridame¹, Gilles Reverdin¹,
Thi Tuyet Trang Chau³, Frédéric Chevallier³, Marion Gehlen³

¹ Laboratoire LOCEAN/IPSL, Sorbonne Université-CNRS-IRD-MNHN, Paris, 75005, France

² Flanders Marine Institute (VLIZ), 8400 Ostend, Belgium

³ Laboratoire LSCE/IPSL, CEA-CNRS-UVSQ, Université Paris-Saclay Gif-sur-Yvette, 91191, France

Correspondence to: Nicolas Metzl (nicolas.metzl@locean.ipsl.fr)

Abstract: The temporal variation of the carbonate system, air-sea CO₂ fluxes and pH is analyzed in the Southern Indian Ocean, south of the Polar Front, based on in-situ data obtained from 1985 to 2021 at a fixed station (50°40'S-68°25'E) and results from a neural network model that reconstructs the fugacity of CO₂ (fCO₂) and fluxes at monthly scale. Anthropogenic CO₂ (C_{ant}) is estimated in the water column and is detected down to the bottom (1600m) in 1985 resulting in an aragonite saturation horizon at 600m that migrated up to 400m in 2021 due to the accumulation of C_{ant}. At subsurface, the trend of C_{ant} is estimated at +0.53 ± 0.01 μmol.kg⁻¹.yr⁻¹ with a detectable increase in the trend in recent years. At the surface during austral winter the oceanic fCO₂ increased at a rate close or slightly lower than in the atmosphere. To the contrary, in summer, we observed contrasting fCO₂ and dissolved inorganic carbon (C_T) trends depending on the decade and emphasizing the role of biological drivers on air-sea CO₂ fluxes and pH inter-annual variability. The regional air-sea CO₂ fluxes evolved from an annual source to the atmosphere of 0.8 molC.m⁻².yr⁻¹ in 1985 to a sink of -0.5 molC.m⁻².yr⁻¹ in 2020. Over 1985-2020, the annual pH trend in surface waters of -0.0165 ± 0.0040.decade⁻¹ was mainly controlled by the accumulation of anthropogenic CO₂, but the summer pH trends were modulated by natural processes that reduced the acidification rate in the last decade. Using historical data from November 1962 we estimated the long-term trend for fCO₂, C_T and pH confirming that the progressive acidification was driven by the atmospheric CO₂ increase. In 59 years this led to a diminution of 11% for both aragonite and calcite saturation state. As atmospheric CO₂ is expected to increase in the future, the pH and carbonate saturation state will decrease at a faster rate than observed in recent years. A projection of future C_T concentrations for a high emission scenario (SSP5-8.5) indicates that the surface pH in 2100 would decrease to 7.32 in winter. This is up to -0.86 lower than pre-industrial pH and -0.71 lower than pH observed in 2020. The aragonite under-saturation in surface waters would be reached as soon as 2050 (scenario SSP5-8.5) and 20 years later for a stabilization scenario (SSP2-4.5) with potential impacts on phytoplankton species and higher trophic levels in the rich ecosystems of the Kerguelen Island area.

Keywords: Ocean Carbonate System, Ocean acidification, anthropogenic CO₂, air-sea CO₂ fluxes, Southern Ocean, Time-series station

42

43 **1 Introduction**

44 The ocean plays an important role in mitigating climate change by taking up a large part of the excess of
45 heat (Cheng et al., 2020; Fox-Kemper et al., 2021) and of CO₂ released by human activities (Sabine et al., 2004;
46 Gruber et al., 2019a; Canadell et al., 2021). Since 1750, the global ocean captured 185 ±35 PgC (Petagramm of
47 Carbon) from a total of 700 ±75 PgC of anthropogenic carbon emissions from fossils fuels and land-use changes
48 (Friedlingstein et al., 2022). The oceanic sink for anthropogenic CO₂ increased progressively from 1.1 ±0.4
49 PgC.yr⁻¹ in the 1960s to 2.3 ±0.4 PgC.yr⁻¹ in the 2000s. Over the decade 2012-2021, the partitioning of the
50 anthropogenic CO₂ uptake was roughly equal between the ocean (2.9 ± 0.4 PgC.yr⁻¹) and the land (3.1 ± 0.6
51 PgC.yr⁻¹) (Friedlingstein et al., 2022). This partitioning has been confirmed for the decade 2013-2022
52 (Friedlingstein et al., 2023).

53 Ocean observations indicate that the Southern Ocean (SO) south of 45°S has been accumulating each
54 year about 0.5 PgC.yr⁻¹ since the 1990s (e.g. Takahashi et al., 2009; Lenton et al., 2013; Rödenbeck et al., 2013;
55 Long et al., 2021; Fay et al, 2023; Gray, 2024). Results based on BGC-Argo floats (Southern Ocean Carbon and
56 Climate Observations and Modeling project, SOCCOM) suggest that the CO₂ sink in the SO might be much
57 lower (0.16 PgC.yr⁻¹ south of 44°S for the period 2015-2017, Gray et al. 2018; Bushinsky et al., 2019) but there
58 is an ongoing debate on the size of the carbon sink in this region depending the periods and methods (Long et al.,
59 2021; Sutton et al., 2021; Hauck et al, 2023b; Gray, 2024). It is also well established that the CO₂ sink in the SO
60 undergoes substantial decadal variability first documented for the 1990s (Le Quéré et al., 2007; Metzl, 2009;
61 Lenton et al., 2013) and subsequently identified for the period 1982-2018 (Landschützer et al., 2015; Kepler
62 and Landschützer, 2019; Mackay et al., 2022; Hauck et al., 2023a, b). However as for the mean state, there are
63 also uncertainties on both the magnitude and phasing of decadal variability in the SO carbon sink mainly due to
64 insufficient sampling (Gloege et al, 2021; Hauck et al, 2023a, b). A recent extension of the period to 1957-2020
65 suggests that the inter-annual to decadal variability of the SO CO₂ sink was most pronounced after the 1980s
66 (Rödenbeck et al., 2022; Bennington et al., 2022). Whatever the variability of the SO CO₂ sink since the 1960s,
67 the ocean continuously absorbs atmospheric CO₂ and the distribution of anthropogenic CO₂ (C_{ant}) in the SO is
68 now relatively well documented (e.g. Pardo et al., 2014; Gruber et al., 2019a) thanks to the GLODAP data
69 synthesis effort for the global ocean (Global Ocean Data Analysis Project, Olsen et al., 2016, 2019, 2020). The
70 SO takes up about 40% of the total anthropogenic carbon that enters the ocean (Khatiwala et al., 2013; Gruber et
71 al., 2019a).

72 The anthropogenic CO₂ uptake in the ocean results in lowering carbonate ion concentrations and pH, a
73 chemical process termed “ocean acidification” (OA) (Caldeira and Wickett 2003; Doney et al., 2009). This
74 decreases the saturation state with respect to carbonate minerals (aragonite, Ω_{ar} and calcite, Ω_{ca}), a process most
75 pronounced in the cold waters at high latitudes where the saturation state is naturally low (Orr et al., 2005;
76 Takahashi et al., 2014; Jiang et al., 2015). The first estimate of C_{ant} distribution in the global ocean (for a
77 nominal year 1994, Sabine et al., 2004) shows that the accumulation of C_{ant} led to an upward migration of the
78 Ω_{ar} and Ω_{ca} saturation horizon in all ocean basins (Feely et al., 2004). This change is particularly pronounced
79 south of the Polar Front (PF) in the SO due to both C_{ant} uptake and the enhanced upwelling of carbon-rich deep
80 waters (e.g. Hauck et al., 2010; Pardo et al., 2017). It has been suggested, through numerical studies, that
81 depending on future CO₂ emission levels, surface waters in the SO could reach under-saturation state for
82 aragonite by 2030-2050 (Orr et al., 2005; Gangstø et al., 2008; McNeil and Matear, 2008; Negrete-Garcia et al.,

83 2019). Such a change would have multiple and detrimental impacts on marine ecosystems (Fabry et al., 2008;
84 Doney et al., 2012; Bopp et al., 2013), in particular calcifying marine organisms, and especially aragonite
85 producers such as pteropods (Hunt et al., 2008; Gardner et al., 2023), but also calcite producing planktonic
86 foraminifera (Moy et al., 2009), coccolithophorids (Beaufort et al., 2011), and non-calcifying species such as the
87 abundant SO diatoms (e.g. Benoiston et al., 2017; Petrou et al., 2019; Weir et al., 2020; Duncan et al., 2022) and
88 krill (Kawaguchi et al., 2013).

89 Hindcast simulations with Global Ocean Biogeochemical Models (GOBM), as well as projections with
90 Earth System Models (ESM) have been used to evaluate the ocean carbon cycle over the past decades and future
91 changes in C_{ant} storage, ocean acidification or impacts of global changes on marine ecosystems. However,
92 current model-based estimates of the contemporary SO CO_2 sink are subject to relatively large uncertainties (e.g.
93 Long et al., 2013; Hauck et al., 2020; Gooya et al., 2023; Hauck et al., 2023a, b; Mayot et al., 2023; DeVries et
94 al, 2023). Difference between GOBM models can reach up to 0.7 PgC.yr^{-1} in the SO (Hauck et al., 2020), which
95 is roughly equivalent to the mean climatological flux of 0.5 PgC.yr^{-1} (McNeil et al., 2007; Takahashi et al., 2009;
96 Lenton et al., 2013). At the high latitudes of the SO ($> 50^\circ\text{S}$) for the 2010s, ESMs from the Coupled Model
97 Intercomparison Project Phase 6 (CMIP6) simulated either a large sink or a modest source of CO_2 (McKinley et
98 al, 2023). This is mainly due to incorrect or missing physical and/or biological processes in the models (e.g.
99 Pilcher et al., 2015; Kessler and Tjiputra, 2016; Mongwe et al., 2018; Lerner et al., 2021) leading to biases in the
100 seasonality of temperature, dissolved inorganic carbon C_T , partial pressure of CO_2 ($p\text{CO}_2$), air-sea CO_2 fluxes,
101 pH or Ω (e.g. McNeil and Sasse 2016; Rodgers et al., 2023; Rustogi et al., 2023; Joos et al., 2023). Such model
102 imperfections should be resolved to gain reliability in future projections of CO_2 uptake, OA, productivity and the
103 responses of the marine ecosystems (Frölicher et al., 2015; Hauck et al., 2015; Sasse et al., 2015; Kessler and
104 Tjiputra, 2016; McNeil and Sasse 2016; Kwiatkowski and Orr, 2018; Negrete-Garcia et al., 2019; Burger et al.,
105 2020; Terharr et al., 2021; Krumhardt et al., 2022; Jiang et al., 2023; Mongwe et al., 2023). In this context, long-
106 term biogeochemical observations are particularly valuable to quantify and understand recent past and current
107 changes, and ultimately evaluate model simulations, as often concluded in modeling studies (e.g. Kessler and
108 Tjiputra, 2016; Gooya et al., 2023; Wright et al., 2023; Hauck et al., 2023a; Mayot et al., 2023; Rodgers et al.,
109 2023).

110 Although the SO south of the Polar Front remains much less observed than other oceanic regions,
111 several observations-based studies have estimated the decrease in pH in surface waters in response to the
112 increase in oceanic CO_2 fugacity, $f\text{CO}_2$ (Mirodikwa et al., 2012; Takahashi et al., 2014; Lauvset et al., 2015;
113 Munro et al., 2015; Xue et al., 2018; Iida et al., 2021; Leseurre et al., 2022; Brandon et al., 2022). Results
114 showed a large range in the pH trends from $-0.008.\text{decade}^{-1}$ to $-0.035.\text{decade}^{-1}$ depending on the period and the
115 region of interest. Most of these analyses were based on summer observations (Table 1) and some studies
116 highlighted contrasting pH trends on a 5-10 years time probably linked to large scale climate variability such as
117 the Southern Annular Mode (SAM) (e.g. Xue et al., 2018). Given such variability, it is important to continue
118 monitoring $f\text{CO}_2$ and pH trends and, if possible, at different seasons as future change in CO_2 uptake and potential
119 tipping points of the carbonate saturation state also depend on seasonality (Sasse et al., 2015). The above
120 observational studies were dedicated to pH changes in surface waters. In contrast to Northern high latitudes (e.g.
121 Olafsson et al., 2009, 2010; Franco et al., 2021; Skjelvan et al., 2022), few studies in the SO evaluated decadal
122 changes of carbonate system properties and acidification in the water column based on time-series stations.
123 These changes in the SO water column were investigated from data collected during cruises generally 3 to 15

124 years apart (e.g., Hauck et al., 2010; Van Heuven et al., 2011; Pardo et al., 2017; Tanhua et al., 2017; Carter et
125 al., 2019).

126 The present study complements in time, seasons, and in the water column, the surface $f\text{CO}_2$ and pH
127 trends investigated by Leseurre et al., (2022) in different regions of the Southern Indian Ocean for the period
128 1998-2019 during austral summer. South of the PF around 50°S , Leseurre et al. (2022) showed that in summer
129 the surface $f\text{CO}_2$ increase and pH decrease over 20 years were mainly driven by the accumulation of
130 anthropogenic CO_2 by about $+0.6 \pm 0.2 \mu\text{mol.kg}^{-1}.\text{yr}^{-1}$ and by a small warming of $+0.03 \pm 0.02 \text{ }^\circ\text{C.yr}^{-1}$. In addition
131 Leseurre et al. (2022) showed that in the recent decade, 2007-2019, the $f\text{CO}_2$ trend was low ($+0.3 \pm 0.2 \mu\text{atm yr}^{-1}$)
132 compared to the previous decade ($+5.3 \pm 0.4 \mu\text{atm yr}^{-1}$ over 1998-2007), highlighting the sensitivity of the $f\text{CO}_2$
133 and pH trends to the selected time period (especially during summer). In particular, they observed relatively
134 stable pH values over 2010-2019 (i.e. no decrease in pH) with no clear explanation on the origin of the slow-
135 down of the $f\text{CO}_2$ and pH trends in surface waters south of the PF in recent years. To complement the analysis
136 by Leseurre et al. (2022) based on summer observations over the period 1998-2019 this study focuses on one
137 location regularly visited south of the Polar Front (around 50°S - 68°E south-west of Kerguelen Island, Figure 1).
138 The analysis period is first extended back to 1985 and forward to 2021 to investigate the recent status of $f\text{CO}_2$
139 and pH. We also evaluate the trends during late winter using sparse data in October/November. The combination
140 of in situ observations and monthly estimates from a neural network model over the period 1985-2020 (Chau et
141 al., 2022) enables to assess potential changes in seasonality of the surface ocean carbonates system (including
142 $f\text{CO}_2$, C_T , pH, Ω) as suggested in recent decades or in future scenarios (Hauck and Völker, 2015; Gallego et al.,
143 2018; Landschützer et al., 2018; Kwiatkowski and Orr, 2018; Kwiatkowski et al., 2020; Lerner et al., 2021;
144 Fassbender et al., 2022; Yun et al., 2022; Rodgers et al., 2023; Joos et al., 2023). The changes observed in
145 surface waters will be related to changes in C_{ant} concentrations estimated in the water column and will be
146 complemented by an analysis of OA at depth between 1985 and 2021. Finally we will explore the long-term
147 change of surface $f\text{CO}_2$ and pH since the 1960s and potential future changes of the carbonate system at this time-
148 series site.

149

150 **2 Data selection, methods and quality control**

151

152 **2.1 Study area and data selection**

153

154 This study focuses on a High Nutrients Low Chlorophyll area (HNLC, Minas and Minas, 1992) in the
155 Indian sector of the Southern ocean (SO) in the Permanent Open Ocean Zone (POOZ) south of the Polar Front
156 (PF) and south-west of Kerguelen Islands (around 50°S - 68°E , Figure 1). The Kerguelen Plateau is an extended
157 topographic feature that controls part of the Antarctic Circumpolar Current (ACC), generates eddies (Daniault
158 and Ménard, 1985) and the northward deflection of the PF just east of the Island (Pauthenet et al., 2018). The
159 Plateau is also a region of relatively high chlorophyll-a (Chl-a) concentration (Moore and Abbott, 2000; Mongin
160 et al., 2008) and strong CO_2 uptake during austral spring-summer that contrasts with the weaker sink over the
161 POOZ/HNLC (Metzl et al., 2006; Jouandet et al., 2008, 2011; Lo Monaco et al., 2014; Leseurre et al., 2022).
162 The POOZ/HNLC region west (upstream) of the Kerguelen Plateau is characterized by rather stable water mass
163 properties (temperature, salinity, oxygen or nutrients) over time and low eddy activity compared to the Plateau
164 (Daniault and Ménard, 1985; Chapman et al., 2015; Dove et al., 2022). In this region, located in the deep

165 Enderby Basin, the flow is not constrained by topography and there is no local upwelling that would import C_T -
166 rich waters to the surface layers as observed on the eastern side of the Kerguelen Plateau (Brady et al., 2021).

167 The Indian sector of the SO is also recognized to host the strongest winds in the SO leading to year-
168 round high gas transfer coefficients (Wanninkhof and Trinanes 2017). As a result, and in contrast to the Atlantic
169 sector of the SO, the Indian region south of 45°S was a periodic annual CO_2 source, especially in the 1960s to
170 the 1980s (Rödenbeck et al., 2022; Bennington et al., 2022; Prend et al., 2022; Gray, 2024). In the POOZ-HNLC
171 region, high winter wind speed (monthly average up to 16 m s⁻¹) and associated heat loss drive deep mixing.
172 Deep winter mixing entrains subsurface properties to the surface layer, increases surface C_T concentrations
173 leading to wintertime outgassing of CO_2 (Metzl et al., 2006). This combination of characteristics makes the
174 region an ideal test-bed for 1-D modeling studies investigating the temporal dynamics and drivers of
175 biogeochemical processes including nutrients, iron, phytoplankton and carbon (Pondaven et al., 1998, 2000;
176 Louanchi et al., 1999, 2001; Jabaud-Jan et al., 2004; Metzl et al., 2006; Mongin et al., 2006, 2007; Kane et al.,
177 2011; Pasquer et al., 2015; Demuyne et al., 2020).

178 Here we used surface and water-column observations around location 50°40'S-68°25'E (Figure 1, Table
179 S1), historically called KERFIX station (KERguelen FIXed station) sampled from 1990 to 1995 in the
180 framework of the WOCE/JGOFS programs (Jeandel et al., 1998). The station was first occupied in March 1985
181 during the INDIGO-1 cruise (Indian Ocean Geochemistry, Poisson, 1985; Poisson et al., 1988) and since 1998 it
182 is regularly visited during the OISO cruises (Océan Indien Service d'Observations, Metzl and Lo Monaco, 1998,
183 <https://doi.org/10.18142/228>). The regular occupation from 1985 to 2021 makes it the longest time-series station
184 in the Southern Ocean POOZ/HNLC area for investigating the inter-annual to decadal trends of carbonate
185 properties in surface waters and across the water-column (0-1600m). Despite the occasional large anomalies in
186 surface waters properties (e.g. lower temperature in December 1998, lower salinity in February 2013) we
187 consider all observations selected for this study both in surface waters and the water-column to be representative
188 of the water masses in this POOZ/HNLC region upstream of the Kerguelen Plateau.

189 Data for the period 1985-2011 were extracted from the GLODAP data-product, version V2.2021
190 (Lauvset et al., 2021 a, b; Table S1a). Observations collected during OISO cruises from 2012 to 2021 will be
191 included in GLODAP-V3. For the surface water properties, all available underway fCO_2 data were selected
192 (Figure 1). This includes one cruise in November 1962 (Keeling and Waterman, 1968) and 41 cruises from 1991
193 to 2021 (Table S1b). All surface temperature, salinity and fCO_2 data were extracted from the SOCAT data-
194 product version v2022 (Surface Ocean CO_2 Atlas, Bakker et al., 2016, 2022) and have an accuracy for fCO_2
195 between 2 to 5 μatm .

196

197 **2.2 Methods**

198

199 The methods for surface underway fCO_2 and biogeochemical properties (oxygen, C_T , total alkalinity A_T ,
200 nutrients) in the water-column for the INDIGO-1, KERFIX and OISO cruises were described in previous studies
201 (e.g. Poisson et al., 1993; Louanchi et al., 2001; Metzl et al., 2006; Metzl, 2009; Mahieu et al., 2020; Leseurre et
202 al., 2022). Here we briefly recall the methods for underway fCO_2 and water-column observations.

203

204 **2.2.1 Surface fCO_2 data**

205

206 For fCO₂ measurements in 1991-2021, sea-surface water was continuously equilibrated with a "thin
207 film" type equilibrator thermostated with surface seawater (Poisson et al., 1993). The xCO₂ in the dried gas was
208 measured with a non-dispersive infrared analyser (NDIR, Siemens Ultramat 5F or 6F). Standard gases for
209 calibration (around 270, 350 and 490 ppm) were measured every 6 hours. To correct xCO₂ dry measurements to
210 fCO₂ *in situ* data, we used polynomials from Weiss and Price (1980) for vapour pressure and from Copin-
211 Montégut (1988, 1989) for temperature. Note that when incorporated in the SOCAT data-base, the original fCO₂
212 data are recomputed (Pfeil et al., 2013) using temperature correction from Takahashi et al. (1993). Given the
213 small difference between equilibrium temperature and sea surface temperature (+0.56 ± 0.30 °C on average for
214 the cruises in 1998-2021), the fCO₂ data from SOCAT used in this analysis (Bakker et al., 2022) are almost
215 identical (within 1 µatm) to the original fCO₂ values from our cruises ([www.ncei.noaa.gov/access/ocean-carbon-](http://www.ncei.noaa.gov/access/ocean-carbon-data-system/oceans/VOS_Program/OISO.html)
216 [data-system/oceans/VOS_Program/OISO.html](http://www.ncei.noaa.gov/access/ocean-carbon-data-system/oceans/VOS_Program/OISO.html)).

217

218 2.2.2 Water column data

219

220 Over the period 1990-1995, water samples were collected during the KERFIX program on the ship *La*
221 *Curieuse* at standard depths using 8 L Niskin bottles mounted on a stainless steel cable and equipped with
222 reversing SIS pressure and temperature probes. Methods and accuracy for the geochemical measurements used
223 in this analysis (A_T, C_T, oxygen, nutrients) are detailed by Jeandel et al. (1998) and by Louanchi et al. (2001).
224 From 1998 onwards, the station was occupied within the framework of the OISO long-term monitoring program
225 onboard the *R.V. Marion-Dufresne*. We used Conductivity-Temperature-Depth (CTD) sensors mounted on a 24
226 bottles rosette equipped with 12 L Niskin bottles. Temperature and salinity measurements have an accuracy of
227 0.002 °C and 0.005 respectively (Mahieu et al., 2020). Samples for A_T and C_T were filled in 500 mL glass bottles
228 and poisoned with 300 µL of saturated mercuric chloride solution to halt biological activity. Discrete C_T and A_T
229 samples were analyzed onboard by potentiometric titration derived from the method developed by Edmond
230 (1970) using a closed cell. Based on replicate samples from the surface or depth, the repeatability for A_T and C_T
231 varies from 1 to 3.5 µmol.kg⁻¹ depending on the cruise. The accuracy of ±3 µmol.kg⁻¹ was ensured by daily
232 analyses of Certified Reference Materials (CRMs) provided by Andrew Dickson's laboratory (Scripps Institute
233 of Oceanography).

234 Dissolved oxygen (O₂) concentration was determined by a sensor fixed on the rosette and values were
235 adjusted based on discrete measurements (Winkler method, Carpenter, 1965) using a potentiometric titration
236 system. Accuracy for O₂ is ±2 µmol.kg⁻¹ (Mahieu et al., 2020). Although long-term deoxygenation in the
237 Southern ocean has been suggested (Ito et al., 2017; Schmidtko et al., 2017; Oschlies et al., 2018), no significant
238 trend in O₂ was identified over 1985-2021 at this station around 50°S in both the surface and the subsurface layer
239 (at the depth of the temperature minimum representing winter water, a layer used for C_{ant} calculations as
240 described later). However, in the station data a small O₂ decrease was detected around 800m in the O₂ minimum
241 layer over 36 years (-0.22 ± 0.07 µmol.kg⁻¹.yr⁻¹). As this has no impact on the interpretation for pH and Ω trends
242 for this analysis, the observed change of O₂ at depth will not be discussed further. Here the O₂ data are mainly
243 used for the calculation of anthropogenic CO₂ concentrations and the observed O₂ change at depth is too small to
244 have an impact on temporal variations of C_{ant} concentrations given the uncertainty of the calculation.

245 Nitrate (NO₃) and silicate (DSi) were analyzed on board or at LOCEAN/Paris by colorimetry following
246 the methods described by Tréguer and Le Corre (1975) for 1998-2008 or from Coverly et al. (2009) for 2009-

247 2021. The uncertainty of NO_3 and DSi measurements is $\pm 0.1 \mu\text{mol.kg}^{-1}$. Based on replicate measurements on
248 deep samples, we estimate an error of about 0.3 % for both nutrients. Phosphate (PO_4) samples were analyzed
249 from a few cruises following the method of Murphy and Riley (1962) revised by Strickland and Parsons (1972)
250 with an uncertainty of $\pm 0.02 \mu\text{mol.kg}^{-1}$. When nutrients data are not available for a cruise, we used
251 climatological values based on the seasonal nutrients cycles inferred from data from 1990 to 2021. This method
252 has a very small impact on the carbonate system calculations and the trend analysis as we did not detect any
253 significant trends in nutrients in surface or at depth since 1985 (not shown) as opposed to what has been
254 observed at higher latitudes of the SO (Iida et al., 2013; Hoppema et al., 2015). However, we will see in section
255 3.1 that the inter-annual variability of nutrients (especially DSi in the HNLC region) might inform on potential
256 changes in biological processes.

257 Samples were collected in the top layers (0-150m) for chlorophyll-a (Chl-a). For that, one to two liters
258 of seawater were filtered onto $0.7 \mu\text{m}$ glass microfiber filters (GF/F, Whatman) and filters were stored at -80°C
259 onboard. Back at the LOCEAN/Paris laboratory, samples were extracted in 90% acetone (Strickland and
260 Parsons, 1972) and the fluorescence of Chl-a was measured on a Turner Type 450 fluorometer for the period
261 1998-2007 and since 2009 at 670 nm on a Hitachi F-4500 spectrofluorometer (Neveux and Lantoiné, 1993).

262

263 2.2.3 Data quality-control and data consistency

264

265 When exploring the trends of ocean properties based on different cruises more than 35 years apart, it is
266 important to first verify the consistency of the data and to correct for any bias or drift. The INDIGO data from
267 1985 (i.e. prior to CRM available for A_T and C_T) were first controlled prior to their incorporation into the
268 original GLODAP product (Sabine et al., 1999; Key et al., 2004) and corrections for A_T and C_T were revisited
269 within the framework of the CARINA project (CARbon IN the Atlantic, Lo Monaco et al., 2010) and the
270 GLODAPv2 synthesis (Olsen et al., 2016). A secondary quality control was performed on the data from the
271 OISO cruises collected between 1998 and 2011 within the CARINA and GLODAP-v2 initiatives (Lo Monaco et
272 al., 2010; Olsen et al., 2016). Significant off-sets were identified for A_T and C_T in samples from the KERFIX
273 cruises (1990-1993) compared to INDIGO and OISO data and it was proposed to correct the original values by -
274 $35 \mu\text{mol.kg}^{-1}$ for C_T and $-49 \mu\text{mol.kg}^{-1}$ for A_T (Metzl et al., 2006). These corrections were applied in GLODAP
275 version v2.2019 (Olsen et al., 2019) and resulted in coherent A_T and C_T concentrations for KERFIX in the deep
276 layers compared to other cruises (Supp. Mat., Table S2, Figure S1). The same data quality control protocol as for
277 GLODAP-v2 was applied to data from OISO cruises for the period 2012-2021 (Mahieu et al., 2020). Given the
278 accuracy of the data no systematic bias (except in 2014) was found for the properties measured in 2012-2021.
279 The time-series of A_T and C_T at depths below 1450 m for all cruises in 1985-2021 show some variability but no
280 trend over 36 years as expected in the bottom waters in this region (Supp. Mat., Figure S1). However, we
281 identified a small bias for C_T in 2014 (cruise OISO-23) where C_T concentrations in the deep water appeared
282 slightly lower ($2228\text{-}2234 \mu\text{mol.kg}^{-1}$ in 2014 compared to the mean value of $2240.7 \pm 3.7 \mu\text{mol.kg}^{-1}$, Table S2,
283 Figure S1). When compared to fCO_2 in surface waters, we also suspect the C_T data in the mixed-layer in 2014 to
284 be too low by about $10 \mu\text{mol.kg}^{-1}$ (Figures S2, S3). Therefore we applied a WOCE/GLODAP flag 3 for C_T data
285 of this cruise and will not use the station data in 2014 for the C_{ant} calculations and the trend analysis described in
286 this study.

287

288 2.2.4 CMEMS-LSCE-FFNN model

289
290 As most of the cruises took place during austral summer and data are not available each year, we
291 completed the observations with the results from an ensemble of feed-forward neural network models (CMEMS-
292 LSCE-FFNN or FFNN for simplicity here, Chau et al., 2022). The FFNN model allows mapping at global scale
293 monthly surface $f\text{CO}_2$ from the SOCAT gridded datasets and ancillary variables. The reconstructed $f\text{CO}_2$ is then
294 used to derive monthly surface C_T and pH fields as well as air-sea CO_2 fluxes. This data product is used to
295 investigate the trends for different seasons and to derive estimates of annual air-sea CO_2 fluxes to interpret the
296 change in CO_2 uptake, if any. For a full description of the model, access to the data and a statistical evaluation of
297 $f\text{CO}_2$ reconstructions please refer to Chau et al. (2022). Within this study, we compared the FFNN $f\text{CO}_2$ with
298 observations from 35 cruises for the years between 1991 and 2020 (Table S3, Figure S2a). Excepted for a few
299 periods (January 1993 and January 2002), model-data differences are generally within $\pm 10 \mu\text{atm}$ with a mean
300 difference of $2.1 \pm 7 \mu\text{atm}$ for the 35 co-located periods. Note that, as opposed to sea surface $f\text{CO}_2$, no temporal
301 trend was identified for the differences between the observed and reconstructed $f\text{CO}_2$ (Figure S2b), i.e. the trends
302 of sea surface $f\text{CO}_2$ derived from the observations and from the FFNN model should be the same. Aside from the
303 $f\text{CO}_2$ reconstructions, surface ocean alkalinity (A_T) fields are also provided by using the multivariate linear
304 regression model LIAR (Carter et al., 2016; 2018) based on sea surface temperature, salinity, and nutrients
305 concentration.

306

307 2.2.5 Calculations of carbonate properties

308
309 Based on the data available for each cruise ($f\text{CO}_2$, or A_T and C_T) or from the FFNN model ($f\text{CO}_2$ and
310 A_T), other carbonate system properties (pH, $[\text{H}^+]$, $[\text{CO}_3^{2-}]$ and Ω) were calculated using the CO2sys program
311 (version CO2sys_v2.5, Orr et al., 2018) developed by Lewis and Wallace (1998) and adapted by Pierrot et al.
312 (2006) with K1 and K2 dissociation constants from Lueker et al. (2000) as recommended (Dickson et al., 2007;
313 Orr et al., 2015; Wanninkhof et al., 2015). The total boron concentration was calculated according to Uppström
314 (1974) and KSO_4 from Dickson (1990). To calculate the properties with the underway surface $f\text{CO}_2$ dataset, we
315 used the A_T/S relationship based on A_T and C_T data from the OISO cruises over the period 1998-2019 in the
316 South Indian sector as described by Leseurre et al. (2022):

317

$$318 A_T = 64.341 \times S + 106.764 \text{ (rmse} = 7.5 \mu\text{mol.kg}^{-1}, n = 4775) \text{ (Eq. 1)}$$

319

320 The use of other A_T/S relationships (e.g. Millero et al., 1998; Jabaud-Jan et al., 2004; Lee et al., 2006;
321 Carter et al., 2018) would change slightly the A_T concentrations but neither the A_T trend nor the interpretation of
322 the C_T , pH or Ω trends. However, as salinity is an important predictor in the calculation of A_T , C_T or pH from
323 $f\text{CO}_2$ data, we have assessed the original underway salinity data and found biases for a few cruises in 1992, 1993
324 and 1995 (Table S1b). For these cruises or when salinity was not measured we used the salinity from the World
325 Ocean Atlas, WOA (Antonov et al., 2006) in the SOCAT data-sets (Pfeil et al., 2013, identified “WOA” in Table
326 S1b). Monthly $f\text{CO}_2$ and A_T data extracted from the CMEMS-LSCE-FFNN datasets at the station location
327 (50.5°S - 68.5°E) over 1985-2020 were used to calculate the carbonate properties in the same way as from
328 observations.

329

330 2.2.6 Comparisons of different datasets and the FFNN model

331

332 To validate the properties calculated using the $f\text{CO}_2$ data for 1991-2021 or from the FFNN model over
333 1985-2020 we compared the calculated values (A_T , C_T , pH, $[\text{H}^+]$, $[\text{CO}_3^{2-}]$, Ω) with those calculated from A_T and
334 C_T data measured in the mixed-layer at the KERFIX/OISO station occupied in 1985 and between 1993 and 2021.
335 For this comparison, we averaged the continuous underway $f\text{CO}_2$ data selected in a box around the station
336 location (50°S - 51.5°S / 67.5 - 69°E , yellow box in Figure 1). Results of the comparisons between various datasets
337 are detailed in the Supplementary Material (Tables S3 and S4). During the period 1993-2021, there are 22 station
338 occupations with co-located underway $f\text{CO}_2$ data for different seasons (but mainly in summer). Since we found a
339 close agreement between measured $f\text{CO}_2$ and the FFNN model (Table S3, Figure S2), mismatches in all
340 calculated carbonate system properties between the underway $f\text{CO}_2$ dataset and the FFNN model are small,
341 falling within the range of the errors associated with the calculations (Orr et al., 2018). For example, for 35 co-
342 located periods, the mean differences in calculated C_T of $1.5 \pm 5 \mu\text{mol.kg}^{-1}$ or pH of -0.002 ± 0.008 are in the
343 range of the theoretical error of about $5 \mu\text{mol.kg}^{-1}$ and 0.007 respectively when taking into account
344 measurements errors on salinity, temperature, nutrients, $f\text{CO}_2$ and A_T (Orr et al., 2018). On the other hand,
345 compared to the station data in the mixed-layer (Table S4), the calculated A_T using Equation 1 is slightly higher
346 by about $5 \mu\text{mol.kg}^{-1}$. This explains the relatively high differences for C_T (mean difference around $8 \mu\text{mol.kg}^{-1}$)
347 and for pH (mean difference around 0.008) calculated with $f\text{CO}_2$ and the A_T/S relationship. The differences of
348 calculated values with observations are, on average, in the range of uncertainties of the carbonate system
349 calculations using A_T - C_T pairs (error for $f\text{CO}_2$ around $13 \mu\text{atm}$ and for pH around 0.0144). Importantly, there is
350 no temporal trend for the differences between calculated and observed properties (Figure S3b). We are thus
351 confident using the selected $f\text{CO}_2$ data for the trend analysis presented in this study. The independent comparison
352 with A_T and C_T measurements in the mixed-layer also indicates that the FFNN model results for A_T and C_T , are
353 close to the observations (Table S4, Table S5, Figure S4) as well as for calculated pH, $[\text{H}^+]$, $[\text{CO}_3^{2-}]$, Ω_{Ca} and
354 Ω_{Ar} . This somehow validates the use of the FFNN data for the trend analysis over the period 1985-2020 and for
355 different seasons, although the FFNN model was not constrained by in-situ $f\text{CO}_2$ before 1991, few data in austral
356 winter since 1991, and no Chl-a satellite data available before 1998. Nevertheless, the model shows a good
357 agreement with observations collected in March 1985 (Table S5, Figure S4).

358

359 3 Results and discussion

360

361 3.1 Variability and trend of sea surface $f\text{CO}_2$ and air-sea CO_2 fluxes: 1985-2021

362

363 The $f\text{CO}_2$ observations around 50°S - 68°E and their mean values for each cruise are shown in Figure 2a.
364 $f\text{CO}_2$ measurements are available for different seasons since 1991, though most of them stem from austral
365 summer (January-February). During austral summer, the ocean $f\text{CO}_2$ was generally lower than in the atmosphere
366 (i.e. the ocean was a CO_2 sink) whereas from July to October it was near equilibrium. The same seasonal change
367 is obtained from the FFNN model for the period 1991-2020 (Figure 2a). The model also indicates that between
368 in 1985 and the mid-1990s the $f\text{CO}_2$ during austral winter (May-September) was always higher than the

369 atmospheric $f\text{CO}_2$ leading to an annual CO_2 source during this period (Figure 3). In 1985 the oceanic $f\text{CO}_2$ from
370 the FFNN model was higher than in the atmosphere from March to October (Figure S4) resulting in an annual
371 CO_2 source of $+0.8 \text{ molC.m}^{-2}.\text{yr}^{-1}$. The model estimates a decrease of the annual CO_2 source until the end of the
372 1990's followed by an increase of the source over the following decade (Figure 3). Around the year 2010, the
373 annual CO_2 flux was around $+0.5 \text{ molC.m}^{-2}.\text{yr}^{-1}$ and then decreased over the last decade to change into an annual
374 CO_2 sink that increased to reach $-0.5 \text{ molC.m}^{-2}.\text{yr}^{-1}$ in 2020. For this reason and given the data available since
375 1991, we evaluated the summer and winter trends in $f\text{CO}_2$, C_T and pH from the FFNN model over 3 periods
376 1991-2001, 2001-2010, 2010-2020 and compared the summer trends with those deduced from observations
377 (Table 2). The analysis of trends and their associated drivers for different seasons and periods will allow to
378 explore links with the variability of primary production and/or the Southern Annual Mode (SAM). Shifts from a
379 negative to a positive SAM index (Figure 3) may have strengthened the upwelling of deep waters and could
380 therefore impact ocean properties throughout the water column including C_T , nutrients, primary production or
381 pH (e.g. Lovenduski and Gruber, 2005; Lenton et al., 2009; Hauck et al., 2013; Hoppema et al., 2015; Pardo et
382 al., 2017).

383 From the first underway measurements obtained at the OISO-KERFIX site in February 2021 to the last
384 measurements used in this study in February 1991, the average oceanic $f\text{CO}_2$ increased by $+50.5 \mu\text{atm}$ (from
385 $344.4 \pm 1.5 \mu\text{atm}$ to $394.9 \pm 1.5 \mu\text{atm}$, Figure 2a). During the same period, the atmospheric CO_2 increased by 57
386 μatm in this region (recorded at Crozet Island, Dlugokencky and Tans, 2022). This first comparison of two
387 cruises 30 years apart indicates that the oceanic $f\text{CO}_2$ increase was close to that of the atmosphere. During the
388 same period, we observed small variations in A_T (average $A_T = 2276.5 \pm 4.5 \mu\text{mol.kg}^{-1}$) and a clear increase in C_T
389 (Figure 4a and S5). This suggests that most of the change observed in oceanic $f\text{CO}_2$ and C_T over the last 30 years
390 is due to the uptake of anthropogenic CO_2 . However, the evolution of air-sea CO_2 fluxes (Figure 3) suggests that
391 other mechanisms were at play over shorter periods, and changes in the air-sea $f\text{CO}_2$ disequilibrium (Figure 2a)
392 suggests that different drivers may be involved in summer and in winter.

393
394 Summer data are characterized by a strong inter-annual variability in both $f\text{CO}_2$ and C_T (Figures 2a and
395 4a) with the ocean being a CO_2 source in January 2002, but a strong sink in January 1993, 1998, 2014, 2016 and
396 2019. In January 1998, when the surface ocean experienced a warm anomaly (Jabaud-Jan et al., 2004), the low
397 $f\text{CO}_2$ of $337 \mu\text{atm}$ and the low C_T of $2110 \mu\text{mol.kg}^{-1}$ (Figure 4a and S5) co-occurred with intense primary
398 production (Figure 5), probably supported by diatoms as suggested by very low DSi concentrations (< 2
399 $\mu\text{mol.kg}^{-1}$ down to 100m, Figure S6). In January 2014 and 2016, mixed-layer DSi concentrations were also
400 remarkably small ($< 5 \mu\text{mol.kg}^{-1}$ down to 75m, Figure S6). In 2014 low DSi coincided with Chl-a levels that
401 started to increase in mid-November 2013 and stayed at high level until February 2014 (Surface $\text{Chl-a} > 0.3$
402 mg.m^{-3} , Figures 5 and S7). The intense primary production contributed to the low $f\text{CO}_2$ of $365 \mu\text{atm}$ reached by
403 mid-January 2014, a value as low as 10 years earlier (Figure 2a). To the contrary, in 2002 relatively low Chl-a
404 (mean $\text{Chl-a} < 0.2 \text{ mg.m}^{-3}$, Figure 5) was associated with higher levels of $f\text{CO}_2$ ($373 \mu\text{atm}$), C_T ($2128 \mu\text{mol.kg}^{-1}$,
405 Figure 4a, Figure S5a) and DSi (Figure S6). This was also associated with higher salinity indicative of
406 entrainment that might be related to storm events that would have occurred few days before the measurements
407 leading to brief positive $f\text{CO}_2$ anomaly as recently observed from Glider data in the subpolar South Atlantic
408 (Nicholson et al., 2022). As opposed to the other periods the ocean was a source of CO_2 in summer 2002 (this
409 particular year was not well reconstructed by the FFNN model, Figure 2a and Figure S2b). The important inter-

410 annual variability observed in summer indicates that in this region historically referred to as HNLC (Minas and
411 Minas, 1992), primary production could significantly impact $f\text{CO}_2$ level in summer (Jabaud-Jan et al., 2004;
412 Pasquer et al., 2015; Gregor et al., 2018), a result that needs to be taken into account when evaluating drivers of
413 inter-annual variability (Rustogi et al., 2023) and the decadal trends of $f\text{CO}_2$ or pH.

414 The Chl-a time-series derived from MODIS suggests higher concentrations in recent years compared to
415 2002-2013, with Chl-a peaks identified in 2014, 2016, 2018, 2019 and 2021 (Figure 5 and S7) when the oceanic
416 $f\text{CO}_2$ in summer was well below the atmospheric level (Figure 2a).

417 The primary production lowers C_T concentrations and $f\text{CO}_2$, i.e. opposite to the C_T increase from
418 anthropogenic CO_2 uptake. These counteracting processes might explain the relatively stable $f\text{CO}_2$ previously
419 observed in the Indian POOZ in summer 2007-2019 with an annual $f\text{CO}_2$ rate of increase of only $+0.3 \pm 0.2$
420 $\mu\text{atm.yr}^{-1}$ (Leseurre et al., 2022). This low rate is confirmed here with the recent data obtained in 2020-2021
421 (Figure 2b and Figure S8). For the period 2010-2021, the oceanic $f\text{CO}_2$ trend in summer derived from
422 observations and the FFNN model is lower than $+1 \mu\text{atm.yr}^{-1}$ (Table 2), i.e. much lower than the atmospheric
423 $f\text{CO}_2$ rate of $+2.4 \mu\text{atm.yr}^{-1}$ and the oceanic $f\text{CO}_2$ trend of $+2.21 \pm 0.17 \mu\text{atm.yr}^{-1}$ estimated in winter by the
424 FFNN model (Table 2, Figure 2b). This rate is also lower compared to the change observed in October ($+2.9$
425 $\mu\text{atm.yr}^{-1}$) albeit being only based on 2 cruises in October 2011 and 2016 (Figure 2a). As the low $f\text{CO}_2$ trend in
426 recent years is detected for summer only this is likely linked to an increase in primary production, as suggested
427 by Chl-a records (Figure 5). From 1998 to 2010 the summer Chl-a concentrations decreased at a rate of -0.099
428 $\pm 0.041 \text{ mg.m}^{-3}.\text{decade}^{-1}$ whereas from 2020 to 2021 Chl-a increased by $+0.078 \pm 0.032 \text{ mg.m}^{-3}.\text{decade}^{-1}$ (Figure
429 5). These trends are coherent with previous studies, e.g. the reduced net primary productivity reported in the
430 Indian Antarctic zone over 1997-2007 (e.g. Arrigo et al., 2008; Takao et al., 2012) and the shift of the Chl-a
431 trend in 2010 also reported at large scale in the HNLC region of the Southern Ocean (Basterretxea et al., 2023).
432 As a consequence, after 2010 the difference between oceanic and atmospheric $f\text{CO}_2$ ($\Delta f\text{CO}_2 = f\text{CO}_2^{\text{occ}} - f\text{CO}_2^{\text{atm}}$)
433 decreased in summer ($-1.4 \mu\text{atm.yr}^{-1}$) and as it remains relatively steady during winter, the annual CO_2 flux
434 progressively varied from a source of $+0.45 \text{ molC.m}^{-2}.\text{yr}^{-1}$ in 2010 to a sink of $-0.63 \text{ molC.m}^{-2}.\text{yr}^{-1}$ in 2020
435 (Figure 3). In addition, as the wind speed was stable during this period ($12.0 \pm 0.9 \text{ m.s}^{-1}$ on average in 2010-2020,
436 Figure 3), the variation of the air-sea CO_2 flux was mainly controlled by $\Delta f\text{CO}_2$ (e.g. Gu et al., 2023) and the
437 decadal variation of primary production imprinted a significant change on the $f\text{CO}_2$ trend and air-sea CO_2 flux in
438 this HNLC region. In the region investigated here, increasing Chl-a levels co-occurred with shifts of the SAM
439 index to a positive state (Figure 3), a link previously suggested south of the Polar Front in the SO but for a short
440 period over 1997-2004 (Lovenduski and Gruber, 2005). Modeling studies also suggest that summertime
441 biological activity could play an important role for the variability of the CO_2 sink in the SO in response to the
442 SAM (Hauck et al, 2013).

443
444 Another process to take into account for interpreting $f\text{CO}_2$ trends is the change in temperature in surface
445 waters. Previous analysis suggested a progressive warming in the region investigated here (Auger et al., 2021 for
446 summer 1993-2017). Over 1998-2019 Leseurre et al. (2022) estimated a warming of Indian POOZ surface
447 waters of $+0.03 \pm 0.02 \text{ }^\circ\text{C.yr}^{-1}$. Extending the time-series for the period 1991-2021 (Figure S9a) we note that the
448 surface temperature presents sub-decadal variability and that the ocean cooled after 2018 with a trend of -0.47
449 $\pm 0.16 \text{ }^\circ\text{C.yr}^{-1}$ over 2018-2021 based on the monthly sea surface temperature (SST, Figure S9b). The trend
450 derived from our in-situ observations in summer over this period was $-0.25 \pm 0.09 \text{ }^\circ\text{C.yr}^{-1}$.

451 In 2019, the lower temperature and relatively high Chl-a led to low $f\text{CO}_2$ (380 μatm , Figure 2a) and low
452 C_T (2128 $\mu\text{mol.kg}^{-1}$) compared to 2018 ($f\text{CO}_2 = 386 \mu\text{atm}$; $C_T = 2137 \mu\text{mol.kg}^{-1}$, Figure 4a). The decrease in
453 observed $f\text{CO}_2$ from summer 2018 to 2019, also reconstructed by the FFNN model (Figure 2a), is contrary to the
454 expected $f\text{CO}_2$ and C_T increase due to anthropogenic uptake. In 2020, although the temperature was also lower
455 than in 2019, the oceanic $f\text{CO}_2$ was higher (392 μatm) probably due to lower primary production as suggested by
456 higher DSI (Figure S6), as well as from C_T (2135 $\mu\text{mol.kg}^{-1}$, Figure 4a) and Chl-a records (Figure 5). In January
457 2021 the temperature was close to that in January 2020, and both $f\text{CO}_2$ and C_T were slightly higher (395 μatm ,
458 2139 $\mu\text{mol.kg}^{-1}$). A_T concentrations were stable between 2018 and 2021 ($2278.9 \pm 1.8 \mu\text{mol.kg}^{-1}$, Figure S5)
459 indicating no effect of A_T on the observed $f\text{CO}_2$ change in this region as opposed to the areas north of the Polar
460 Front in the Indian Ocean where A_T variations are often linked to coccolithophores blooms (Balch et al., 2016;
461 Smith et al., 2017).

462 The inter-annual and pluri-annual variability observed over 1991-2021 highlights the competitive
463 processes that drive C_T , $f\text{CO}_2$ or pH temporal variations. In order to separate natural and anthropogenic
464 contributions, the anthropogenic CO_2 signal is estimated in the following section.

465

466 **3.2 Anthropogenic CO_2**

467 **3.2.1 Anthropogenic CO_2 in the water column**

468

469 To calculate anthropogenic CO_2 concentrations (C_{ant}), we used the TrOCA method developed by
470 Touratier et al. (2007) and previously applied in the southern Indian Ocean (Mahieu et al., 2020; Leseurre et al.,
471 2022). Such an indirect method is not suitable for evaluating C_{ant} concentrations in surface waters due to
472 biological activity and gas exchange and we restrict the C_{ant} calculations below the productive layer around
473 150m. In the region south of the Polar Front, a well-defined subsurface temperature minimum is observed each
474 year characterizing the Winter Water (WW) at depth range 150-250m (Figure 6a).

475

476 The C_T and C_{ant} concentrations increased over time in the water column, a signal that is most
477 pronounced in the top layers (200-400m, Figure 6b). In the deep layer, the presence of the Indo-Pacific Deep
478 Water (IPDW) around 600-800m is identified by a maximum of C_T ($C_T > 2250 \mu\text{mol.kg}^{-1}$) and a minimum of O_2
479 (O_2 close to or $< 180 \mu\text{mol.kg}^{-1}$, Figure S10) (Talley, 2013; Chen et al., 2022). In the IPDW layer restricted to
480 the neutral density (ND) range 27.75-27.85 kg.m^{-3} there is no significant change in C_T over time (Figure S10). In
481 that layer the C_{ant} concentrations in 1985 (17.3 $\mu\text{mol.kg}^{-1}$) were almost identical to those evaluated in 2021 (21.2
482 $\mu\text{mol.kg}^{-1}$), considering the uncertainty in the C_{ant} calculations ($\pm 6.5 \mu\text{mol.kg}^{-1}$, Touratier et al., 2007). Below
483 800m, the C_{ant} concentrations were small but not null (Figure 6b). The average C_{ant} concentration below 800m
484 for all years and seasons was $8.0 \pm 5.3 \mu\text{mol.kg}^{-1}$ ($n=123$) with a very small change detected over time ($C_{\text{ant}} = 7.7$
485 $\pm 1.3 \mu\text{mol.kg}^{-1}$ in 1985 and $C_{\text{ant}} = 10.4 \pm 0.6 \mu\text{mol.kg}^{-1}$ in 2021). As discussed above (section 2.2.3) the C_T and A_T
486 concentrations in the bottom layer ($>1450\text{m}$) were stable over 1985-2021 (Table S2, Figure S1).

487

488 **3.2.2 Anthropogenic CO_2 trend in the Winter Water**

489

490 To separate the natural and anthropogenic signals in surface waters for the driver analysis we assume
491 that C_{ant} in the WW is representative of C_{ant} in the mixed-layer (ML). This is confirmed with few stations

492 occupied during winter showing that C_{ant} concentrations in the WW in summer are almost equal to C_{ant} in the
493 ML during the preceding winter (Figure S11). The evolution of C_{ant} in the WW from 1985 to 2021 is presented
494 in Figure 7a for all seasons. In 1985 the C_{ant} concentration in the WW was $47.1 \mu\text{mol.kg}^{-1}$ and C_{ant} reached a
495 maximum of $71.7 \mu\text{mol.kg}^{-1}$ in 2021. The data selected at 200m present some inter-annual variability such as the
496 relatively low C_{ant} in 1998, 2005 and 2020 probably related to natural variability. In 1998 and in 2020 the O_2
497 concentrations were slightly lower in the WW ($< 300 \mu\text{mol.kg}^{-1}$) explaining the lower C_{ant} concentration (44.8
498 $\mu\text{mol.kg}^{-1}$ in 1998 and $53.8 \mu\text{mol.kg}^{-1}$ in 2020) but no anomaly was observed for C_T . This suggests that the
499 biological contribution may have been overestimated (lower O_2 is interpreted by the TrOCA method as more
500 organic matter remineralization which should be associated with higher C_T). This could be instead related to a
501 change in mixing or circulation. In 2005 anomalies of C_T , A_T and O_2 concur to explain the lower C_{ant} (43.9
502 $\mu\text{mol.kg}^{-1}$).

503 From 1985 to 2021, we estimated a C_{ant} trend in WW of $+0.49 \pm 0.09 \mu\text{mol.kg}^{-1}.\text{yr}^{-1}$. When the C_{ant}
504 anomalies in 1998, 2005 and 2020 were discarded, this C_{ant} trend was $+0.53 \pm 0.01 \mu\text{mol.kg}^{-1}.\text{yr}^{-1}$ (Figure 7a). As
505 expected, the C_{ant} concentrations in the ocean are positively related to atmospheric CO_2 (slope $+0.26 \pm 0.04$
506 $\mu\text{mol.kg}^{-1}.\mu\text{atm}^{-1}$, Figure 7b). Interestingly the slope observed south of the PF in the Indian Ocean is close to that
507 observed in the Antarctic Intermediate waters (AAIW) in the South Atlantic ($+0.23 \pm 0.05 \mu\text{mol.kg}^{-1}.\mu\text{atm}^{-1}$,
508 Fontela et al., 2021). Gruber et al. (2019 a, b) evaluated C_{ant} changes between 1994 and 2007 in the global ocean.
509 In the South Indian sector, they estimated a mean C_{ant} accumulation at the surface of $+6.0 \pm 1.1 \mu\text{mol kg}^{-1}$ in the
510 band 50-55°S south of the PF. At our station location (50-52°S/68°E) in the layer 0-250m, the C_{ant} accumulated
511 from 1994 to 2007 was $+5.7 \pm 1.5 \mu\text{mol kg}^{-1}$. In 13 years, this corresponds to a trend of $+0.44 \pm 0.11 \mu\text{mol.kg}^{-1}.\text{yr}^{-1}$.
512 Gruber et al. (2019 a, b) did not use the data presented here allowing for an independent comparison to the
513 present study. Estimates of C_{ant} accumulation by Gruber et al. (2019 a, b) are in agreement with ours for the
514 period 1994-2007 ($+0.49 \pm 0.01 \mu\text{mol.kg}^{-1}.\text{yr}^{-1}$) but lower than reported here in recent years ($+0.61 \pm 0.01$
515 $\mu\text{mol.kg}^{-1}.\text{yr}^{-1}$ over 2008-2021). Indeed our estimates over 3 decades indicate an increase in the uptake of
516 anthropogenic CO_2 with time (Figure 4b).

517
518

519 3.2.3 Anthropogenic and surface C_T seasonal trends

520

521 The C_{ant} trend in the WW over 1985-2021 ($+0.53 \pm 0.01 \mu\text{mol.kg}^{-1}.\text{yr}^{-1}$) is slightly lower than the annual
522 surface C_T trend derived from the FFNN model for 1985-2020 ($+0.58 \pm 0.05 \mu\text{mol.kg}^{-1}.\text{yr}^{-1}$ Figure 4a, Table 2)
523 suggesting that anthropogenic CO_2 uptake explains 86% of the C_T increase in surface waters. Over 1991-2020
524 the surface C_T trend appears slightly higher in January than in August (Figure 4b, Table 2). This suggests that in
525 addition to the increase of C_T due to anthropogenic CO_2 other processes such as the variability of the biological
526 activity, vertical mixing or upwelling contributed to the observed trend. Indeed, as for $f\text{CO}_2$ (Figures 2b), the C_T
527 growth rate also depends on seasons and decades (Figure 4b). Over 1991-2001 the C_T trend from the
528 observations ($+0.05 \pm 0.64 \mu\text{mol.kg}^{-1}.\text{yr}^{-1}$, Table 2) is highly uncertain due to few data and the large variability
529 (Figures 4a, b). The FFNN model showed that the C_T trend in summer was faster than the trend in C_{ant} (Figure
530 4b), suggesting that natural processes would have increased C_T . This could be explained by an increase in
531 vertical mixing due to the increase in wind speed (Figure 3). On the contrary, the winter C_T trend was lower than
532 the C_{ant} trend estimated in subsurface waters (Figure 4b).

533 Over 2001-2010 the C_T trends were much faster than over the previous decade and they were the same
534 for both seasons (Figure 4b, Table 2). For this decade the summer C_T trends from the observations and the FFNN
535 model are coherent. They were also twice the C_{ant} rate in the WW, which could be explained by enhanced
536 upwelling of C_T -rich deep waters during this period after the SAM reached a high positive index (Figure 3;
537 Lenton and Matear, 2007; Le Quéré et al., 2007; Hauck et al., 2013). However, over this period we did not detect
538 any clear change at depth for ocean properties (except for C_T and C_{ant}) that would support this assumption
539 (enhanced upwelling). The rapid C_T (and fCO_2) trend for this decade is probably due to processes occurring at
540 the surface (e.g. biological activity, as discussed later) rather than changes in the water column (vertical mixing
541 or upwelling). Over the last decade C_T trends were lower than over the previous one (Figure 4b). For summer,
542 this is identified from both observations and the FFNN model. In winter the C_T trend (from FFNN) is close to
543 C_{ant} indicative of the anthropogenic CO_2 accumulation. The low C_T trend at the surface in summer, about half the
544 C_{ant} trend, is likely due to the increase of primary production after 2010 as described above (Figure 5). Thus, it
545 appears that the impact of biological activity and its variability in summer could counteract that of anthropogenic
546 CO_2 and explain the low temporal change of the carbonate system at the surface in recent years.

547
548 Given the differences of the fCO_2 and C_T trends in summer and winter (Figures 2b and 4b, Table 2) we
549 explored the temporal variations of the seasonality. For each year we estimated the differences between August
550 and January (Figure 8a). The seasonal amplitude for C_T was on average $26.1 \pm 3.4 \mu mol.kg^{-1}$ and for fCO_2 15.1
551 $\pm 5.6 \mu atm$. Some large inter-annual variations appear related to the variability of Chl-a in summer (Figure 8a).
552 Interestingly the fCO_2 seasonal amplitude reached a minimum around 2008-2010, then increased over 2010-
553 2020. This signal also appears correlated with the evolution of surface Chl-a in summer (Figure 8). This supports
554 the conclusion that low phytoplanktonic biomass between 2008 and 2010 reduced the seasonal amplitude of
555 fCO_2 .

556 The inter-annual variability of the seasonality is clearly identified when comparing C_T with C_T
557 calculated due only to C_{ant} accumulation (Figure S12). This supports the conclusion that in addition to the C_{ant}
558 accumulation, the variations of phytoplanktonic biomass imprinted inter-annual variability on C_T and fCO_2 in
559 summer. This holds for the seasonal amplitude as the results for winter follows the C_{ant} trend (Figure 4b, Figure
560 S12a). The same is true for pH for which reduced seasonal amplitude was found when the production was low
561 (not shown). However, over 36 years (1985-2020) we did not identify a long-term trend of the seasonal
562 amplitude for C_T or for fCO_2 as suggested by other studies (Landschützer et al., 2018; Rodgers et al., 2023;
563 Shadwick et al 2023). Our results highlight a variability over 5-10 years (Figure 8a) and suggest a potential
564 change in seasonality and annual CO_2 sink if primary production changes in the future (e.g. Bopp et al., 2013;
565 Leung et al., 2015; Fu et al., 2016; Kwiatkowski et al., 2020; Krumhardt et al., 2022; Seifert et al., 2023).

566

567 **3.3 Anthropogenic CO_2 drives acidification in surface waters and in the water column**

568

569 **3.3.1 Surface pH trend**

570

571 To explore the temporal change of pH in surface waters we used the fCO_2 observations and the monthly
572 results from the FFNN model. For both data-sets pH was calculated from fCO_2 and A_T reconstructed as
573 described in section 2.2.5. Figure 9a presents the time-series of pH at the surface (the same time-series for $[H^+]$

574 concentrations is shown in Figure S13). For the full period, 1985-2020, the annual pH trend derived from the
575 FFNN model is $-0.0165 \pm 0.0004 \text{ decade}^{-1}$ (Table 2) exactly the same as derived at large scale in the Southern
576 Ocean (south of 44°S) for the period 1993-2018 (Iida et al., 2021, Table 1) but when restricted to this period,
577 1993-2018, the trend from the FFNN model appears slightly faster ($-0.0182 \pm 0.0006 \text{ decade}^{-1}$). This is less than
578 the pH trend derived from pCO_2 data in the SO SubPolar Seasonally Stratified biome around $40\text{-}50^\circ\text{S}$ (SO-
579 SPSS) for 1981-2011 ($-0.020 \pm 0.002 \text{ decade}^{-1}$, Table 1, Lauvset et al., 2015) and close to the pH trend based on
580 OceanSODA-ETH reconstructed fields in the SO-SPSS for the period 1982-2021 ($-0.0189 \pm 0.0010 \text{ decade}^{-1}$, Ma
581 et al., 2023). However, as for fCO_2 and C_T , we estimated different pH trends in summer and winter, as well as
582 depending on the periods (Figure 9b, Table 2).

583 The winter pH decrease estimated over the last two decades was twice as fast as estimated during the
584 previous one, mirroring the winter fCO_2 trends (Table 2). In summer, the pH trend presents a large variability at
585 decadal scale as it was three times faster over 2001-2010 than during the previous and following decades (Figure
586 9b, Table 2). Although the trends based on the observations are less robust because the cruises were not
587 conducted each year, the reduced pH trend in summer after 2010 is confirmed from in-situ data (Figure 9b, Table
588 2).

589
590 Our results show that the pH trend varied significantly from decade to decade and that part of the
591 variations could be explained by the evolution of phytoplanktonic biomass, but overall the decrease of pH since
592 1985 was mainly driven by the accumulation of anthropogenic CO_2 . This is revealed in the Winter Water when
593 comparing pH and pre-industrial pH (Figure 10a). Here, the pre-industrial pH (pH-PI) was calculated after
594 subtracting C_{ant} values from the observed C_T concentrations for each sample in the WW layer. Interestingly the
595 pH trend in the WW of $-0.0161 \pm 0.0033 \text{ decade}^{-1}$ (here deduced from the station A_T and C_T data over 1985-
596 2021) is very close to the annual trend at the surface deduced from the FFNN model over 1985-2020 (-0.0165
597 $\pm 0.0004 \text{ decade}^{-1}$). This trend is slightly faster than the pH trends of $-0.0134 \pm 0.001 \text{ decade}^{-1}$ recently estimated
598 in subsurface waters (100-210m) of the Southern Ocean south of the PF and derived for years 1994-2017 from
599 historical data and BGC-Argo floats (Mazloff et al., 2023). For the same period, 1994-2017, at the OISO-
600 KERFIX station we estimated a pH trend in the WW of $-0.0168 \pm 0.0043 \text{ decade}^{-1}$ and of -0.0186 ± 0.0006
601 decade^{-1} in surface waters from the FFNN model.

602
603 As for other properties (A_T , O_2 , temperature, salinity and nutrients), the pre-industrial pH (pH-PI) does
604 not change over time in the WW (mean pH-PI = 8.173 ± 0.020 , $n=45$, Figure 10a). The pH-PI in the WW is in
605 the range of the pre-industrial surface pH value in the Southern Ocean (8.2 for year 1750 and 8.18 for year 1850)
606 derived from Earth system Models (Jiang et al., 2023, their Table S9). In the WW at our location the modern pH
607 (1985-2021) was on average -0.147 ± 0.021 lower than pre-industrial pH. In 1985 pH in the WW was -0.119
608 lower than pH-PI and in 2021 it was -0.184 lower than pH-PI (Figure 10a). The progressive decrease of pH was
609 clearly linked to C_{ant} concentrations in the WW layer and the pH decrease identified below that layer in the water
610 column (Figure 10b).

611 3.3.2 Temporal change in the water column

612
613

614 From 1985 to 2021, signals of decreasing pH and increasing C_T in surface waters are propagated in the
615 water column down to about 500m. As mentioned above the data in 1985 (first occupation of the station) reveal
616 significant C_{ant} levels across the water column (Figure 6b). Therefore the pH down to the bottom was already
617 lower in 1985 than at pre-industrial times (Figure 10b). However, the largest C_{ant} increases were found in the top
618 layers and changes in pH from 1985 to 2021 were small below 500m (Figure 10b, Figure S14). While
619 observations for all years fall on a common linear relationship between C_{ant} and pH_{ant} for depths greater than 500
620 m, the change in pH for a given level of C_{ant} increases with time for layers shallower than 500 m (Figure 11).

621
622 The increase in C_{ant} concentrations over time (Figure 6b) also leads to a decrease of carbonate ion
623 concentrations [CO_3^{2-}] and of Ω_{ar} and Ω_{ca} (Figure S14, S15). These decreases are well identified since the pre-
624 industrial era in the whole water column but in the last 36 years, observations do not show any appreciable
625 changes below 500m (Figure 11). The aragonite saturation horizon ($\Omega_{ar}=1$) was found around 600m in 1985 and
626 around 400m in recent years (2015-2021, Figures S14, S15). Moreover, during the period covered by
627 observations (1985-2021), we did not detect abrupt change of the aragonite saturation horizon from one year to
628 the next (nor between winter and summer, Figure S16). This contrasts with previous regional studies in the SO
629 and most notably with results from the layers close to the deep minimum of carbonate ion concentrations (Hauri
630 et al., 2015; Negrete-Garcia et al., 2019). At our station the [CO_3^{2-}] minimum lies around 500-600m (Figure S14,
631 S15) and, along with the superimposed C_{ant} accumulation, explains the upward shift of the aragonite and calcite
632 saturation horizon between the pre-industrial and modern periods (Figure S15). At pre-industrial time under-
633 saturation with regard to aragonite ($\Omega_{ar}<1$) was found at the bottom only (1600m) whereas between 1985 and
634 2021 it was found in the water column below 600 m or 400 m (Figure S15). The subsurface pre-industrial Ω_{ar}
635 value was around 1.9-2 (Figure S15) and in the range of Ω_{ar} value in the Southern Ocean at pre-industrial time
636 from ESM models (Jiang et al., 2023, their Figure 4).

637 The aragonite under-saturation already occurred in 1985 at 600-700m, a layer corresponding to the
638 [CO_3^{2-}] minimum (Figure S15) and a small increase of C_T just above this layer (via C_{ant} accumulation) would
639 rapidly shift the aragonite saturation horizon above 600m. This might have already occurred and could explain
640 that Ω_{ar} value was 1.02 at 350m in 2021 (Figure S15). These results suggest that for pelagic calcifiers living in
641 subsurface waters (150m or deeper) such as pteropods and foraminifera (e.g. Hunt et al., 2008; Meilland et al.,
642 2018) the impact of acidification might occur sooner than at the surface.

643 For the interpretation of the trend analysis based on observations, only data below 150m could be used
644 as C_{ant} was not evaluated in the surface layer. At 200m, based on A_T and C_T data, we estimated a decrease in pH
645 from 1985 to 2021 by -0.059 (Figure 10b), corresponding to an increase by +1.1 $nmol.kg^{-1}$ in $[H^+]$ (Figure S13),
646 and a decrease by -0.16 in Ω_{ar} (Figure S15). Over 36 years, this represents about 30% of the total change since
647 the pre-industrial era for pH (-0.184), $[H^+]$ (+3.5 $nmol.kg^{-1}$) and Ω_{ar} (-0.6). This is mainly linked to the C_{ant}
648 change that also represents over 36 years 30% of the total accumulation (+24.6 $\mu mol.kg^{-1}$ from 1985 to 2021 for
649 a total concentration of +71.7 $\mu mol.kg^{-1}$ at 200m in 2021, Figure 7). We conclude that the accumulation of
650 anthropogenic CO_2 drives the change of the carbonate system in subsurface waters and probably also in surface
651 waters.

652 In order to quantify the propagation of surface trends to depth, the temporal variations of carbonate
653 system properties at the surface for both summer and winter derived from the FFNN model are compared to the
654 changes observed across the water column (Figure 12). The comparison shows that the seasonal amplitude of

655 surface waters properties was of a similar magnitude to the observed changes in the mixed layer between 1985
656 and 2021. For example, the C_T and Ω_{ar} seasonal amplitude, respectively around $20 \mu\text{mol.kg}^{-1}$ and 0.2,
657 corresponds to the C_T increase and Ω_{ar} decrease from 1985 to 2021. The comparisons also highlight that in
658 summer the FFNN results were close to observations in the mixed-layer (e.g. C_T was $2120 \mu\text{mol.kg}^{-1}$ in 1985 and
659 $2140 \mu\text{mol.kg}^{-1}$ in 2021). In winter, at the surface, C_T was higher and pH, $[\text{CO}_3^{2-}]$, Ω_{ar} were lower (from the
660 FFNN model, blue line in Figure 12). The winter surface values in 1985 and 2020/2021 are in good agreement
661 with observations at depth in the winter water (150-200m). As an example, in 1985 surface C_T in winter was
662 $2145.5 \mu\text{mol.kg}^{-1}$, which corresponds to the concentration measured at 150m during summer (purple line in
663 Figure 12). In 2020, the winter C_T at the surface ($2168.3 \mu\text{mol.kg}^{-1}$) is equal to C_T concentrations observed at
664 150-180 m in January 2020 or in 2021. For Ω_{ar} , the surface value derived from the FFNN model in winter 1985
665 (1.6) was equal to the Ω_{ar} observed at 125 m in March 1985. In 2020, the surface winter estimate of Ω_{ar} (1.42)
666 was equal to Ω_{ar} observed at 100-150 m in January 2020 or 2021. The same correspondences between winter
667 surface and WW data were identified for pH and $[\text{CO}_3^{2-}]$ (Figure 12). This supports the use of winter and
668 summer surface data from the FFNN model to investigate the seasonal Ω_{ar} trends and their projection in the
669 future.

670 The surface water Ω_{ar} (Ω_{ca}) trend from the FFNN model in summer of $-0.0059.\text{yr}^{-1}$ ($-0.0094.\text{yr}^{-1}$) was
671 stronger than the winter of $-0.0050.\text{yr}^{-1}$ ($-0.0079.\text{yr}^{-1}$) and also higher than the trend derived from observations in
672 the WW ($-0.0043.\text{yr}^{-1}$ for Ω_{ar} and $-0.0069.\text{yr}^{-1}$ for Ω_{ca}). Our results indicate that the change of carbonate
673 properties in the years 1985-2021 were mainly driven by C_{ant} accumulation in surface waters and across the
674 water column. However, a potential increase in primary productivity after 2010 mitigated the effects of
675 increasing C_{ant} accumulation in response to increasing atmospheric CO_2 leading to relatively stable summer C_T
676 and $f\text{CO}_2$ and to a stronger CO_2 sink (Figure 3). Consequently, when restricted to the period 2010-2020, the
677 trend of Ω_{ar} in surface waters in summer was much smaller, $-0.024 \pm 0.027 \text{ decade}^{-1}$ than during the preceding
678 period. This was much smaller than derived from all the data over 1985-2021 ($-0.048.\text{decade}^{-1}$) or estimated
679 from reconstructed fields in the SO-SPSS over 1982-2021 ($-0.0616.\text{decade}^{-1}$, Ma et al., 2023). It underscores the
680 uncertainty in extrapolating time-series to the future depending on the selection of data and periods.

681
682

683 **3.4 Long-term change in surface water, from the sixties to the future.**

684

685 The data described above allowed evaluating the temporal variations of the properties of the carbonate
686 system and C_{ant} over 1985-2021 along with a comparison to the pre-industrial state in the water column. The
687 results over 36 years informed on the recent changes, inter-annual variations and trends, but the time-series
688 appears somehow short to extrapolate the trends over time. What was the change of the carbonate system in
689 surface waters before 1985 and what will be its future evolution ?

690

691 **3.4.1 Back to the sixties: observed trends since 1962.**

692

693 To explore the long-term change, we start by comparing our recent data with observations from the
694 LUSIAD cruise conducted in 1962-1963 (Keeling and Waterman, 1968). Some data from this cruise were
695 obtained in mid-November 1962 south of the Polar Front, in the region south-west off Kerguelen Islands.

696 Because of the seasonality, we compared the November 1962 data with our observations obtained in October-
697 November in 1995, 2011 and 2016, and with the FFNN model results for November (Figure 13). The C_T
698 concentration, pH, Ω_{ar} and Ω_{ca} for 1962 were calculated using fCO_2 data and A_T (from the A_T/S relationship Eq.
699 1) with salinity from the World Ocean Atlas (Antonov et al, 2006).

700

701 First, we note that the measured SST in November 1962 ($1.7^\circ C$) was slightly lower compared to recent
702 years (on average by about $-0.6^\circ C$), but SST as low as $1.8^\circ C$ for this season was also found in other years (e.g.
703 November 1995, 2014). The change in SST is unlikely to explain the long-term increase in fCO_2 or decrease in
704 pH since 1962 (Figure 13). In 1962, the oceanic fCO_2 was $324 \mu atm$, which is slightly higher than in the
705 atmosphere ($\Delta fCO_2 = +8 \mu atm$, a small source), whereas in November 1985-2020 the ocean was a small CO_2 sink
706 on average ($\Delta fCO_2 = -3.3 \pm 4.5 \mu atm$). The C_T concentration in 1962 ($2135 \mu mol.kg^{-1}$) was much lower than
707 observed since 1995 and the pH (8.115) was much higher than in the last three decades (Figure 13). Compared to
708 1962, pH in 2016 was -0.078 lower, i.e. representing 70% of the pH decrease of -0.11 in the global ocean since
709 the beginning of the industrial era (Jiang et al, 2019). In November 1962, surface C_T was lower by -15.1
710 $\mu mol.kg^{-1}$ compared to the data in October 1995, i.e. a trend of $+0.46 \mu mol.kg^{-1}.yr^{-1}$ over 33 years close to the
711 C_{ant} trend observed in the WW over 1985-2021 as described above ($+0.53 \pm 0.01 \mu mol.kg^{-1}.yr^{-1}$). Having the C_T
712 value in 1962, we can project the C_T in time by adding the C_{ant} concentration based on the relationship observed
713 between C_{ant} and atmospheric CO_2 (Figure 7b) assuming that the anthropogenic CO_2 uptake since the sixties is
714 representative of the C_T change (i.e. the change of C_T due to natural variability was small). This projection is
715 shown for all properties (red dashed-lines in Figure 13) and confirms that the progressive C_{ant} accumulation
716 explained most of the C_T and fCO_2 increase in surface waters since 1962. We note that the C_T derived from the
717 FFNN model suggests slightly lower C_T compared to the C_{ant} projection especially before 2006. The difference
718 of projected C_T and the FFNN model (on average $-2.2 \pm 2.7 \mu mol.kg^{-1}$) is within the uncertainty of C_T
719 calculations (error is $\pm 5 \mu mol.kg^{-1}$ when using the A_T/fCO_2 pairs) and the trend of the difference over 1985-2020
720 ($-0.15 \mu mol.kg^{-1}.yr^{-1}$) is too small to be related with confidence to changes associated with natural processes. On
721 the other hand, the oceanic fCO_2 recalculated with the projected C_{ant} trend suggested that for this season
722 (November) the ocean moved from a CO_2 source in 1962-1985 ($\Delta fCO_2 > 0$) to a sink in 1986-2021 ($\Delta fCO_2 < 0$)
723 in line with results from the FFNN model. The recalculated fCO_2 with C_{ant} (dashed red line in Figure 13) was
724 close to that observed in 1995 or from the FFNN model in 1985-2014 (mean difference over 1985-2014 is -1.2
725 $\pm 5.2 \mu atm$). After 2016, the recalculated fCO_2 suggest a stronger sink and the difference with observations in
726 2011 and 2016 or the FFNN model is slightly higher (mean difference over 2016-2020 is $-8.8 \pm 1.5 \mu atm$).
727 Although the differences are in the range of the error in fCO_2 calculation using A_T-C_T pairs ($\pm 13 \mu atm$), this
728 might indicate that after 2016 a process could contribute to increase fCO_2 faster than the effect of C_{ant} only. This
729 difference could be due to the warming that occurred after 2016 when SST was higher than $2^\circ C$ and up to $3^\circ C$ in
730 November 2017 (Figures 13 and S9). The same could be applied for pH that was slightly lower than the pH
731 recalculated from C_{ant} trend after 2015 (the mean difference between recalculated pH and FFNN-pH over 1985-
732 2020 is only 0.002 ± 0.006). Therefore, we conclude that for November the pH decrease since 1962 was mainly
733 driven by the accumulation of anthropogenic CO_2 . Aragonite and calcite saturation states also show a clear
734 decrease since 1962 (Figure 13), a diminution of 11% over 59 years for both Ω_{ar} and Ω_{ca} . Based on these results
735 over almost 60 years that confirm the conclusions from the observations in 1985-2021, we now evaluate the
736 long-term change of the carbonate system in surface waters in the future.

737

738 3.4.2 Projecting the observed trends in the future

739

740 The trends of the properties based on observations in 1962-2021 and the FFNN model in 1985-2020
741 indicate relatively linear trends linked to C_{ant} uptake albeit with some decadal variability in summer (Figure 4). A
742 simple linear extrapolation of the trends in the future suggests that aragonite under-saturation in surface waters
743 would be reached in year 2110 for the winter season and 2120 for summer (Figure S17) whereas the subsurface
744 trend suggests under-saturation in 2090. In year 2100, surface pH and $[H^+]$ would be around 7.9 and 12 nmol.kg^{-1}
745 (Figure S17). However, ESM CMIP6 models suggest that under a high emission scenario (SSP5-8.5), pH in
746 2100 in the Southern Ocean near 50°S would be around 7.65 and $[H^+]$ around 22 nmol.kg^{-1} (Jiang et al., 2023,
747 their figure 4). This shows that the simple linear extrapolation based on recent observed trends (Figure S17)
748 underestimated the future change of the carbonate system for a high emission scenario as previously shown in
749 the South-Eastern Indian Ocean based on summer trends derived from observations in 1969-2003 (Midorikawa
750 et al., 2012, their figure 4).

751 To better investigate the changes for the next decades, we assumed that the C_{ant} trend for the modern
752 period (Figure 7) that experienced a “business as usual” scenario after the sixties is representative of the future
753 changes in the surface ocean carbonate system. For this analysis, we used two emissions scenarios (Shared
754 Socioeconomic Pathways, SSP, Meinshausen et al., 2020) with atmospheric $x\text{CO}_2$ reaching 1135 ppm in 2100 (a
755 “high” emission scenario SSP5-8.5) or $x\text{CO}_2$ reaching 603 ppm in 2100 after a stabilization around 2080
756 (scenario SSP2-4.5). This enables to simulate future C_T concentrations for summer or winter (Figure 14) and to
757 calculate other carbonate properties using C_T and A_T (Figure 15, Table 3) in response to approximated future
758 changes in physical and geochemical properties excluding impacts of changes in atmospheric and oceanic
759 circulation. As the calculated properties are sensitive to A_T values, we used a fixed A_T of $2280 \text{ } \mu\text{mol.kg}^{-1}$ or
760 applied a correction based on the long-term change of sea surface salinity observed in the last 6 decades (1960-
761 2017), i.e. a freshening in the Southern Ocean of around -0.01 to $-0.02.\text{decade}^{-1}$ (Durack and Wijffels, 2010;
762 Cheng et al., 2020b). The decrease in salinity in the South Indian Ocean ($-0.02 \pm 0.01 \text{ decade}^{-1}$) was recently
763 analyzed by Akhoudas et al. (2023) who showed that in the years 1993-2021 the freshening was mainly due to
764 an increase in precipitations linked to the acceleration of the atmospheric hydrological cycle. From our data in
765 the mixed-layer over 1985-2021, we estimated a trend in salinity of $-0.021 \pm 0.004 \text{ decade}^{-1}$. For the A_T
766 sensitivity test we thus selected a salinity trend of $-0.01.\text{decade}^{-1}$ in 1962-1985 and $-0.02.\text{decade}^{-1}$ after 1985 and
767 applied these trends to simulate A_T over 1960-2100 using the $A_T/\text{Salinity}$ relationship (Equation 1). This leads to
768 a salinity of 33.650 and A_T of $2272 \text{ } \mu\text{mol.kg}^{-1}$ in the year 2100, about $8 \text{ } \mu\text{mol.kg}^{-1}$ lower than observed in 2021
769 ($2280 \text{ } \mu\text{mol.kg}^{-1}$). Compared to the C_T change from 2021 to 2100 ($+50$ and $+193 \text{ } \mu\text{mol.kg}^{-1}$ for the “low” and
770 “high” emissions scenario, Figure 14), the impact of the A_T decrease has a minor effect on the future change for
771 pH, $[\text{CO}_3^{2-}]$ and Ω (Table 3). For example, in winter for the SSP5-8.5 scenario, when the A_T decrease is taken
772 into account, pH in 2100 is 7.316 and Ω_{Ar} is 0.33 against 7.372 and 0.34 when A_T is constant (Table 3). In both
773 cases, the surface aragonite under-saturation ($\Omega_{\text{Ar}}=1$) in winter occurred in 2055, whereas in summer it is
774 identified in 2070. The effect of lower A_T in the future appeared also small compared to the seasonal differences
775 of pH and Ω in 2100.

776 As noted above, the Southern Ocean experienced a warming in recent decades (e.g. Auger et al., 2021)
777 and it is projected that warming will continue in the future (IPCC, 2022). Therefore, to test the sensitivity of

778 calculated properties to warming we applied a warming of $+0.0125^{\circ}\text{C}\cdot\text{yr}^{-1}$ in 1985-2020 and $+0.025^{\circ}\text{C}\cdot\text{yr}^{-1}$ after
779 2020 (Azarian et al, 2023). As for A_T , these results are compared for winter using constant SST (Table 3 ~~2~~). The
780 effect of the long-term warming does mainly impact the projection of $[\text{H}^+]$ and pH (Table 3).

781 These sensitivity tests for temperature and A_T showed that as for the observed period 1962-2021 (Figure
782 13), the projection in the future depends mainly on the anthropogenic CO_2 accumulation. Here, the C_T
783 concentrations were calculated using the C_{ant} versus atmospheric CO_2 relationship (Figure 7b). We thus tested
784 the results for winter based on the error associated with this relationship (Figure S18). This leads to either higher
785 or lower C_T compared to the original calculation (Figure 14). For the SSP5-8.5 scenario, the winter C_T
786 concentrations in 2100 range between 2328 and 2378 $\mu\text{mol}\cdot\text{kg}^{-1}$, higher than simulated in the ESM CMIP6
787 models around 50°S (2300 $\mu\text{mol}\cdot\text{kg}^{-1}$, Jiang et al., 2023). As in the ESM models, the projected C_T concentration
788 in 2100 at our location for the SSP2-4.5 scenario is much lower 2217 $\mu\text{mol}\cdot\text{kg}^{-1}$ (Figure 14). The future change
789 of the carbonate system is not significantly different using low or high C_{ant} accumulation (Figure S18) but this
790 test gives a range of years to reach aragonite and calcite under-saturation. In winter (SSP5-8.5 scenario),
791 aragonite (calcite) would reach under-saturation between year 2050 and 2060 (between year 2070 and 2080).
792 Note that for summer we derived under-saturation for Ω_{Ar} in year 2065 and for Ω_{Ca} in year 2085. For the SSP2-
793 4.5 scenario, where C_T is 143 $\mu\text{mol}\cdot\text{kg}^{-1}$ lower in 2100 compared to SSP5-8.5, aragonite under-saturation would
794 not be reached before 2070 (Figure 15).

795

796 **4 Summary and concluding remarks**

797

798 The times-series of high quality observations collected between 1985 and 2021 and the results from the
799 FFNN model at one location, south of the Polar Front in the Southern Indian Ocean (50°S - 68°E) presented in
800 this analysis offered new results on the inter-annual variability, decadal to long-term trends of the carbonate
801 system in surface waters, air-sea CO_2 fluxes and associated drivers. The evaluation of anthropogenic CO_2
802 concentrations in the water column indicated that the trends of the carbonate species are mainly driven by the
803 anthropogenic CO_2 uptake leading to a progressive acidification in surface waters and at depth.

804 In 1985, the C_{ant} concentrations were approaching 50 $\mu\text{mol}\cdot\text{kg}^{-1}$ at 200 m and C_{ant} was detected in the
805 water column down to the bottom (1600m). This explains why aragonite under-saturation was observed at 600-
806 700m in 1985, where $[\text{CO}_3^{2-}]$ concentration was at its minimum, whereas for the pre-industrial era the whole
807 water column was super-saturated (this study Figure S15; Lauvset et al., 2020, their Figure S15). 36 years later,
808 because of the anthropogenic CO_2 accumulation, we observed an upward migration of the aragonite saturation
809 horizon that was found around 400 m in 2021 (a shoaling rate of around $-6\text{ m}\cdot\text{yr}^{-1}$).

810 At subsurface, in the Winter Water layer, the C_{ant} trend is estimated at $+0.53 \pm 0.01\ \mu\text{mol}\cdot\text{kg}^{-1}\cdot\text{yr}^{-1}$ over
811 1985-2021 with a detectable increase of the trend in recent years. The C_{ant} concentrations in the ocean are closely
812 related to the atmospheric CO_2 concentrations and the slope we observed south of the PF in the Indian sector of
813 $+0.263 \pm 0.042\ \mu\text{mol}\cdot\text{kg}^{-1}\cdot\mu\text{atm}^{-1}$ is close to that observed in the AAIW in the South Atlantic (Fontela et al.,
814 2021). This suggests that local observations in the South Indian POOZ captured the link between C_{ant} and
815 atmospheric CO_2 at larger scale.

816 In surface waters, over 1991-2020 the oceanic $f\text{CO}_2$ increased at a rate close or slightly lower than in
817 the atmosphere (Figure 2b) and the C_T trend followed the C_{ant} accumulation (Figure 4b, S12a). However in the
818 last decade both observations and the FFNN model showed low $f\text{CO}_2$ trends in summer (less than $1\ \mu\text{atm}\cdot\text{yr}^{-1}$).

819 The change in summer trend appears related to primary production as revealed by a decrease of Chl-a in 1998-
820 2010 followed by an increase after 2010. Biological activity counteracts the C_T increase due to C_{ant} , resulting in
821 rather stable C_T and fCO_2 in summer during the last decade. As a result, the region moved from an annual source
822 of $+0.8 \text{ molC.m}^{-2}.\text{yr}^{-1}$ in 1985 to a sink of $-0.5 \text{ molC.m}^{-2}.\text{yr}^{-1}$ in 2020. Adding historical data from November
823 1962 that indicate an annual source of $2.2 \text{ molC.m}^{-2}.\text{yr}^{-1}$, and extrapolating to the entire South Indian POOZ (50-
824 $58^\circ\text{S}/20\text{-}120^\circ\text{E}$, 6.5 Mkm^2), suggest that this region changed from a CO_2 source of 0.17 PgC.yr^{-1} in 1962,
825 reduced to 0.06 PgC.yr^{-1} in 1985 and a CO_2 sink of $-0.04 \text{ PgC.yr}^{-1}$ in 2020. This can be compared with
826 reconstructed fluxes from a data-based model that produced a CO_2 source around 0.10 PgC.yr^{-1} in 1960-1990
827 and a sink around $-0.05 \text{ PgC.yr}^{-1}$ in 2020 in the south Indian sector (Rödenbeck et al., 2022, their Figure 6).
828 Based on the FFNN reconstructions, the increase of the ocean CO_2 sink was particularly pronounced after 2011
829 (Figure 3) when phytoplankton biomass was increasing in this HNLC region and occurred when the SAM index
830 was in a positive state. Although observations in the water column do not suggest enhanced upwelling, we
831 cannot eliminate the possibility that the SAM influenced changes in primary production.

832 For October/November, the estimated increase in C_T concentration in surface waters over 54 years ($+21$
833 $\mu\text{mol.kg}^{-1}$) was almost equal to the increase of C_{ant} ($+22.3 \mu\text{mol.kg}^{-1}$). As a result, surface ocean pH dropped
834 from 8.11 in 1962 to 8.044 in 2020. Over a multi-decadal time scale (30 years or more), acidification in the
835 South Indian POOZ was mainly controlled by the uptake of anthropogenic CO_2 . However, our data also indicate
836 a modulation of the summer pH trend by natural processes. After 2010, a very small pH trend was estimated in
837 summer ($-0.0098.\text{decade}^{-1} \pm 0.0042$) when the region experienced an increase in primary productivity. On the
838 opposite, in winter, the pH trends continuously increased with time. At the subsurface (Winter Water layer), the
839 trend of pH based on A_T and C_T data over 1985-2021 ($-0.0161 \pm 0.0033.\text{decade}^{-1}$) is also almost equal to the
840 annual surface trend from the FFNN model. A simple extrapolation of the trends in the WW indicated that
841 under-saturation ($\Omega < 1$) would be reached at year 2090 for aragonite and year 2180 for calcite. However, as
842 atmospheric CO_2 is expected to increase and ocean C_T will increase in the future, pH and Ω will decrease at a
843 faster rate than observed in the last decades. A projection of future C_T concentrations based on two emission
844 scenarios, excluding changes in ocean circulation, indicated that the winter surface pH in 2100 would decrease to
845 7.32 for a high emission scenario (SSP5-8.5) or to 7.782 for a low emission scenario (SSP2-4.5). This is up to -
846 0.86 lower than pre-industrial pH and -0.71 lower than pH observed in 2020. For the winter season the aragonite
847 under-saturation in surface would be reached around 2050 for a high emissions scenario and 2070 for a low
848 emission scenario.

849 The time-series presented here for the Southern Ocean, along with other historical time-series of A_T and
850 C_T in the water-column (BATS, HOT, ESTOC, KNOT, Iceland or Irminger seas; Bates et al., 2014; Lange et al.,
851 2023) or the recent BGC-Argo floats in the Southern Ocean (Mazloff et al., 2023) offer useful data for the
852 evaluation of biogeochemical and Earth system models, especially for the physical and biological drivers of the
853 carbonate system not well represented in current models at seasonal to decadal scales in the Southern Ocean (e.g.
854 Hauck et al., 2023a; Rodgers et al., 2023; Joos et al., 2023). Observing the decadal changes of the carbonate
855 system in the water column is also an important step to extend the evaluation of biogeochemical and ESM
856 models below the surface (Jiang et al., 2023). It is important to maintain such time-series for monitoring the
857 future evolution of the ocean CO_2 sink, of the acidification and its impact on phytoplankton species and higher
858 trophic levels. This is especially the case in Marine Protected Area such as the French Sub-Antarctic islands
859 including the Kerguelen Archipelago which was listed as a UNESCO World Heritage site in 2019.

860
861
862
863
864
865
866
867
868
869
870
871
872
873
874
875
876
877
878
879
880
881
882
883
884
885
886
887
888
889
890
891
892
893
894
895
896
897
898
899
900
901
902

Data availability:

Data used in this study are available in SOCAT (www.socat.info) for fCO₂ surface data, in GLODAP (www.glodap.info) for water-column data and at NCEI/OCADS (www.ncei.noaa.gov/access/ocean-carbon-data-system/oceans/VOS_Program/OISO.html). The CMEMS-LSCE-FFNN model data are available at E.U. Copernicus Marine Service Information (<https://resources.marine.copernicus.eu/products>).

Authors contributions:

CLM and NM are co-I of the ongoing OISO project. CLM, NM, CL and CR participated to OISO cruises. Underway fCO₂ was measured by CLM, NM, CL, and qualified by CLM and NM. Nutrients data were measured and qualified by CLM and CL. Chl-a data were measured and qualified by CR. Water column data were qualified by CLM, NM, CL, CR and GR. MG, FC and TTTC developed the CMEMS-LSCE-FFNN model and provided the model results. NM started the analysis, wrote the draft of the manuscript and prepared the figures. All authors contributed to revising the draft manuscript.

Competing interest: The authors declare that they have no conflict of interest.

Acknowledgments: The OISO program was supported by the French institutes INSU (Institut National des Sciences de l'Univers) and IPEV (Institut Polaire Paul-Emile Victor), OSU Ecce-Terra (at Sorbonne Université), the French programs SOERE/Great-Gases and ICOS-France. We thank the French Oceanographic Fleet for financial and logistic support for the OISO program (<https://campagnes.flotteoceanographique.fr/series/228/>). We thank the captains and crew of *R.R.V. Marion Dufresne* and the staff at IFREMER, GENAVIR and IPEV. We also thank Jonathan Fin and Claude Mignon for their help during the OISO cruises. The development of the neural network model benefited from funding by the French INSU-GMMC project "PPR-Green-Grog (grant no 5-DS-PPR-GGREOG), the EU H2020 project AtlantOS (grant no 633211), as well as through the Copernicus Marine Environment Monitoring Service (project 83-CMEMS-TAC-MOB). We thank all colleagues that contributed to the quality control of ocean data made available through CARINA and GLODAP (www.glodap.info). The Surface Ocean CO₂ Atlas (SOCAT, www.socat.info) is an international effort, endorsed by the International Ocean Carbon Coordination Project (IOCCP), the Surface Ocean Lower Atmosphere Study (SOLAS) and the Integrated Marine Biogeochemistry and Ecosystem Research program (IMBER), to deliver a uniformly quality-controlled surface ocean CO₂ database. We thank the associate editor, Ismael Hernández-Carrasco, and two anonymous reviewers for their detailed comments and supportive reviews.

References

Akhoudas, C. H., Sallée, J.-B., Reverdin, G., Haumann, F. A., Pauthenet, E., Chapman, C. C., Margirier, F., Lo Monaco, C., Metzl, N., Meilland, J., and Stranne, C.: Isotopic evidence for an intensified hydrological cycle in the Indian sector of the Southern Ocean. *Nat Commun* 14, 2763. <https://doi.org/10.1038/s41467-023-38425-5>, 2023

Aminot, A., and Kérouel, R.: *Hydrologie des écosystèmes marins: paramètres et analyses*. Ed. Ifremer, 336 p., 2004

903 Antonov, J. I., Locarnini, R. A., Boyer, T. P., Mishonov, A. V., and Garcia, H. E.: World Ocean Atlas 2005, in:
904 Volume 2: Salinity, edited by: Levitus, S., NOAA Atlas NESDIS 62, US Government Printing Office,
905 Washington, DC, 182 pp., <https://repository.library.noaa.gov/view/noaa/1127>, 2006.
906

907 Arrigo, K. R., van Dijken, G. L., and Bushinsky, S.: Primary production in the Southern Ocean, 1997–2006, *J.*
908 *Geophys. Res.-Oceans*, 113, C08004, doi:doi:10.1029/2007jc004551, 2008.
909

910 Auger, M., Morrow, R., Kestenare, E., Sallée, J.-B., and Cowley, R.: Southern Ocean in-situ temperature trends
911 over 25 years emerge from interannual variability, *Nat. Commun.*, 12, 514,
912 <https://doi.org/10.1038/s41467-020-20781-1>, 2021
913

914 Azarian, C., Bopp, L., Pietri, A., Sallée, J.-B., and d'Ovidio, F.: Current and projected patterns of warming and
915 marine heatwaves in the Southern Indian Ocean, *Progress in Oceanography*,
916 doi:<https://doi.org/10.1016/j.pocean.2023.103036>, 2023
917

918 Bakker, D. C. E., Pfeil, B., Landa, C. S., Metzl, N., O'Brien, K. M., Olsen, A., Smith, K., Cosca, C., Harasawa,
919 S., Jones, S. D., Nakaoka, S.-I., Nojiri, Y., Schuster, U., Steinhoff, T., Sweeney, C., Takahashi, T., Tilbrook, B.,
920 Wada, C., Wanninkhof, R., Alin, S. R., Balestrini, C. F., Barbero, L., Bates, N. R., Bianchi, A. A., Bonou, F.,
921 Boutin, J., Bozec, Y., Burger, E. F., Cai, W.-J., Castle, R. D., Chen, L., Chierici, M., Currie, K., Evans, W.,
922 Featherstone, C., Feely, R. A., Fransson, A., Goyet, C., Greenwood, N., Gregor, L., Hankin, S., Hardman-
923 Mountford, N. J., Harlay, J., Hauck, J., Hoppema, M., Humphreys, M. P., Hunt, C. W., Huss, B., Ibáñez, J. S.
924 P., Johannessen, T., Keeling, R., Kitidis, V., Körtzinger, A., Kozyr, A., Krasakopoulou, E., Kuwata, A.,
925 Landschützer, P., Lauvset, S. K., Lefèvre, N., Lo Monaco, C., Manke, A., Mathis, J. T., Merlivat, L., Millero, F.
926 J., Monteiro, P. M. S., Munro, D. R., Murata, A., Newberger, T., Omar, A. M., Ono, T., Paterson, K., Pearce, D.,
927 Pierrot, D., Robbins, L. L., Saito, S., Salisbury, J., Schlitzer, R., Schneider, B., Schweitzer, R., Sieger, R.,
928 Skjelvan, I., Sullivan, K. F., Sutherland, S. C., Sutton, A. J., Tadokoro, K., Telszewski, M., Tuma, M., Van
929 Heuven, S. M. A. C., Vandemark, D., Ward, B., Watson, A. J., and Xu, S. : A multi-decade record of high-
930 quality fCO₂ data in version 3 of the Surface Ocean CO₂ Atlas (SOCAT), *Earth Syst. Sci. Data*, 8, 383-413,
931 doi:10.5194/essd-8-383-2016, 2016.
932

933 Bakker, D. C. E. et al: Surface Ocean CO₂ Atlas Database Version 2022 (SOCATv2022) (NCEI Accession
934 0253659). NOAA National Centers for Environmental Information. Dataset. <https://doi.org/10.25921/1h9f-nb73>.
935 Last Accessed [21 June 2022], 2022
936

937 Balch, W.M., Bates, N.R., Lam, P.J., Twining, B.S., Rosengard, S. Z., Bowler, B.C., Drapeau, D.T., Garley, R.,
938 Lubelczyk, L.C., Mitchell, C., and Rauschenberg, S.: Factors regulating the Great Calcite Belt in the Southern
939 Ocean and its biogeochemical significance. *Global Biogeochem. Cycles*, 30, doi: 10.1002/2016GB005414, 2016
940

941 Basterretxea, G., Font-Muñoz, J. S., Hernández-Carrasco, I., and Sañudo-Wilhelmy, S. A.: Global variability of
942 high-nutrient low-chlorophyll regions using neural networks and wavelet coherence analysis, *Ocean Sci.*, 19,
943 973–990, <https://doi.org/10.5194/os-19-973-2023>, 2023.
944

945 Bates, N., Astor, Y., Church, M., Currie, K., Dore, J., González-Dávila, M., Lorenzoni, L., Muller-Karger, F.,
946 Olafsson, J., and Santa-Casiano, M.: A Time-Series View of Changing Ocean Chemistry Due to Ocean Uptake
947 of Anthropogenic CO₂ and Ocean Acidification, *Oceanography*, 27, 126–141,
948 <https://doi.org/10.5670/oceanog.2014.16>, 2014.
949

950 Beaufort, L., Probert, I., de Garidel-Thoron, T., Bendif, E.M., Ruiz-Pino, D., Metzl, N., Goyet, C., Buchet, N.,
951 Coupel, P., Grelaud, M., Rost, B., Rickaby, R.E.M., and de Vargas C.: Sensitivity of coccolithophores to
952 carbonate chemistry and ocean acidification. *Nature*, doi:10.1038/nature10295. 2011
953

954 Bennington, V., Gloege, L., and McKinley, G. A.: Variability in the global ocean carbon sink from 1959 to 2020
955 by correcting models with observations. *Geophysical Research Letters*, 49, e2022GL098632.
956 <https://doi.org/10.1029/2022GL098632>, 2022
957

958 Benoiston, A.-S., Ibarbalz, F. M., Bittner, L., Guidi, L., Jahn, O., Dutkiewicz, S., and Bowler, C.: The evolution
959 of diatoms and their biogeochemical functions. *Phil. Trans. R. Soc. B* 372: 20160397.
960 <http://dx.doi.org/10.1098/rstb.2016.0397>, 2017
961

962 Bopp, L., Resplandy, L., Orr, J. C., Doney, S. C., Dunne, J. P., Gehlen, M., Halloran, P., Heinze, C., Ilyina, T.,
963 S  f  rian, R., Tjiputra, J., and Vichi, M.: Multiple stressors of ocean ecosystems in the 21st century: projections
964 with CMIP5 models, *Biogeosciences*, 10, 6225–6245, <https://doi.org/10.5194/bg-10-6225-2013>, 2013.
965

966 Brady, R. X., Maltrud, M. E., Wolfram, P. J., Drake, H. F., and Lovenduski, N. S.: The influence of ocean
967 topography on the upwelling of carbon in the Southern Ocean. *Geophysical Research Letters*, 48,
968 e2021GL095088. <https://doi.org/10.1029/2021GL095088>, 2021
969

970 Brandon, M., Goyet, C., Touratier, F., Lef  vre, N., Kestenare, E., and Morrow, R.: Spatial and temporal
971 variability of the physical, carbonate and CO₂ properties in the Southern Ocean surface waters during austral
972 summer (2005-2019), *Deep-Sea Research Part I*, <https://doi.org/10.1016/j.dsr.2022.103836>, 2022
973

974 Burger, F. A., John, J. G., and Fr  licher, T. L.: Increase in ocean acidity variability and extremes under
975 increasing atmospheric CO₂, *Biogeosciences*, 17, 4633–4662, <https://doi.org/10.5194/bg-17-4633-2020>, 2020
976

977 Bushinsky, S. M., Landsch  tzer, P., R  denbeck, C., Gray, A. R., Baker, D., Mazloff, M. R., Resplandy, L.,
978 Johnson, K. S., and Sarmiento, J. L.: Reassessing Southern Ocean air-sea CO₂ flux estimates with the addition of
979 biogeochemical float observations. *Global Biogeochemical Cycles*, 33. doi: 10.1029/2019GB006176, 2019
980

981 Caldeira, K., and Wickett, M.: Anthropogenic carbon and ocean pH. *Nature*, 425, 365. doi: 10.1038/425365a,
982 2003
983

984 Canadell, J. G., Monteiro, P. M. S., Costa, M. H., Cotrim da Cunha, L., Cox, P. M., Eliseev, A. V., Henson, S.,
985 Ishii, M., Jaccard, S., Koven, C., Lohila, A., Patra, P. K., Piao, S., Rogelj, J., Syampungani, S., Zaehle, S., and
986 Zickfeld, K.: Global Carbon and other Biogeochemical Cycles and Feedbacks, in: *Climate Change 2021: The*
987 *Physical Science Basis. Contribution of Working Group I to the Sixth Assessment Report of the*
988 *Intergovernmental Panel on Climate Change*, edited by: Masson-Delmotte, V., Zhai, P., Pirani, A., Connors, S.
989 L., P  an, C., Berger, S., Caud, N., Chen, Y., Goldfarb, L., Gomis, M. I., Huang, M., Leitzell, K., Lonnoy, E.,
990 Matthews, J. B. R., Maycock, T. K., Waterfield, T., Yelek  i, O., Yu, R., and Zhou, B., Cambridge University
991 Press, Cambridge, United Kingdom and New York, NY, USA, 673–816, doi:10.1017/9781009157896, 2021
992

993 Carpenter, J. H.: The Accuracy of the Winkler Method for Dissolved Oxygen Analysis, *Limnol. Oceanogr.*, 10,
994 135–140, <https://doi.org/10.4319/lo.1965.10.1.0135>, 1965.
995

996 Carter, B. R., Williams, N. L., Gray, A. R., and Feely, R. A.: Locally interpolated alkalinity regression for global
997 alkalinity estimation. *Limnol. Oceanogr.: Methods* 14: 268–277. doi:10.1002/lom3.10087, 2016
998

999 Carter, B. R., Feely, R. A., Williams, N. L., Dickson, A. G., Fong, M. B., and Takeshita, Y.: Updated methods
1000 for global locally interpolated estimation of alkalinity, pH, and nitrate. *Limnology and Oceanography: Methods*,
1001 16: 119-131. doi: 10.1002/lom3.10232, 2018
1002

1003 Carter, B. R., Feely, R. A., Wanninkhof, R., Kouketsu, S., Sonnerup, R. E., Pardo, P. C., et al: Pacific
1004 anthropogenic carbon between 1991 and 2017. *Global Biogeochemical Cycles*, 33, 597–617.
1005 <https://doi.org/10.1029/2018GB006154>, 2019
1006

1007 Chapman, C., Mcc Hogg, A., Kiss, A., and Rintoul, S.: The dynamics of Southern Ocean storm tracks. *Journal of*
1008 *Physical Oceanography*, 45 (3), pp.884 - 903. 10.1175/JPO-D-14-0075.1, 2015

1009

1010 Chau, T. T. T., Gehlen, M., and Chevallier, F.: A seamless ensemble-based reconstruction of surface ocean $p\text{CO}_2$
1011 and air-sea CO_2 fluxes over the global coastal and open oceans, *Biogeosciences*, 19, 1087–1109,
1012 <https://doi.org/10.5194/bg-19-1087-2022>, 2022.

1013

1014 Chen, H., Haumann, F. A., Talley, L. D., Johnson, K. S., and Sarmiento, J. L.: The deep ocean's carbon exhaust.
1015 *Global Biogeochemical Cycles*. doi: <https://doi.org/10.1002/essoar.10507757.1>, 2022

1016

1017 Cheng, L. J., Abraham, J., Zhu, J., Trenberth, K. E., Fasullo, J., Boyer, T., Locarnini, R., Zhang, B., Yu, F. J.,
1018 Wan, L. Y., Chen, X. R., Song, X. Z., Liu, Y. L., and Mann, M. E.: Record-setting ocean warmth continued in
1019 2019, *Adv. Atmos. Sci*, 37, 137-142. <https://doi.org/10.1007/s00376-020-9283-7>, 2020a

1020

1021 Cheng L., K. E. Trenberth, N. Gruber, J. P. Abraham, J. Fasullo, G. Li, M. E. Mann, X. Zhao, Jiang Zhu:
1022 Improved estimates of changes in upper ocean salinity and the hydrological cycle. *Journal of Climate*. doi:
1023 <https://doi.org/10.1175/JCLI-D-20-0366.1>, 2020b

1024

1025 Copin-Montégut, C.: A new formula for the effect of temperature on the partial pressure of CO_2 in seawater.
1026 *Marine Chemistry*, 25, 29-37. [https://doi.org/10.1016/0304-4203\(88\)90012-6](https://doi.org/10.1016/0304-4203(88)90012-6), 1988.

1027

1028 Copin-Montégut, C.: A new formula for the effect of temperature on the partial pressure of CO_2 in seawater.
1029 Corrigendum. *Marine Chemistry*, 27, 143-144. [https://doi.org/10.1016/0304-4203\(89\)90034-0](https://doi.org/10.1016/0304-4203(89)90034-0), 1989.

1030

1031 Coverly, S. C., Aminot, A., and R. K erouel: Nutrients in Seawater Using Segmented Flow Analysis, In: Practical
1032 Guidelines for the Analysis of Seawater, Edited by: Oliver Wurl, CRC Press,
1033 <https://doi.org/10.1201/9781420073072>, 2009

1034

1035 Daniault, N., and M enard, Y.: Eddy kinetic energy distribution in the Southern Ocean from altimetry and FGGE
1036 drifting buoys, *J. Geophys. Res.*, 90 (C6), 11877–11889, doi:10.1029/JC090iC06p11877, 1985

1037

1038 Demuynck, P., Tyrrell, T., Naveira Garabato, A., Moore, M. C., and Martin, A. P.: Spatial variations in silicate-
1039 to-nitrate ratios in Southern Ocean surface waters are controlled in the short term by physics rather than biology,
1040 *Biogeosciences*, 17, 2289–2314, <https://doi.org/10.5194/bg-17-2289-2020>, 2020.

1041

1042 DeVries, T., Yamamoto, K., Wanninkhof, R., Gruber, N., Hauck, J., M uller, J. D., et al.: Magnitude, trends, and
1043 variability of the global ocean carbon sink from 1985-2018. *Global Biogeochemical Cycles*, 37,
1044 e2023GB007780, doi:10.1029/2023GB007780, 2023.

1045

1046 Dickson, A. G.: Standard potential of the reaction: $\text{AgCl}(s) + \frac{1}{2}\text{H}_2(g) = \text{Ag}(s) + \text{HCl}(aq)$, and the standard
1047 acidity constant of the ion HSO_4^- in synthetic sea water from 273.15 to 318.15 K. *J. Chem. Thermodyn.* **22**:
1048 113–127. doi:10.1016/0021-9614(90)90074-Z, 1990

1049

1050 Dickson, A. G., Sabine, C. L. and Christian, J. R. (Eds.): Guide to Best Practices for Ocean CO_2 Measurements.
1051 *PICES Special Publication 3*, 191 pp., [https://www.ncei.noaa.gov/access/ocean-carbon-acidification-data-](https://www.ncei.noaa.gov/access/ocean-carbon-acidification-data-system/oceans/Handbook_2007.html)
1052 [system/oceans/Handbook_2007.html](https://www.ncei.noaa.gov/access/ocean-carbon-acidification-data-system/oceans/Handbook_2007.html), 2007

1053

1054 Dlugokencky, E. and Tans, P.: Trends in atmospheric carbon dioxide, National Oceanic & Atmospheric
1055 Administration, Earth System Research Laboratory (NOAA/ESRL), available at: [http://](http://www.esrl.noaa.gov/gmd/ccgg/trends/global.html)
1056 www.esrl.noaa.gov/gmd/ccgg/trends/global.html, (last access: 8 January 2022), 2022

1057

1058 Doney, S. C., Fabry, V. J., Feely, R. A., and Kleypas, J. A.: Ocean Acidification: The Other CO_2 Problem,
1059 *Annu. Rev. Mar. Sci.*, 1, 169–192, <https://doi.org/10.1146/annurev.marine.010908.163834>, 2009.

1060

1061 Doney, S. C., Ruckelshaus, M., Duffy, J. E., Barry, J. P., Chan, F., English, C. A., Galindo, H. M., Grebmeier, J.
1062 M., Hollowed, A. B., Knowlton, N., Polovina, J., Rabalais, N. N., Sydeman, W. J., and Talley, L. D.: Climate
1063 change impacts on marine ecosystems, *Annu. Rev. Mar. Sci.*, 4, 11–37. 10.1146/annurev-marine-041911-
1064 111611, 2012.

1065

1066 Dove, L. A., Balwada D., Thompson, A. F., and Gray, A. R.: Enhanced ventilation in energetic regions of the
1067 Antarctic Circumpolar Current. *Geophys. Res. Lett.* 49(13):e2021GL097574,
1068 <https://doi.org/10.1029/2021GL097574>. 2022.

1069

1070 Duncan, R.J., Nielsen, D.A., Sheehan, C.E., Deppeler, S., Hancock, A.M., Schulz, K.G., Davidson, A.T. and
1071 Petrou, K.: Ocean acidification alters the nutritional value of Antarctic diatoms. *New Phytol*, 233: 1813-1827.
1072 <https://doi-org.insu.bib.cnrs.fr/10.1111/nph.17868>, 2022

1073

1074 Durack, P. J. and Wijffels, S. E.: Fifty-year trends in global ocean salinities and their relationship to broad-scale
1075 warming. *J. Climate*, 23, 4342–4362, <https://doi.org/10.1175/2010JCLI3377.1>, 2010

1076

1077 Fabry, V. J., Seibel, B. A., Feely, R. A., and Orr, J. C.: Impacts of ocean acidification on marine fauna and
1078 ecosystem processes. – *ICES Journal of Marine Science*, 65: 414–432, doi: 10.1093/icesjms/fsn048, 2008

1079

1080 Fassbender, A. J., Schlunegger, S., Rodgers, K. B., and Dunne, J. P.: Quantifying the role of seasonality in the
1081 marine carbon cycle feedback: An ESM2M case study. *Global Biogeochemical Cycles*, 36, e2021GB007018.
1082 doi:10.1029/2021GB007018, 2022

1083

1084 Fay, A. R., Munro, D. R., McKinley, G. A., Pierrot, D., Sutherland, S. C., Sweeney, C., and Wanninkhof, R.:
1085 Updated climatological mean delta fCO₂ and net sea–air CO₂ flux over the global open ocean regions, *Earth*
1086 *Syst. Sci. Data Discuss.* [preprint], <https://doi.org/10.5194/essd-2023-429>, in review, 2023, accepted in press.

1087

1088 Fox-Kemper, B., Hewitt, H. T. , Xiao, C., Adalgeirsdottir, G., Drijfhout, S. S., Edwards, T. L., Golledge, N. R.,
1089 Hemer, M., Kopp, R. E., Krinner, G., Mix, A., Notz, D., Nowicki, S., Nurhati, I. S., Ruiz, L., Sallée, J.-B.,
1090 Slangen, A. B. A., and Yu, Y.: *Climate Change 2021: The Physical Science Basis. Contribution of Working*
1091 *Group I to the Sixth Assessment Report of the Intergovernmental Panel on Climate Change*, chapter Ocean,
1092 Cryosphere and Sea Level Change, pages 1211-1362. Cambridge University Press, United Kingdom and New
1093 York, NY, USA, August 2021. doi:10.1017/9781009157896.

1094

1095 Fontela, M., Vélo, A., Gilcoto, M., and Pérez, F.: Anthropogenic CO₂ and Ocean Acidification in Argentine
1096 Basin Water Masses over Almost Five Decades of Observations. *Science of The Total Environment*, 779.
1097 <https://doi.org/10.1016/j.scitotenv.2021.146570>, 2021

1098

1099 Franco, A. C., Ianson, D., Ross, T., Hamme, R. C., Monahan, A. H., Christian, J. R., et al.: Anthropogenic and
1100 climatic contributions to observed carbon system trends in the northeast Pacific. *Global Biogeochemical Cycles*,
1101 35, e2020GB006829. Doi: 10.1029/2020GB006829, 2021

1102

1103 Friedlingstein, P., O'Sullivan, M., Jones, M. W., Andrew, R. M., Gregor, L., Hauck, J., Le Quéré, C., Luijkx, I.
1104 T., Olsen, A., Peters, G. P., Peters, W., Pongratz, J., Schwingshackl, C., Sitch, S., Canadell, J. G., Ciais, P.,
1105 Jackson, R. B., Alin, S. R., Alkama, R., Arneeth, A., Arora, V. K., Bates, N. R., Becker, M., Bellouin, N., Bittig,
1106 H. C., Bopp, L., Chevallier, F., Chini, L. P., Cronin, M., Evans, W., Falk, S., Feely, R. A., Gasser, T., Gehlen,
1107 M., Gkritzalis, T., Gloege, L., Grassi, G., Gruber, N., Gürses, Ö., Harris, I., Hefner, M., Houghton, R. A., Hurtt,
1108 G. C., Iida, Y., Ilyina, T., Jain, A. K., Jersild, A., Kadono, K., Kato, E., Kennedy, D., Klein Goldewijk, K.,
1109 Knauer, J., Korsbakken, J. I., Landschützer, P., Lefèvre, N., Lindsay, K., Liu, J., Liu, Z., Marland, G., Mayot, N.,
1110 McGrath, M. J., Metzl, N., Monacchi, N. M., Munro, D. R., Nakaoka, S.-I., Niwa, Y., O'Brien, K., Ono, T.,
1111 Palmer, P. I., Pan, N., Pierrot, D., Pockock, K., Poulter, B., Resplandy, L., Robertson, E., Rödenbeck, C.,
1112 Rodriguez, C., Rosan, T. M., Schwinger, J., Séférian, R., Shutler, J. D., Skjelvan, I., Steinhoff, T., Sun, Q.,

1113 Sutton, A. J., Sweeney, C., Takao, S., Tanhua, T., Tans, P. P., Tian, X., Tian, H., Tilbrook, B., Tsujino, H.,
1114 Tubiello, F., van der Werf, G. R., Walker, A. P., Wanninkhof, R., Whitehead, C., Willstrand Wranne, A.,
1115 Wright, R., Yuan, W., Yue, C., Yue, X., Zaehle, S., Zeng, J., and Zheng, B.: Global Carbon Budget 2022, *Earth*
1116 *Syst. Sci. Data*, 14, 4811–4900, <https://doi.org/10.5194/essd-14-4811-2022>, 2022.

1117

1118 Friedlingstein, P., O'Sullivan, M., Jones, M. W., Andrew, R. M., Bakker, D. C. E., Hauck, J., Landschützer, P.,
1119 Le Quéré, C., Luijkx, I. T., Peters, G. P., Peters, W., Pongratz, J., Schwingshackl, C., Sitch, S., Canadell, J. G.,
1120 Ciais, P., Jackson, R. B., Alin, S. R., Anthoni, P., Barbero, L., Bates, N. R., Becker, M., Bellouin, N., Decharme,
1121 B., Bopp, L., Brasika, I. B. M., Cadule, P., Chamberlain, M. A., Chandra, N., Chau, T.-T.-T., Chevallier, F.,
1122 Chini, L. P., Cronin, M., Dou, X., Enyo, K., Evans, W., Falk, S., Feely, R. A., Feng, L., Ford, D. J., Gasser, T.,
1123 Ghattas, J., Gkritzalis, T., Grassi, G., Gregor, L., Gruber, N., Gürses, Ö., Harris, I., Hefner, M., Heinke, J.,
1124 Houghton, R. A., Hurtt, G. C., Iida, Y., Ilyina, T., Jacobson, A. R., Jain, A., Jarníková, T., Jersild, A., Jiang, F.,
1125 Jin, Z., Joos, F., Kato, E., Keeling, R. F., Kennedy, D., Klein Goldewijk, K., Knauer, J., Korsbakken, J. I.,
1126 Körtzinger, A., Lan, X., Lefèvre, N., Li, H., Liu, J., Liu, Z., Ma, L., Marland, G., Mayot, N., McGuire, P. C.,
1127 McKinley, G. A., Meyer, G., Morgan, E. J., Munro, D. R., Nakaoka, S.-I., Niwa, Y., O'Brien, K. M., Olsen, A.,
1128 Omar, A. M., Ono, T., Paulsen, M., Pierrot, D., Pocock, K., Poulter, B., Powis, C. M., Rehder, G., Resplandy, L.,
1129 Robertson, E., Rödenbeck, C., Rosan, T. M., Schwinger, J., Séférian, R., Smallman, T. L., Smith, S. M.,
1130 Sospedra-Alfonso, R., Sun, Q., Sutton, A. J., Sweeney, C., Takao, S., Tans, P. P., Tian, H., Tilbrook, B., Tsujino,
1131 H., Tubiello, F., van der Werf, G. R., van Ooijen, E., Wanninkhof, R., Watanabe, M., Wimart-Rousseau, C.,
1132 Yang, D., Yang, X., Yuan, W., Yue, X., Zaehle, S., Zeng, J., and Zheng, B.: Global Carbon Budget 2023, *Earth*
1133 *Syst. Sci. Data*, 15, 5301–5369, <https://doi.org/10.5194/essd-15-5301-2023>, 2023.

1134

1135 Frölicher, T. L., Sarmiento, J. L., Paynter, D. J., Dunne, J. P., Krasting, J. P., and Winton, M.: Dominance of the
1136 southern ocean in anthropogenic carbon and heat uptake in CMIP5 models. *Journal of Climate*, 28(2), 862–886.
1137 <https://doi.org/10.1175/JCLI-D-14-00117.1>, 2015

1138

1139 Fu, W., Randerson, J. T., and Moore, J. K.: Climate change impacts on net primary production (NPP) and export
1140 production (EP) regulated by increasing stratification and phytoplankton community structure in the CMIP5
1141 models, *Biogeosciences*, 13, 5151–5170, <https://doi.org/10.5194/bg-13-5151-2016>, 2016.

1142

1143 Gallego, M. A., Timmermann, A., Friedrich, T., and Zeebe, R. E.: Drivers of future seasonal cycle changes in
1144 oceanic $p\text{CO}_2$, *Biogeosciences*, 15, 5315–5327, <https://doi.org/10.5194/bg-15-5315-2018>, 2018.

1145

1146 Gangstø, R., Gehlen, M., Schneider, B., Bopp, L., Aumont, O., and Joos, F.: Modeling the marine aragonite
1147 cycle: changes under rising carbon dioxide and its role in shallow water CaCO_3 dissolution, *Biogeosciences*, 5,
1148 1057–1072, <https://doi.org/10.5194/bg-5-1057-2008>, 2008.

1149

1150 Gardner J., Peck, V. L., Bakker, D. C. E., Tarling, G. A. and Manno, C.: Contrasting life cycles of Southern
1151 Ocean pteropods alter their vulnerability to climate change. *Front. Mar. Sci.* 10:1118570.
1152 doi: 10.3389/fmars.2023.1118570, 2023

1153

1154 Gloege, L., McKinley, G. A., Landschützer, P., Fay, A. R., Frölicher, T. L., Fyfe, J. C., et al: Quantifying errors
1155 in observationally based estimates of ocean carbon sink variability. *Global Biogeochemical Cycles*, 35,
1156 e2020GB006788. <https://doi.org/10.1029/2020GB006788>, 2021.

1157

1158 Gooya, P., Swart, N. C., and Hamme, R. C.: Time-varying changes and uncertainties in the CMIP6 ocean carbon
1159 sink from global to local scale, *Earth Syst. Dynam.*, 14, 383–398, <https://doi.org/10.5194/esd-14-383-2023>,
1160 2023.

1161

1162 Gray, A., Johnson, K. S., Bushinsky, S. M., Riser, S. C., Russell, J. L., Talley, L. D., et al.: Autonomous
1163 biogeochemical floats detect significant carbon dioxide outgassing in the high-latitude Southern Ocean.
1164 *Geophysical Research Letters*, 45, 9049–9057. <https://doi.org/10.1029/2018GL078013>, 2018.

1165

1166 Gray, A., R.: The Four-Dimensional Carbon Cycle of the Southern Ocean. *Annu. Rev. Mar. Sci.* 16:23.1–23.28.
1167 <https://doi.org/10.1146/annurev-marine-041923-104057>, 2024.
1168
1169 Gregor, L., Kok, S., and Monteiro, P. M. S.: Interannual drivers of the seasonal cycle of CO₂ in the Southern
1170 Ocean, *Biogeosciences*, 15, 2361-2378, <https://doi.org/10.5194/bg-15-2361-2018>, 2018.
1171
1172 Gruber, N., Clement, D., Carter, B. R., Feely, R. A., van Heuven, S., Hoppema, M., Ishii, M., Key, R. M.,
1173 Kozyr, A., Lauvset, S. K., Lo Monaco, C., Mathis, J. T., Murata, A., Olsen, A., Perez, F. F., Sabine, C. L.,
1174 Tanhua, T., and Wanninkhof, R.: The oceanic sink for anthropogenic CO₂ from 1994 to 2007, *Science* vol. 363
1175 (issue 6432), pp. 1193-1199. DOI: 10.1126/science.aau5153, 2019a.
1176
1177 Gruber, N., Clement, D., Carter, B. R., Feely, R. A., Heuven, S., van, Hoppema, M., Ishii, M., Key, R. M.,
1178 Kozyr, A., Lauvset, S. K., Lo Monaco, C., Mathis, J. T., Murata, A., Olsen, A., Perez, F. F., Sabine, C. L.,
1179 Tanhua, T., and Wanninkhof, R.: The oceanic sink for anthropogenic CO₂ from 1994 to 2007 – the data (NCEI
1180 Accession 0186034), NOAA National Centers for Environmental Information [data set],
1181 <https://doi.org/10.25921/wdn2-pt10>, 2019b.
1182
1183 Gruber, N., Landschützer, P., and Lovenduski, N. S.: The Variable Southern Ocean Carbon Sink, *Annu.*
1184 *Rev. Mar. Sci.*, Vol. 11, doi:10.1146/annurev-marine-121916-063407, 2019c.
1185
1186 Gu, Y., Katul, G. G., & Cassar, N. Multiscale temporal variability of the global air-sea CO₂ flux anomaly.
1187 *Journal of Geophysical Research: Biogeosciences*, 128, e2022JG006934. <https://doi.org/10.1029/2022JG006934>,
1188 2023
1189
1190 Hauri, C., Friedrich, T., and Timmermann, A.: Abrupt onset and prolongation of aragonite undersaturation
1191 events in the Southern Ocean, *Nature Climate Change*, doi:10.1038/nclimate2844, 2015.
1192
1193 Hauck J., Hoppema, M., Bellerby, R. G. J., Völker, C., and Wolf-Gladrow, D.: Data-based estimation of
1194 anthropogenic carbon and acidification in the Weddell Sea on a decadal timescale. *J. Geophys. Res.* 115,
1195 C03004. doi:10.1029/2009jc005479, 2010
1196
1197 Hauck, J., Völker, C., Wang, T., Hoppema, M., Losch, M., and Wolf-Gladrow, D. A.: Seasonally different
1198 carbon flux changes in the Southern Ocean in response to the southern annular mode. *Global Biogeochemical*
1199 *Cycles*, 27(4), 1236–1245. <https://doi.org/10.1002/2013GB004600>, 2013
1200
1201 Hauck, J. and Völker, C.: Rising atmospheric CO₂ leads to large impact of biology on Southern Ocean CO₂
1202 uptake via changes of the Revelle factor, *Geophys. Res. Lett.*, 42, 1459–1464, doi:10.1002/2015GL063070,
1203 2015
1204
1205 Hauck, J., Volker, C., Wolf-Gladrow, D. A., Laufkotter, C., Vogt, M., Aumont, O., et al.: On the Southern
1206 Ocean CO₂ uptake and the role of the biological carbon pump in the 21st century. *Global Biogeochemical*
1207 *Cycles*, 29(9), 1451–1470. <https://doi.org/10.1002/2015GB005140>, 2015
1208
1209 Hauck, J., Zeising, M., Le Quéré, C., Gruber, N., Bakker, D. C. E., Bopp, L., Chau, T. T., Gürses, Ö., Ilyina, T.,
1210 Landschützer, P., Lenton, A., Resplandy, L., Rödenbeck, C., Schwinger, J., and Séférian, R.: Consistency and
1211 challenges in the ocean carbon sink estimate for the Global Carbon Budget. *Front. Mar. Sci.* doi:
1212 10.3389/fmars.2020.571720, 2020
1213
1214 Hauck, J., Nissen, C., Landschützer, P., Rödenbeck, C., Bushinsky, S., and Olsen, A.: Sparse observations
1215 induce large biases in estimates of the global ocean CO₂ sink: an ocean model subsampling experiment. *Phil.*
1216 *Trans. R. Soc. A* 381: 20220063. <https://doi.org/10.1098/rsta.2022.0063>, 2023a
1217

1218 Hauck, J., Gregor, L., Nissen, C., Patara, L., Hague, M., Mongwe, P., et al.: The Southern Ocean carbon cycle
1219 1985–2018: Mean, seasonal cycle, trends, and storage. *Global Biogeochemical Cycles*, 37, e2023GB007848.
1220 <https://doi.org/10.1029/2023GB007848>, 2023b

1221

1222 Hersbach, H., Bell, B., Berrisford, P., Hirahara, S., Horányi, A., Muñoz-Sabater, J., Nicolas, J., Peubey, C.,
1223 Radu, R., Schepers, D., Simmons, A., Soci, C., Abdalla, S., Abellan, X., Balsamo, G., Bechtold, P., Biavati, G.,
1224 Bidlot, J., Bonavita, M., De Chiara, G., Dahlgren, P., Dee, D., Diamantakis, M., Dragani, R., Flemming, J.,
1225 Forbes, R., Fuentes, M., Geer, A., Haimberger, L., Healy, S., Hogan, R. J., Hólm, E., Janisková, M., Keeley, S.,
1226 Laloyaux, P., Lopez, P., Lupu, C., Radnoti, G., de Rosnay, P., Rozum, I., Vamborg, F., Villaume, S., and
1227 Thépaut, J.-N.: The ERA5 global reanalysis, *Q. J. Roy. Meteor. Soc.*, 146, 1999–2049,
1228 <https://doi.org/10.1002/qj.3803>, 2020.

1229

1230 Hoppema, M., Bakker, K., van Heuven, S. M. A. C., van Ooijen, J. C., and de Baar, H. J. W.: Distributions,
1231 trends and inter-annual variability of nutrients along a repeat section through the Weddell Sea (1996–2011).
1232 *Marine Chemistry*, 177, 545–553. <https://doi.org/10.1016/j.marchem.2015.08.007>, 2015

1233

1234 Hunt, B. P. V., Pakhomov, E. A., Hosie, G. W., Siegel, V., Ward, P., and Bernard, K.: Pteropods in Southern
1235 Ocean ecosystems, *Progress in Oceanography*, Volume 78, Issue 3, Pages 193–221,
1236 <https://doi.org/10.1016/j.pocean.2008.06.001>, 2008

1237

1238 Iida, T., Odate, T., and Fukuchi, M.: Long-term trends of nutrients and apparent oxygen utilization south of the
1239 polar front in Southern Ocean intermediate water from 1965 to 2008. *PLoS One*, 8, e71766.
1240 <https://doi.org/10.1371/journal.pone.0071766>, 2013

1241

1242 Iida, Y., Takatani, Y., Kojima, A., and Ishii, M.: Global trends of ocean CO₂ sink and ocean acidification: an
1243 observation based reconstruction of surface ocean inorganic carbon variables, *J. Oceanogr.*, 77, 323–358,
1244 <https://doi.org/10.1007/s10872-020-00571-5>, 2021.

1245

1246 IPCC: Changing Ocean, Marine Ecosystems, and Dependent Communities. in *The Ocean and Cryosphere in a*
1247 *Changing Climate* 447–588 (Cambridge University Press, 2022). doi:10.1017/9781009157964.007, 2022

1248

1249 Ito, T., Minobe, S., Long, M. C., Deutsch, C. Upper ocean O₂ trends: 1958–2015. *Geophysical Research Letters*
1250 44, 4214–4223, <https://doi.org/10.1002/2017GL073613>, 2017.

1251

1252 Jabaud-Jan, A., Metzl, N., Brunet, C., Poisson, A., and Schauer, B.: Variability of the Carbon Dioxide System in
1253 the Southern Indian Ocean (20°S–60°S): the impact of a warm anomaly in austral summer 1998. *Global*
1254 *Biogeochemical Cycles*, Vol. 18, No. 1, GB1042,10.1029/2002GB002017, 2004

1255

1256 Jeandel, C., Ruiz-Pino, D., Gjata, E., Poisson, A., Brunet, C., Charriaud, E., Dehairs, F., Delille, D., Fiala, M.,
1257 Fravallo, C., Miquel, J. C., Park, Y. H., Pondaven, P., Quéguiner, B., Razouls, S., Schauer, B., and Tréguer, P.:
1258 KERFIX, a time-series station in the Southern Ocean: a presentation. *Journal of Marine Systems*, 17, 1–4, 555–
1259 569., [https://doi.org/10.1016/S0924-7963\(98\)00064-5](https://doi.org/10.1016/S0924-7963(98)00064-5), 1998

1260

1261 Jiang, L.-Q., Feely, R. A., Carter, B. R., Greeley, D. J., Gledhill, D. K., and Arzayus K. M.: Climatological
1262 distribution of aragonite saturation state in the global oceans, *Global Biogeochem. Cycles*, 29, 1656–1673,
1263 doi:10.1002/2015GB005198, 2015.

1264

1265 Jiang, L.-Q., Carter, B. R., Feely, R. A., Lauvset, S. K., and Olsen, A.: Surface ocean pH and buffer capacity:
1266 past, present and future. *Sci Rep* 9, 18624, doi:10.1038/s41598-019-55039-4, 2019

1267

1268 Jiang, L.-Q., Dunne, J., Carter, B. R., Tjiputra, J. F., Terhaar, J., Sharp, J. D., et al.: Global surface ocean
1269 acidification indicators from 1750 to 2100. *Journal of Advances in Modeling Earth Systems*, 15,
1270 e2022MS003563. <https://doi.org/10.1029/2022MS003563>, 2023

1271
1272 Joos, F., Hameau, A., Frölicher, T. L., and Stephenson, D. B.: Anthropogenic attribution of the increasing
1273 seasonal amplitude in surface ocean pCO₂. *Geophysical Research Letters*, 50, e2023GL102857.
1274 <https://doi.org/10.1029/2023GL102857>, 2023
1275
1276 Jouandet, M.-P., Blain, S., Metzl, N., Brunet, C., Trull, T., and Obernosterer, I.: A seasonal carbon budget for a
1277 naturally iron fertilized bloom (Kerguelen I. Southern Ocean). *Deep-Sea Res II*, 55, 856-867.
1278 doi:10.1016/j.dsr2.2007.12.037, 2008
1279
1280 Jouandet M.P., Blain, S., Metzl, N., and Mongin, C.: Interannual variability of the net community production and
1281 air-sea CO₂ flux in a natural iron fertilization region of the Southern Ocean. (Kerguelen plateau), *Antarctic*
1282 *Science*, doi:10.1017/S0954102011000411, 2011
1283
1284 Kane, A., Moulin, C., Thiria, S., Bopp, L., Berrada, M., Tagliabue, A., Crépon, M., Aumont, O., and Badran, F.:
1285 Improving the parameters of a global ocean biogeochemical model via variational assimilation of in situ data at
1286 five time series stations, *J. Geophys. Res.*, 116, C06011, doi:10.1029/2009JC006005, 2011
1287
1288 Kawaguchi, S., Ishida, A., King, R. et al.: Risk maps for Antarctic krill under projected Southern Ocean
1289 acidification. *Nature Clim. Change*, 3, 843–847, DOI: 10.1038/NCLIMATE1937, 2013
1290
1291 Keeling, C. D., and Waterman, L. S.: Carbon dioxide in surface ocean waters: 3. Measurements on Lusiad
1292 Expedition 1962–1963, *J. Geophys. Res.*, 73(14), 4529– 4541, doi:10.1029/JB073i014p04529, 1968
1293
1294 Keppler, L. and Landschützer, P.: Regional Wind Variability Modulates the Southern Ocean Carbon Sink, *Sci.*
1295 *Rep.-UK*, 9, 7384, <https://doi.org/10.1038/s41598-019-43826-y>, 2019.
1296
1297 Kessler, A. and Tjiputra, J.: The Southern Ocean as a constraint to reduce uncertainty in future ocean carbon
1298 sinks, *Earth Syst. Dynam.*, 7, 295-312, doi:10.5194/esd-7-295-2016, 2016.
1299
1300 Key, R. M., Kozyr, A., Sabine, C. L., Lee, K., Wanninkhof, R., Bullister, J. L., Feely, R. A., Millero, F. J.,
1301 Mordy, C., and Peng, T. H.: A global ocean carbon climatology: Results from Global Data Analysis Project
1302 (GLODAP), *Global Biogeochemical Cycles*, 18, GB4031, <https://doi.org/10.1029/2004GB002247>, 2004.
1303
1304 Khatiwala, S., Tanhua, T., Mikaloff Fletcher, S., Gerber, M., Doney, S. C., Graven, H. D., Gruber, N.,
1305 McKinley, G. A., Murata, A., Ríos, A. F., and Sabine, C. L.: Global ocean storage of anthropogenic carbon,
1306 *Biogeosciences*, 10, 2169–2191, <https://doi.org/10.5194/bg-10-2169-2013>, 2013.
1307
1308 Krumhardt, K. M., Long, M. C., Sylvester, Z. T. and Petrik, C. M.: Climate drivers of Southern Ocean
1309 phytoplankton community composition and potential impacts on higher trophic levels. *Front. Mar. Sci.*
1310 9:916140. doi: 10.3389/fmars.2022.916140, 2022
1311
1312 Kwiatkowski, L., and Orr, J. C.: Diverging seasonal extremes for ocean acidification during the twenty-first
1313 century. *Nature Climate Change*, 8(2), 141–145. <https://doi.org/10.1038/s41558-017-0054-0>, 2018
1314
1315 Kwiatkowski, L., Torres, O., Bopp, L., Aumont, O., Chamberlain, M., Christian, J. R., Dunne, J. P., Gehlen, M.,
1316 Ilyina, T., John, J. G., Lenton, A., Li, H., Lovenduski, N. S., Orr, J. C., Palmieri, J., Santana-Falcón, Y.,
1317 Schwinger, J., Séférian, R., Stock, C. A., Tagliabue, A., Takano, Y., Tjiputra, J., Toyama, K., Tsujino, H.,
1318 Watanabe, M., Yamamoto, A., Yool, A., and Ziehn, T.: Twenty-first century ocean warming, acidification,
1319 deoxygenation, and upper-ocean nutrient and primary production decline from CMIP6 model projections,
1320 *Biogeosciences*, 17, 3439–3470, <https://doi.org/10.5194/bg-17-3439-2020>, 2020.
1321
1322 Lange, N., Fiedler, B., Álvarez, M., Benoit-Cattin, A., Benway, H., Buttigieg, P. L., Coppola, L., Currie, K.,
1323 Flecha, S., Honda, M., Huertas, I. E., Lauvset, S. K., Muller-Karger, F., Körtzinger, A., O'Brien, K. M.,

1324 Ólafsdóttir, S. R., Pacheco, F. C., Rueda-Roa, D., Skjelvan, I., Wakita, M., White, A., and Tanhua, T.: Synthesis
1325 Product for Ocean Time-Series (SPOTS) – A ship-based biogeochemical pilot, *Earth Syst. Sci. Data Discuss.*
1326 [preprint], <https://doi.org/10.5194/essd-2023-238>, in review, 2023. accepted in press.
1327

1328 Landschützer, P., Gruber, N., Haumann, F. A., Rödenbeck, C., Bakker, D. C. E., Van Heuven, S., Hoppema, M.,
1329 Metzl, N., Sweeney, C., Takahashi, T., Tilbrook, B., and Wanninkhof, R.: The reinvigoration of the Southern
1330 Ocean carbon sink, *Science*, 349, 1221–1224, <https://doi.org/10.1126/science.aab2620>, 2015.
1331

1332 Landschützer, P., Gruber, N., Bakker, D. C. E., Stemmler, I., and Six, K. D.: Strengthening seasonal marine CO₂
1333 variations due to increasing atmospheric CO₂. *Nature Climate Change*, 8(2), 146–150.
1334 <https://doi.org/10.1038/s41558-017-0057-x>, 2018
1335

1336 Lauvset, S. K., Gruber, N., Landschützer, P., Olsen, A., and Tjiputra, J.: Trends and drivers in global surface
1337 ocean pH over the past 3 decades. *Biogeosciences*, 12, 1285–1298, doi:10.5194/bg-12-1285-2015, 2015
1338

1339 Lauvset, S. K., Carter, B. R., Perez, F. F., Jiang, L.-Q., Feely, R. A., Velo, A., and Olsen, A.: Processes Driving
1340 Global Interior Ocean pH Distribution, *Global Biogeochem. Cycles*, 34, e2019GB006 229,
1341 <https://doi.org/10.1029/2019GB006229>, 2020.
1342

1343 Lauvset, S. K., Lange, N., Tanhua, T., Bittig, H. C., Olsen, A., Kozyr, A., Álvarez, M., Becker, S., Brown, P. J.,
1344 Carter, B. R., Cotrim da Cunha, L., Feely, R. A., van Heuven, S., Hoppema, M., Ishii, M., Jeansson, E.,
1345 Jutterström, S., Jones, S. D., Karlsen, M. K., Lo Monaco, C., Michaelis, P., Murata, A., Pérez, F. F., Pfeil, B.,
1346 Schirnack, C., Steinfeldt, R., Suzuki, T., Tilbrook, B., Velo, A., Wanninkhof, R., Woosley, R. J., and Key, R. M.:
1347 An updated version of the global interior ocean biogeochemical data product, GLODAPv2.2021, *Earth Syst. Sci.*
1348 *Data*, 13, 5565–5589, <https://doi.org/10.5194/essd-13-5565-2021>, 2021a.
1349

1350 Lauvset, Siv K.; Lange, Nico; Tanhua, Toste; Bittig, Henry C.; Olsen, Are; Kozyr, Alex; Álvarez, Marta;
1351 Becker, Susan; Brown, Peter J.; Carter, Brendan R.; Cotrim da Cunha, Leticia; Feely, Richard A.; van Heuven,
1352 Steven M. A. C.; Hoppema, Mario; Ishii, Masao; Jeansson, Emil; Jutterström, Sara; Jones, Steve D.; Karlsen,
1353 Maren K.; Lo Monaco, Claire; Michaelis, Patrick; Murata, Akihiko; Pérez, Fiz F.; Pfeil, Benjamin; Schirnack,
1354 Carsten; Steinfeldt, Reiner; Suzuki, Toru; Tilbrook, Bronte; Velo, Antón; Wanninkhof, Rik; Woosley, Ryan J.;
1355 Key, Robert M.: Global Ocean Data Analysis Project version 2.2021 (GLODAPv2.2021) (NCEI Accession
1356 0237935). [subset used GLODAPv2.2021_Indian_Ocean.cvs]. NOAA National Centers for Environmental
1357 Information. Dataset. <https://doi.org/10.25921/ttgg-n825>., Accessed 2/8/2021. 2021b.
1358

1359 Lee, K., Tong, L. T., Millero, F. J., Sabine, C. L., Dickson, A. G., Goyet, C., Park, G. H., Wanninkhof, R., Feely,
1360 R. A., and Key, R. M.: Global relationships of total alkalinity with salinity and temperature in surface waters of
1361 the world's oceans. *Geophys. Res. Lett.* 33, L19605. doi10.1029/2006GL027207, 2006.
1362

1363 Lenton, A., Codron, F., Bopp, L., Metzl, N., Cadule, P., Tagliabue, A., and Le Sommer, J.: Stratospheric ozone
1364 depletion reduces ocean carbon uptake and enhances ocean acidification. *Geophys. Res. Lett.*, 36, L12606, 2009.
1365 doi:10.1029/2009GL038227, 2009
1366

1367 Lenton, A., Tilbrook, B., Law, R. M., Bakker, D., Doney, S. C., Gruber, N., Ishii, M., Hoppema, M.,
1368 Lovenduski, N. S., Matear, R. J., McNeil, B. I., Metzl, N., Mikaloff Fletcher, S. E., Monteiro, P. M. S.,
1369 Rödenbeck, C., Sweeney, C., and Takahashi, T.: Sea–air CO₂ fluxes in the Southern Ocean for the period 1990–
1370 2009, *Biogeosciences*, 10, 4037–4054, <https://doi.org/10.5194/bg-10-4037-2013>, 2013.
1371

1372 Le Quéré, C., Rödenbeck, C., Buitenhuis, E. T., Conway, T. J., Langenfelds, R., Gomez, A., Labuschagne, C.,
1373 Ramonet, M., Nakazawa, T., Metzl, N., Gillett, N., and Heimann, M.: Saturation of the Southern Ocean CO₂
1374 Sink Due to Recent Climate Change, *Science*, 316, 1735–1738, <https://doi.org/10.1126/science.1136188>, 2007.
1375

1376 Lerner, P., Romanou, A., Kelley, M., Romanski, J., Ruedy, R., and Russell, G.: Drivers of air-sea CO₂ flux
1377 seasonality and its long-term changes in the NASA-GISS model CMIP6 submission. *Journal of Advances in*
1378 *Modeling Earth Systems*, 13, e2019MS002028. <https://doi.org/10.1029/2019MS002028>, 2021.
1379

1380 Leseurre, C., Lo Monaco, C., Reverdin, G., Metzl, N., Fin, J., Mignon, C., and Benito, L.: Summer trends and
1381 drivers of sea surface fCO₂ and pH changes observed in the southern Indian Ocean over the last two decades
1382 (1998–2019), *Biogeosciences*, 19, 2599–2625, <https://doi.org/10.5194/bg-19-2599-2022>, 2022.
1383

1384 Leung, S., Cabré, A., and Marinov, I.: A latitudinally banded phytoplankton response to 21st century climate
1385 change in the Southern Ocean across the CMIP5 model suite, *Biogeosciences*, 12, 5715–5734,
1386 <https://doi.org/10.5194/bg-12-5715-2015>, 2015.
1387

1388 Lewis E., and Wallace, D. W. R.: Program developed for CO₂ system calculations. ORNL/CDIAC-105. Carbon
1389 Dioxide Information Analysis Center, Oak Ridge National Laboratory, US. Dept. of Energy, Oak Ridge, TN,
1390 1998.
1391

1392 Lo Monaco, C., Goyet, C., Metzl, N., Poisson, A., and Touratier, F.: Distribution and inventory of anthropogenic
1393 CO₂ in the Southern Ocean: Comparison of three databased methods, *J. Geophys. Res.-Oceans*, 110, C09S02,
1394 <https://doi.org/10.1029/2004JC002571>, 2005.
1395

1396 Lo Monaco, C., Álvarez, M., Key, R. M., Lin, X., Tanhua, T., Tilbrook, B., Bakker, D. C. E., van Heuven, S.,
1397 Hoppema, M., Metzl, N., Ríos, A. F., Sabine, C. L., and Velo, A.: Assessing the internal consistency of the
1398 CARINA database in the Indian sector of the Southern Ocean, *Earth Syst. Sci. Data*, 2, 51–70,
1399 <https://doi.org/10.5194/essd-2-51-2010>, 2010.
1400

1401 Lo Monaco, C., Metzl, N., D’Ovidio, F., Llorc, J., and Ridame, C.: Rapid establishment of the CO₂ sink
1402 associated with Kerguelen’s bloom observed during the KEOPS2/OISO20 cruise, *Biogeosciences Discuss.*, 11,
1403 17543–17578, <https://doi.org/10.5194/bgd-11-17543-2014>, 2014.
1404

1405 Long, M. C., Lindsay, K., Peacock, S., Moore, J. K., and Doney, S. C.: Twentieth-Century Oceanic Carbon
1406 Uptake and Storage in CESM1(BGC), *J. Climate*, 26 (18), 6775–6800, doi:10.1175/JCLI-D-12-00184.1, 2013.
1407

1408 Long, M. C., Stephens, B. B., McKain, K., Sweeney, C., Keeling, R. F., Kort, E. A., Morgan, E. J., Bent, J. D.,
1409 Chandra, N., Chevallier, F., Commane, R., Daube, B. C., Krummel, P. B., Loh, Z., Lujikx, I. T., Munro, D.,
1410 Patra, P., Peters, W., Ramonet, M., Rödenbeck, C., Stavert, A., Tans, P., and Wofsy, S. C.: Strong Southern
1411 Ocean carbon uptake evident in airborne observations, *Science*, 374, 1275–1280,
1412 <https://doi.org/10.1126/science.abi4355>, 2021.
1413

1414 Louanchi, F., Ruiz-Pino, D., and Poisson, A.: Temporal variations of mixed layer oceanic CO₂ at JGOFS-
1415 KERFIX time-series station: Physical versus biogeochemical processes. *Journal of Marine Research* 57(1): 165-
1416 187. <https://doi.org/10.1357/002224099765038607>, 1999.
1417

1418 Louanchi, F., Ruiz-Pino, D. P., Jeandel, C., Brunet, C., Schauer, B., Masson, A., Fiala, M., and Poisson, A.:
1419 Dissolved inorganic carbon, alkalinity, nutrient and oxygen seasonal and interannual variations at the Antarctic
1420 Ocean JGOFS-KERFIX site. *Deep Sea Research Part I: Oceanographic Research Papers* 48(7): 1581-1603,
1421 [https://doi.org/10.1016/S0967-0637\(00\)00086-8](https://doi.org/10.1016/S0967-0637(00)00086-8), 2001.
1422

1423 Lovenduski, N. S., and Gruber, N.: Impact of the Southern Annular Mode on Southern Ocean circulation and
1424 biology, *Geophys. Res. Lett.*, 32, L11603, doi:10.1029/2005GL022727, 2005.
1425

1426 Lueker, T. J., Dickson, A. G., and Keeling, C. D.: Ocean pCO₂ calculated from dissolved inorganic carbon,
1427 alkalinity, and equations for K-1 and K-2: validation based on laboratory measurements of CO₂ in gas and
1428 seawater at equilibrium. *Marine Chemistry* 70, 105-119. [https://doi.org/10.1016/S0304-4203\(00\)00022-0](https://doi.org/10.1016/S0304-4203(00)00022-0), 2000.

1429
1430 Ma, D., Gregor, L., and Gruber, N.: Four decades of trends and drivers of global surface ocean acidification.
1431 Global Biogeochemical Cycles, 37, e2023GB007765. 10.1029/2023GB007765, 2023.
1432
1433 Mackay, N., Watson, A. J., Suntharalingam, P. et al.: Improved winter data coverage of the Southern Ocean CO₂
1434 sink from extrapolation of summertime observations. Commun Earth Environ 3, 265,
1435 <https://doi.org/10.1038/s43247-022-00592-6>, 2022.
1436
1437 Mahieu, L., Lo Monaco, C., Metzl, N., Fin, J., and Mignon, C.: Variability and stability of anthropogenic CO₂ in
1438 Antarctic Bottom Water observed in the Indian sector of the Southern Ocean, 1978–2018, Ocean Sci., 16, 1559–
1439 1576, <https://doi.org/10.5194/os-16-1559-2020>, 2020.
1440
1441 Marshall, G. J.: Trends in the Southern Annular Mode from observations and reanalyses. J. Clim., 16, 4134–
1442 4143, doi:10.1175/1520-0442%282003%29016<4134%3ATITSAM>2.0.CO%3B2, 2003.
1443
1444 Mayot, N., Le Quéré, C., Rödenbeck, C., Bernardello, R., Bopp, L., Djeutchouang, L. M., Gehlen, M., Gregor,
1445 L., Gruber, N., Hauck, J., Iida, Y., Ilyina, T., Keeling, R. F., Landschützer, P., Manning, A. C., Patara, L.,
1446 Resplandy, L., Schwinger, J., Séférian, R., Watson, A. J., Wright, R. M. and Zeng, J.: Climate-driven variability
1447 of the Southern Ocean CO₂ sink. Phil. Trans. R. Soc. A. 381: 20220055, <http://doi.org/10.1098/rsta.2022.0055>,
1448 2023
1449
1450 Mazloff, M. R., Verdy, A., Gille, S. T., Johnson, K. S., Cornuelle, B. D., and Sarmiento, J.: Southern Ocean
1451 acidification revealed by biogeochemical-Argo floats. *Journal of Geophysical Research: Oceans*, 128,
1452 e2022JC019530. <https://doi.org/10.1029/2022JC019530>, 2023.
1453
1454 McKinley, G. A., Bennington, V. S., Meinshausen, M., and Nicholls, Z.: Modern air-sea flux distributions
1455 reduce uncertainty in the future ocean carbon sink, Environmental Research Letters, 18, doi:10.1088/1748-
1456 9326/acc195, 2023.
1457
1458 McNeil, B. I. and Matear, R. J.: Southern Ocean acidification: A tipping point at 450-ppm atmospheric
1459 CO₂, P. Natl. Acad. Sci. USA, 105, 18860–18864, <https://doi.org/10.1073/pnas.0806318105>, 2008.
1460
1461 McNeil, B. I. and Sasse, T. P.: Future ocean hypercapnia driven by anthropogenic amplification of the natural
1462 CO₂ cycle, Nature, 529, 383–386, doi:10.1038/nature16156, 2016
1463
1464 McNeil, B. I., Metzl, N., Key, R. M., Matear, R. J. and Corbiere, A.: An empirical estimate of the Southern
1465 Ocean air-sea CO₂ flux, Global Biogeochem. Cycles, Vol. 21, No. 3, GB3011 10.1029/2007GB002991, 2007.
1466
1467 Meinshausen, M., Nicholls, Z. R. J., Lewis, J., Gidden, M. J., Vogel, E., Freund, M., et al.: The shared
1468 socioeconomic pathway (SSP) greenhouse gas concentrations and their extensions to 2500. Geoscientific Model
1469 Development, 13(8), 3571–3605. <https://doi.org/10.5194/gmd-13-3571-2020>, 2020.
1470
1471 Metzl, N., and Lo Monaco, C.: OISO- Océan Indien Service d'Observation,
1472 <https://doi.org/10.18142/228>, 1998.
1473
1474 Metzl, N., Brunet, C., Jabaud-Jan, A., Poisson, A., and Schauer, B.: Summer and winter air–sea CO₂ fluxes in
1475 the Southern Ocean, Deep-Sea Res., 53, 1548–1563, <https://doi.org/10.1016/j.dsr.2006.07.006>, 2006.
1476
1477 Metzl, N.: Decadal increase of oceanic carbon dioxide in Southern Indian Ocean surface waters (1991–2007),
1478 Deep-Sea Res. Pt. II, 56, 607–619, <https://doi.org/10.1016/j.dsr2.2008.12.007>, 2009.
1479

1480 Midorikawa, T., Inoue, H. Y., Ishii, M., Sasano, D., Kosugi, N., Hashida, G., Nakaoka, S., and Suzuki, T.:
1481 Decreasing pH trend estimated from 35-year time series of carbonate parameters in the Pacific sector of the
1482 Southern Ocean in summer, *Deep-Sea Res.*, 61, 131–139, <https://doi.org/10.1016/j.dsr.2011.12.003>, 2012.
1483
1484 Millero, F. J., Lee, K., and Roche, M.: Distribution of alkalinity in the surface waters of the major oceans, *Mar.*
1485 *Chem.*, 60, 111–130, [https://doi.org/10.1016/S0304-4203\(97\)00084-4](https://doi.org/10.1016/S0304-4203(97)00084-4), 1998.
1486
1487 Minas, H. J., and Minas, M.: Net community production in high nutrient-low chlorophyll waters of the tropical
1488 and Antarctic oceans – grazing vs iron hypothesis, *Oceanol. Acta*, 15, 145–162, 1992.
1489
1490 Mongin, M., Nelson, D. M., Pondaven, P., and Tréguer, P.: Simulation of upper-ocean biogeochemistry with a
1491 flexible-composition phytoplankton model: C, N and Si cycling and Fe limitation in the Southern Ocean. *Deep*
1492 *Sea Research Part II: Topical Studies in Oceanography*, Elsevier, 2006, 53 (5-7), pp.601-619.
1493 [10.1016/j.dsr2.2006.01.021](https://doi.org/10.1016/j.dsr2.2006.01.021), 2006.
1494
1495 Mongin, M., Nelson, D. M., Pondaven P., and Tréguer, P.: Potential phytoplankton responses to iron and
1496 stratification changes in the Southern Ocean based on a flexible-composition phytoplankton model. *Global*
1497 *Biogeochemical Cycles* 21 (GB4020), [/http://dx.doi.org/10.1029/2007GB002972S](http://dx.doi.org/10.1029/2007GB002972S), 2007.
1498
1499 Mongin, M., Molina, E., and Trull, T. W.: Seasonality and scale of the Kerguelen plateau phytoplankton bloom:
1500 A remote sensing and modeling analysis of the influence of natural iron fertilization in the Southern Ocean.
1501 *Deep Sea Research Part II: Topical Studies in Oceanography*, Vol 55, Issues 5–7, Pages 880-892,
1502 <https://doi.org/10.1016/j.dsr2.2007.12.039>. 2008.
1503
1504 Mongwe, N. P., Vichi, M., and Monteiro, P. M. S.: The seasonal cycle of pCO₂ and CO₂ fluxes in the Southern
1505 Ocean: diagnosing anomalies in CMIP5 Earth system models, *Biogeosciences*, 15, 2851–2872,
1506 <https://doi.org/10.5194/bg-15-2851-2018>, 2018.
1507
1508 Mongwe, P., Gregor, L., Tjiputra, J., Hauck, J., Ito, T., Danek, C., Vichi, M., Thomalla S., and Monteiro, M. S.:
1509 A shift in the mechanism of CO₂ uptake in the Southern Ocean under high emission-scenario, DOI:
1510 [10.21203/rs.3.rs-2849464/v1](https://doi.org/10.21203/rs.3.rs-2849464/v1), 2023.
1511
1512 Moore, J. K. and Abbott, M. R.: Phytoplankton chlorophyll distributions and primary production in the Southern
1513 Ocean, *J. Geophys. Res.-Oceans*, 105, 28709–28722, <https://doi.org/10.1029/1999JC000043>, 2000
1514
1515 Moy, A. D., Palmer, M. R., Howard, W. R., Bijma, J., Cooper, M. J., Calvo, E., Pelejero, C., Gagan M. K. and
1516 Chalk, T. B.: Reduced calcification in modern Southern Ocean planktonic foraminifera. *Nature Geosci* 2, 276–
1517 280. <https://doi-org.insu.bib.cnrs.fr/10.1038/ngeo460>, 2009.
1518
1519 Negrete-García, G., Lovenduski, N. S., Hauri, C., Krumhardt, K. M., and Lauvset, S. K.: Sudden
1520 emergence of a shallow aragonite saturation horizon in the Southern Ocean. *Nature Climate Change*, 1758-
1521 6798, [10.1038/s41558-019-0418-8](https://doi.org/10.1038/s41558-019-0418-8), 2019.
1522
1523 Neveux, J., and Lantoiné, F.: Spectrofluorometric assay of chlorophylls and phaeopigments using the least
1524 squares approximation technique, *Deep-Sea Res. I*, 40(9), 1747-1765, [https://doi.org/10.1016/0967-](https://doi.org/10.1016/0967-0637(93)90030-7)
1525 [0637\(93\)90030-7](https://doi.org/10.1016/0967-0637(93)90030-7), 1993.
1526
1527 Nicholson S. A., Whitt, D. B., Fer, I., du Plessis, M. D., Lebéhot A. D., et al.: Storms drive outgassing of CO₂ in
1528 the subpolar Southern Ocean. *Nat. Commun.* 13:158. <https://doi.org/10.1038/s41467-021-27780-w>, 2022
1529
1530 Olafsson, J., Olafsdottir, S. R., Benoit-Cattin, A., Danielsen, M., Arnarson, T. S., and Takahashi, T.: Rate of
1531 Iceland Sea acidification from time series measurements. *Biogeosciences* 6, 2661–2668.
1532 <https://doi.org/10.5194/bg-6-2661-2009>, 2009.

1533
1534 Olafsson, J., Olafsdottir, S. R., Benoit-Cattin, A., and Takahashi, T.: The Irminger Sea and the Iceland Sea time
1535 series measurements of sea water carbon and nutrient chemistry 1983–2006. *Earth Syst. Sci. Data* 2, 99–104.
1536 <https://doi.org/10.5194/essd-2-99-2010>, 2010.
1537
1538 Olsen, A., Key, R. M., van Heuven, S., Lauvset, S. K., Velo, A., Lin, X., Schirnick, C., Kozyr, A., Tanhua, T.,
1539 Hoppema, M., Jutterström, S., Steinfeldt, R., Jeansson, E., Ishii, M., Pérez, F. F., and Suzuki, T.: The Global
1540 Ocean Data Analysis Project version 2 (GLODAPv2) – an internally consistent data product for the world ocean,
1541 *Earth Syst. Sci. Data*, 8, 297–323, <https://doi.org/10.5194/essd-8-297-2016>, 2016.
1542
1543 Olsen, A., Lange, N., Key, R. M., Tanhua, T., Álvarez, M., Becker, S., Bittig, H. C., Carter, B. R., Cotrim da
1544 Cunha, L., Feely, R. A., van Heuven, S., Hoppema, M., Ishii, M., Jeansson, E., Jones, S. D., Jutterström, S.,
1545 Karlsen, M. K., Kozyr, A., Lauvset, S. K., Lo Monaco, C., Murata, A., Pérez, F. F., Pfeil, B., Schirnick, C.,
1546 Steinfeldt, R., Suzuki, T., Telszewski, M., Tilbrook, B., Velo, A., and Wanninkhof, R.: GLODAPv2.2019 – an
1547 update of GLODAPv2, *Earth Syst. Sci. Data*, 11, 1437–1461, <https://doi.org/10.5194/essd-11-1437-2019>, 2019.
1548
1549 Olsen, A., Lange, N., Key, R. M., Tanhua, T., Bittig, H. C., Kozyr, A., Álvarez, M., Azetsu-Scott, K., Becker, S.,
1550 Brown, P. J., Carter, B. R., Cotrim da Cunha, L., Feely, R. A., van Heuven, S., Hoppema, M., Ishii, M.,
1551 Jeansson, E., Jutterström, S., Landa, C. S., Lauvset, S. K., Michaelis, P., Murata, A., Pérez, F. F., Pfeil, B.,
1552 Schirnick, C., Steinfeldt, R., Suzuki, T., Tilbrook, B., Velo, A., Wanninkhof, R., and Woosley, R. J.: An updated
1553 version of the global interior ocean biogeochemical data product, GLODAPv2.2020, *Earth Syst. Sci. Data*, 12,
1554 3653–3678, <https://doi.org/10.5194/essd-12-3653-2020>, 2020.
1555
1556 Orr, J. C., Fabry, V. J., Aumont, O., Bopp, L., Doney, S. C., Feely, R. A., Gnanadesikan, A., Gruber, N., Ishida,
1557 A., Joos, F., Key, R. M., Lindsay, K., Maier-Reimer, E., Matear, R., Monfray, P., Mouchet, A., Najjar, R. G.,
1558 Plattner, G.-K., Rodgers, K. B., Sabine, C. L., Sarmiento, J. L., Schlitzer, R., Slater, R. D., Totterdell, I. J.,
1559 Weirig, M.-F., Yamanaka, Y., and Yool, A.: Anthropogenic ocean acidification over the twenty-first century and
1560 its impact on calcifying organisms, *Nature*, 437, 681–686, <https://doi.org/10.1038/nature04095>, 2005.
1561
1562 Orr, J. C., Epitalon, J.-M., and Gattuso, J.-P.: Comparison of ten packages that compute ocean carbonate
1563 chemistry, *Biogeosciences*, 12(5), 1483–1510, doi:10.5194/bg-12-1483-2015, 2015.
1564
1565 Orr, J. C., Epitalon, J.-M., Dickson, A. G., and Gattuso, J.-P.: Routine uncertainty propagation for the marine
1566 carbon dioxide system, *Marine Chemistry*, Vol. 207, 84–107, doi:10.1016/j.marchem.2018.10.006., 2018.
1567
1568 Oeschies, A., Brandt, P., Stramma, L., and Schmidtko, S.: Drivers and mechanisms of ocean deoxygenation. *Nat.*
1569 *Geosci.* 11, 467–473. doi: 10.1038/s41561-018-0152-2, 2018.
1570
1571 Pardo, P. C., Pérez, F. F., Khatiwala, S., and Ríos, A. F.: Anthropogenic CO₂ estimates in the Southern Ocean:
1572 Storage partitioning in the different water masses, *Prog. Oceanogr.*, 120, 230–242,
1573 <https://doi.org/10.1016/j.pocean.2013.09.005>, 2014.
1574
1575 Pardo, P. C., Tilbrook, B., Langlais, C., Trull, T. W., and Rintoul, S. R.: Carbon uptake and biogeochemical
1576 change in the Southern Ocean, south of Tasmania. *Biogeosciences*, 14(22), 5217–5237.
1577 <https://doi.org/10.5194/bg-14-5217-2017>, 2017.
1578
1579 Pasquer, B., Metzl, N., Goosse, H., and Lancelot, C.: What drives the seasonality of air-sea CO₂ fluxes in the
1580 ice-free zone of the Southern Ocean: A 1D coupled physical-biogeochemical model approach. *Marine*
1581 *Chemistry*, 177 (3): 554–565. doi:10.1016/j.marchem.2015.08.008, 2015.
1582
1583 Pauthenet, E., Roquet, F., Madec, G., Guinet, C., Hindell, M., McMahon, C. R., Harcourt, R., and Nerini, D.:
1584 Seasonal Meandering of the Polar Front Upstream of the Kerguelen Plateau, *Geophys. Res. Lett.*, 45, 9774–
1585 9781, <https://doi.org/10.1029/2018GL079614>, 2018.

1586
1587 Petrou, K., Baker, K. G., Nielsen, D. A., Hancock, A. M., Schulz, K. G. and Davidson, A. T.: Acidification
1588 diminishes diatom silica production in the Southern Ocean. *Nature Climate Change*, 9, 781-786,
1589 <https://doi.org/10.1038/s41558-019-0557-y>, 2019.
1590
1591 Pierrot, D., Lewis, E., and Wallace, D. W. R.: MS Excel Program Developed for CO₂ System Calculations
1592 ORNL/CDIAC-105, Carbon Dioxide Inf. Anal. Cent., Oak Ridge Natl. Lab., U. S. Dept. of Energy, Oak Ridge,
1593 Tenn., https://cdiac.ess-dive.lbl.gov/ftp/co2sys/CO2SYS_calc_XLS_v2.1/ (last access: 3 March 2022), 2006.
1594
1595 Pilcher, D. J., Brody, S. R., Johnson, L., and Bronselaer, B.: Assessing the abilities of CMIP5 models to
1596 represent the seasonal cycle of surface ocean pCO₂, *J. Geophys. Res. Oceans*, 120, 4625–4637,
1597 doi:10.1002/2015JC010759, 2015.
1598
1599 Pfeil, B., Olsen, A., Bakker, D. C. E., Hankin, S., Koyuk, H., Kozyr, A., Malczyk, J., Manke, A., Metzl, N.,
1600 Sabine, C. L., Akl, J., Alin, S. R., Bates, N., Bellerby, R. G. J., Borges, A., Boutin, J., Brown, P. J., Cai, W.-J.,
1601 Chavez, F. P., Chen, A., Cosca, C., Fassbender, A. J., Feely, R. A., González-Dávila, M., Goyet, C., Hales,
1602 B., Hardman-Mountford, N., Heinze, C., Hood, M., Hoppema, M., Hunt, C. W., Hydes, D., Ishii, M.,
1603 Johannessen, T., Jones, S. D., Key, R. M., Körtzinger, A., Landschützer, P., Lauvset, S. K., Lefèvre, N.,
1604 Lenton, A., Lourantou, A., Merlivat, L., Midorikawa, T., Mintrop, L., Miyazaki, C., Murata, A., Nakadate, A.,
1605 Nakano, Y., Nakaoka, S., Nojiri, Y., Omar, A. M., Padin, X. A., Park, G.-H., Paterson, K., Perez, F. F., Pierrot,
1606 D., Poisson, A., Ríos, A. F., Santana-Casiano, J. M., Salisbury, J., Sarma, V. V. S. S., Schlitzer, R.,
1607 Schneider, B., Schuster, U., Sieger, R., Skjelvan, I., Steinhoff, T., Suzuki, T., Takahashi, T., Tedesco, K.,
1608 Telszewski, M., Thomas, H., Tilbrook, B., Tjiputra, J., Vandemark, D., Veness, T., Wanninkhof, R., Watson,
1609 A. J., Weiss, R., Wong, C. S., and Yoshikawa-Inoue, H.: A uniform, quality controlled Surface Ocean CO₂ Atlas
1610 (SOCAT), *Earth Syst. Sci. Data*, 5, 125-143, doi:10.5194/essd-5-125-2013, 2013.
1611
1612 Poisson, A.: INDIGO 1 - MD 43 cruise, RV Marion Dufresne, <https://doi.org/10.17600/85000111>, 1985.
1613
1614 Poisson, A., Schauer, B., and Brunet, C. : MD43/INDIGO 1, Cruise report; Les rapports des campagnes à la mer,
1615 85(06). Les publications de la Mission de Recherche des Terres Australes et Antarctiques Françaises, Paris, 267
1616 pp., 1988.
1617
1618 Poisson, A., Metzl, N., Brunet, C., Schauer, B., Bres, B., Ruiz-Pino, D., and Louanchi, F.: Variability of sources
1619 and sinks of CO₂ in the western Indian and southern oceans during the year 1991, *J. Geophys. Res. Oceans*, 98,
1620 22759–22778, <https://doi.org/10.1029/93JC02501>, 1993.
1621
1622 Pondaven, P., Fravallo, C., Ruiz-Pino, D., Tréguer, P., Quéguiner, B., and Jeandel, C.: Modelling the silica pump
1623 in the Permanently Open Ocean Zone of the Southern Ocean, *J. Mar. Syst.*, 17, 1-4, 587–619,
1624 [https://doi.org/10.1016/S0924-7963\(98\)00066-9](https://doi.org/10.1016/S0924-7963(98)00066-9), 1998.
1625
1626 Pondaven, P., Ruiz-Pino, D., Fravallo, C., Tréguer, P., and Jeandel, C.: Interannual variability of Si and N cycles
1627 at the time-series station KERFIX between 1990 and 1995 – a 1-D modelling study, *Deep-Sea Res. Pt. I*, 47, 2,
1628 223–257, [https://doi.org/10.1016/S0967-0637\(99\)00053-9](https://doi.org/10.1016/S0967-0637(99)00053-9), 2000.
1629
1630 Prend, C. J., Gray, A. R., Talley, L. D., Gille, S. T., Haumann, F. A., Johnson, K. S., et al.: Indo-Pacific sector
1631 dominates Southern Ocean carbon outgassing. *Global Biogeochemical Cycles*, 36, e2021GB007226.
1632 <https://doi.org/10.1029/2021GB007226>, 2022.
1633
1634 Racapé, V., Lo Monaco, C., Metzl, N., and Pierre, C.: Summer and winter distribution of $\delta^{13}\text{C}_{\text{DIC}}$ in surface
1635 waters of the South Indian Ocean (20°S-60°S). *Tellus-B*, DOI: 10.1111/j.1600-0889.2010.00504, 2010.
1636

1637 Reynolds, R. W., Rayner, N. A., Smith, T. M., Stokes, D. C., and Wang, W.: An improved in situ and satellite
1638 SST analysis for climate. *J. Clim.* 15, 1609–1625. [https://doi.org/10.1175/1520-0442\(2002\)015<1609:AIISAS>2.0.CO;2](https://doi.org/10.1175/1520-0442(2002)015<1609:AIISAS>2.0.CO;2), 2002.

1640
1641 Rödenbeck, C., Keeling, R. F., Bakker, D. C. E., Metzl, N., Olsen, A., Sabine, C., and Heimann, M.: Global
1642 surface-ocean pCO₂ and sea–air CO₂ flux variability from an observation-driven ocean mixed-layer scheme,
1643 *Ocean Sci.*, 9, 193–216, <https://doi.org/10.5194/os-9-193-2013>, 2013.

1644
1645 Rödenbeck, C., DeVries, T., Hauck, J., Le Quéré, C., and Keeling, R. F.: Data-based estimates of
1646 interannual sea–air CO₂ flux variations 1957–2020 and their relation to environmental drivers,
1647 *Biogeosciences*, 19, 2627–2652, <https://doi.org/10.5194/bg-19-2627-2022>, 2022.

1648
1649 Rodgers, K. B., Schwinger, J., Fassbender, A. J., Landschützer, P., Yamaguchi, R., Frenzel, H., et al.: Seasonal
1650 variability of the surface ocean carbon cycle: A synthesis. *Global Biogeochemical Cycles*, 37, e2023GB007798.
1651 <https://doi.org/10.1029/2023GB007798>, 2023

1652
1653 Rustogi, P., Landschützer, P., Brune, S. et al.: The impact of seasonality on the annual air-sea carbon flux and its
1654 interannual variability. *Clim. Atmos. Sci.*, 6, 66, <https://doi.org/10.1038/s41612-023-00378-3>, 2023.

1655
1656 Sabine, C. L., Key, R. M., Johnson, K. M., Millero, F. J., Poisson, A., Sarmiento, J. L., Wallace, D. W. R., and
1657 Winn, C. D.: Anthropogenic CO₂ inventory of the Indian Ocean, *Global Biogeochemical Cycles*, 13, 179-198,
1658 <https://doi.org/10.1029/1998GB900022>, 1999.

1659
1660 Sabine, C. L., Feely, R. A., Gruber, N., Key, R. M., Lee, K., Bullister, J. L., Wanninkhof, R., Wong, C. S.,
1661 Wallace, D. W. R., Tilbrook, B., Millero, F. J., Peng, T.-H., Kozyr, A., Ono, T., and Rios, A. F.: The Oceanic
1662 Sink for Anthropogenic CO₂, *Science*, 305, 367–371, <https://doi.org/10.1126/science.1097403>, 2004.

1663
1664 Sasse, T. P., McNeil, B. I., Matear, R. J., and Lenton, A.: Quantifying the influence of CO₂ seasonality on future
1665 aragonite undersaturation onset, *Biogeosciences*, 12, 6017–6031, <https://doi.org/10.5194/bg-12-6017-2015>,
1666 2015.

1667
1668 Schlitzer, R.: Ocean Data View, Ocean Data View, <http://odv.awi.de> (last access: 13 March 2019), 2018.

1669
1670 Schmidtko, S., Stramma, L., and Visbeck, M.: Decline in global oceanic oxygen content during the past five
1671 decades, *Nature*, 542, 335–339, <https://doi.org/10.1038/nature21399>, 2017.

1672
1673 Seifert, M., Nissen, C., Rost, B., Vogt, M., Völker, C., and Hauck, J.: Interaction matters: Bottom-up driver
1674 interdependencies alter the projected response of phytoplankton communities to climate change. *Global Change
1675 Biology*, 00, 1– 25. <https://doi.org/10.1111/gcb.16799>, 2023.

1676
1677 Shadwick, E. H., Wynn-Edwards, C. A., Matear, R.J., Jansen, P., Schulz, E. and Sutton, A. J.: Observed
1678 amplification of the seasonal CO₂ cycle at the Southern Ocean Time Series. *Front. Mar. Sci.* 10:1281854. doi:
1679 10.3389/fmars.2023.1281854, 2023

1680
1681 Skjelvan, I., Lauvset, S. K., Johannessen, T., et al.: Decadal trends in Ocean Acidification from the Ocean
1682 Weather Station M in the Norwegian Sea, *Journal of Marine Systems*,
1683 <https://doi.org/10.1016/j.jmarsys.2022.103775>, 2022.

1684
1685 Smith, H. E. K., Poulton, A. J., Garley, R., Hopkins, J., Lubelczyk, L. C., Drapeau, D. T., Rauschenberg, S.,
1686 Twining, B. S., Bates, N. R., and Balch, W. M.: The influence of environmental variability on the biogeography
1687 of coccolithophores and diatoms in the Great Calcite Belt, *Biogeosciences*, 14, 4905–4925,
1688 <https://doi.org/10.5194/bg-14-4905-2017>, 2017.

1689

1690 Strickland, J. D. H. and Parsons, T. R.: A Practical Hand Book of Seawater Analysis. Fisheries Research Board
1691 of Canada Bulletin, 2nd Edition., 310 p. pp., 1972.
1692
1693 Sutton, A. J., Williams, N. L., and Tilbrook, B.: Constraining Southern Ocean CO₂ Flux Uncertainty Using
1694 Uncrewed Surface Vehicle Observations, *Geophys. Res. Lett.*, 48, e2020GL091748,
1695 <https://doi.org/10.1029/2020GL091748>, 2021.
1696
1697 Takahashi, T., Olafsson, J., Goddard, J. G., Chipman, D. W., and Sutherland, S. C.: Seasonal variation of CO₂
1698 and nutrients in the high-latitude surface oceans: A comparative study, *Global Biogeochem. Cycles*, 7(4), 843–
1699 878, doi:10.1029/93GB02263, 1993.
1700
1701 Takahashi, T., Sutherland, S. C., Wanninkhof, R., Sweeney, C., Feely, R. A., Chipman, D. W., Hales, B.,
1702 Friederich, G., Chavez, F., Sabine, C., Watson, A., Bakker, D. C. E., Schuster, U., Metzl, N., Yoshikawa-Inoue,
1703 H., Ishii, M., Midorikawa, T., Nojiri, Y., Körtzinger, A., Steinhoff, T., Hoppema, M., Olafsson, J., Arnarson, T.
1704 S., Tilbrook, B., Johannessen, T., Olsen, A., Bellerby, R., Wong, C. S., Delille, B., Bates, N. R., and de Baar, H.
1705 J. W.: Climatological mean and decadal change in surface ocean pCO₂, and net sea–air CO₂ flux over the
1706 global oceans, *Deep-Sea Res. Pt. II*, 56, 554–577, <https://doi.org/10.1016/j.dsr2.2008.12.009>, 2009a.
1707
1708 Takahashi, T., Sutherland, S. C., Wanninkhof, R., Sweeney, C., Feely, R. A., Chipman, D. W., Hales, B.,
1709 Friederich, G., Chavez, F., Sabine, C., Watson, A., Bakker, D. C. E., Schuster, U., Metzl, N., Yoshikawa-Inoue,
1710 H., Ishii, M., Midorikawa, T., Nojiri, Y., Körtzinger, A., Steinhoff, T., Hoppema, M., Olafsson, J., Arnarson, T.
1711 S., Tilbrook, B., Johannessen, T., Olsen, A., Bellerby, R., Wong, C. S., Delille, B., Bates, N. R., and de Baar, H.
1712 J. W.: Corrigendum to “Climatological mean and decadal change in surface ocean pCO₂, and net sea–air CO₂
1713 flux over the global oceans” [*Deep Sea Res. II* 56 (2009) 554–577], *Deep Sea Research Part I: Oceanographic*
1714 *Research Papers*, 56, 11, 2075–2076, <https://doi.org/10.1016/j.dsr.2009.07.007>. 2009b.
1715
1716 Takao, S., Hirawake, T., Wright, S. W., and Suzuki, K.: Variations of net primary productivity and
1717 phytoplankton community composition in the Indian sector of the Southern Ocean as estimated from ocean color
1718 remote sensing data, *Biogeosciences*, 9, 3875–3890, doi:10.5194/bg-9-3875-2012, 2012.
1719
1720 Talley, L. D.: Closure of the global overturning circulation through the Indian, Pacific, and Southern Oceans:
1721 Schematics and transports. *Oceanography*, 26(1), 80–97. <https://doi.org/10.5670/oceanog.2013.07>, 2013.
1722
1723 Tanhua, T., Hoppema, M., Jones, E. M., Stöven, T., Hauck, J., Dávila, M. G., Santana-Casiano, M., Álvarez, M.,
1724 and Strass, V. H.: Temporal changes in ventilation and the carbonate system in the Atlantic sector of the
1725 Southern Ocean, *Deep Sea Res. Part II Top. Stud. Oceanogr.*, 138, 26–38,
1726 <https://doi.org/10.1016/j.dsr2.2016.10.004>, 2017.
1727
1728 Touratier, F., Azouzi, L. and Goyet, C.: CFC-11, $\Delta 14\text{C}$ and 3H tracers as a means to assess anthropogenic CO₂
1729 concentrations in the ocean. *Tellus B*, 59(2), 318–325, doi:10.1111/j.1600-0889.2006.00247.x, 2007.
1730
1731 Tréguer, P., and Le Corre, P.: Manuel d’analyse des sels nutritifs dans l’eau de mer (utilisation de
1732 l’autoanalyseur II Technicon), 2nd ed., 110 pp., L.O.C.U.B.O., Brest, 1975.
1733
1734 Uppström, L. R.: The boron/chlorinity ratio of deep-sea water from the Pacific Ocean, *Deep Sea Research and*
1735 *Oceanographic Abstracts*, 21, 161–162, [https://doi.org/10.1016/0011-7471\(74\)90074-6](https://doi.org/10.1016/0011-7471(74)90074-6), 1974.
1736
1737 van Heuven, S. M. A. C., Hoppema, M., Huhn, O., Slagter, H. A., and de Baar, H. J. W.: Direct observation of
1738 increasing CO₂ in the Weddell Gyre along the Prime Meridian during 1973–2008, *Deep-Sea Res. Pt. II*, 58,
1739 2613–2635, <https://doi.org/10.1016/j.dsr2.2011.08.007>, 2011.
1740
1741 Vázquez-Rodríguez, M., Touratier, F., Lo Monaco, C., Waugh, D. W., Padin, X. A., Bellerby, R. G. J., Goyet,
1742 C., Metzl, N., Ríos, A. F., and Pérez, F. F.: Anthropogenic carbon distributions in the Atlantic Ocean: data-based

1743 estimates from the Arctic to the Antarctic, *Biogeosciences*, 6, 439–451, <https://doi.org/10.5194/bg-6-439-2009>,
1744 2009.

1745

1746 Wanninkhof, R., and Trinanes, J.: The impact of changing wind speeds on gas transfer and its effect on
1747 global air-sea CO₂ fluxes, *Global Biogeochem. Cycles*, 31, doi:10.1002/2016GB005592, 2017.

1748

1749 Wanninkhof, R., Barbero, L., Byrne, R., Cai, W.-J., Huang, W.-J., Zhang, J.-Z., Baringer, M., and Langdon, C.:
1750 Ocean acidification along the Gulf Coast and East Coast of the USA, *Continental Shelf Research*, 98, 54-71,
1751 <https://doi.org/10.1016/j.csr.2015.02.008>, 2015

1752

1753 Weir, I., Fawcett, S., Smith, S., Walker, D., Bornman, T., and Fietz, S.: Winter biogenic silica and diatom
1754 distributions in the Indian sector of the Southern Ocean, *Deep Sea Research Part I: Oceanographic Research*
1755 *Papers*, Volume 166, 103421, <https://doi.org/10.1016/j.dsr.2020.103421>, 2020.

1756

1757 Weiss, R. F. and Price, B. A.: Nitrous oxide solubility in water and seawater. *Marine Chemistry*, 8(4), 347–359,
1758 doi:10.1016/0304-4203(80)90024-9, 1980.

1759

1760 Wright, R. M., Le Quéré, C., Mayot, N., Olsen, A., and Bakker, D.: Fingerprint of climate change on Southern
1761 Ocean carbon storage. *Global Biogeochemical Cycles*, 37, e2022GB007596. Doi: 10.1029/2022GB007596,
1762 2023.

1763

1764 Xue, L., Cai, W. J., Takahashi, T. et al.: Climatic modulation of surface acidification rates through summertime
1765 wind forcing in the Southern Ocean. *Nat. Commun.*, 9, 3240, Doi:10.1038/s41467-018-05443-7, 2018.

1766

1767 Yun, J., Jeong, S., Gruber, N., Gregor, L., Ho, C.-H., Piao, S., Ciais, P., Schimel, D., and Kwon, E. Y.: Enhance
1768 seasonal amplitude of atmospheric CO₂ by the changing Southern Ocean carbon sink, *Science Advances*, 8, 41,
1769 doi: 10.1126/sciadv.abq0220, 2022.

1770

1771

1772 Tables

1773

1774 Table 1: Trends of oceanic fCO₂ (µatm.yr⁻¹) and pH (decade⁻¹) in the Southern Ocean south of the Polar Front
 1775 based on observations. IO: Indian Ocean sector. PO: Pacific Ocean sector. AO: Atlantic Ocean sector. SO SPSS:
 1776 Southern Ocean SubPolar Seasonally Stratified biome (around 50-60°S). PZ: Polar Zone. NR: Not Reported.
 1777 Standard-deviations when available are given in brackets.
 1778

1779

1780	Period	Season	Zone	Trend fCO ₂ µatm.yr ⁻¹	Trend pH decade ⁻¹	Reference
1781						
1782						
1783	1991-2000	Summer	IO PZ 55-60°S	2.93	-0.035	Xue et al (2018)
1784	2001-2011	Summer	IO PZ 55-60°S	1.41	-0.016	Xue et al (2018)
1785						
1786	2005-2019	Summer	IO PZ 54-64°S	NR	-0.026(0.003)	Brandon et al (2022)
1787						
1788	1998-2019	Summer	IO 50°S-68°E	1.9 (0.3)	-0.019 (0.004)	Leseurre et al (2022)
1789	1998-2019	Summer	IO 55°S-63°E	2.1 (0.3)	-0.022 (0.003)	Leseurre et al (2022)
1790	1998-2007	Summer	IO 55°S-63°E	5.3 (0.4)	-0.050 (0.016)	Leseurre et al (2022)
1791	2006-2019	Summer	IO 55°S-63°E	0.3 (0.2)	no trend	Leseurre et al (2022)
1792						
1793	1969-2003	Summer	PO 55-62°S	1.7 (0.2)	-0.020 (0.003)	Midorikawa (2012)
1794						
1795	2002-2012	Annual	Drake North	2.21 (0.55)	-0.023 (0.007)	Takahashi (2014)
1796	2002-2012	Annual	Drake South	1.50 (0.65)	-0.015 (0.008)	Takahashi (2014)
1797						
1798	2002-2015	Summer	Drake North	1.95 (0.55)	-0.021 (0.006)	Munro et al (2015)
1799	2002-2015	Winter	Drake North	1.92 (0.24)	-0.018 (0.003)	Munro et al (2015)
1800	2002-2015	Summer	Drake South	1.30 (0.85)	-0.017 (0.010)	Munro et al (2015)
1801	2002-2015	Winter	Drake South	0.67 (0.39)	-0.008 (0.004)	Munro et al (2015)
1802	2002-2015	Annual	Drake North	1.74 (0.15)	-0.019 (0.002)	Munro et al (2015)
1803	2002-2015	Annual	Drake South	1.16 (0.27)	-0.015 (0.003)	Munro et al (2015)
1804						
1805	1981-2011	Annual	SO SPSS	1.44 (0.10)	-0.020 (0.002)	Lauvset et al (2015)
1806	1991-2011	Annual	SO SPSS	1.46 (0.11)	-0.021 (0.002)	Lauvset et al (2015)
1807						
1808	1993-2018	Annual	SO 44-75°S	NR	-0.0165 (0.0001)	Iida et al (2021)

1809

1810

1811

1812

1813

1814 Table 2: Trends of oceanic $f\text{CO}_2$ ($\mu\text{atm.yr}^{-1}$), pH (TS.decade^{-1}) and C_T ($\mu\text{mol.kg}^{-1}.\text{yr}^{-1}$) at the OISO-KERFIX location
 1815 ($50^\circ40'S-68^\circ25'E$) in the Southern Indian Ocean for different periods based on observations (Obs.) and the FFNN model
 1816 (FFNN). Standard-deviations are given in brackets.

1817

1818

1819

1820

1821

1822

1823

1824

1825

1826

1827

1828

1829

1830

1831

1832

1833

1834

1835

1836

1837

1838

1839

1840

1841

1842

1843

1844

Period	Season	Trend $f\text{CO}_2$ $\mu\text{atm.yr}^{-1}$	Trend pH TS.decade^{-1}	Trend C_T $\mu\text{mol.kg}^{-1}.\text{yr}^{-1}$	
1962-2016	November	1.31 (0.32)	-0.014 (0.002)	0.47 (0.01)	Obs.
1991-2021	Summer	2.10 (0.22)	-0.022 (0.002)	0.57 (0.16)	Obs.
1991-2001	Summer	0.76 (0.90)	-0.009 (0.010)	0.05 (0.64)	Obs.
2001-2010	Summer	3.23 (1.07)	-0.035 (0.011)	1.03 (0.77)	Obs.
2010-2020	Summer	0.84 (0.77)	-0.008 (0.008)	0.70 (0.68)	Obs.
1985-2020	Summer	1.71 (0.08)	-0.018 (0.001)	0.68 (0.05)	FFNN
1991-2020	Summer	1.85 (0.11)	-0.020 (0.001)	0.68 (0.07)	FFNN
1991-2001	Summer	1.18 (0.26)	-0.013 (0.004)	0.60 (0.30)	FFNN
2001-2010	Summer	2.87 (0.25)	-0.030 (0.003)	1.08 (0.24)	FFNN
2010-2020	Summer	0.98 (0.40)	-0.010 (0.004)	0.38 (0.26)	FFNN
1985-2020	Winter	1.64 (0.05)	-0.017 (0.001)	0.55 (0.04)	FFNN
1991-2020	Winter	1.78 (0.15)	-0.018 (0.001)	0.56 (0.05)	FFNN
1991-2001	Winter	0.98 (0.09)	-0.010 (0.001)	0.18 (0.14)	FFNN
2001-2010	Winter	1.99 (0.10)	-0.021 (0.001)	1.02 (0.12)	FFNN
2010-2020	Winter	2.21 (0.17)	-0.022 (0.002)	0.69 (0.30)	FFNN
1985-2020	Annual	1.57 (0.03)	-0.0165(0.0004)	0.58 (0.05)	FFNN

1845
 1846
 1847
 1848
 1849
 1850
 1851
 1852
 1853
 1854
 1855
 1856
 1857
 1858
 1859
 1860
 1861
 1862
 1863
 1864
 1865
 1866
 1867
 1868
 1869
 1870
 1871
 1872
 1873
 1874
 1875
 1876
 1877
 1878

Table 3: Results of the simulated properties for year 2020, 2050 and 2100 for two emission scenarios (SSP5-8.5 and SSP2-4.5). For 2020 the results based on observations in January (Obs) and the FFNN model in January and August also listed. Sensitivity tests: “SSP85 W-T” is for winter with constant temperature and “SSP85 W-A-T” is for winter with constant A_T and temperature.

Method	Year	Atm-CO ₂ ppm	fCO ₂ μatm	C _T μmol.kg ⁻¹	A _T μmol.kg ⁻¹	pH TS	[H ⁺] nmol.kg ⁻¹	[CO ₃ ²⁻] μmol.kg ⁻¹	Ωca	Ωar
Obs Jan	2020	410.6	391.9	2142.2	2281.8	8.044	9.04	105.2	2.53	1.59
Std obs.			(2.0)	(0.7)	(0.3)	(0.002)	(0.04)	(0.5)	(0.01)	(0.01)
FFNN Jan	2020	410.6	385.1	2138.5	2280.1	8.051	8.90	106.3	2.55	1.61
SSP Summer	2020	414.9	375.4	2137.5	2282.1	8.061	8.70	108.0	2.60	1.63
FFNN Aug	2020	410.6	410.0	2168.3	2289.8	8.024	9.45	94.2	2.27	1.42
SSP Winter	2020	414.9	434.5	2167.3	2282.1	8.001	9.98	90.4	2.18	1.37
SSP585 Summer	2050	562.8	526.5	2177.2	2278.3	7.928	11.79	84.2	2.02	1.28
SSP585 Winter	2050	562.8	624.7	2207.0	2278.3	7.857	13.91	68.5	1.65	1.04
SSP585 W-A-T	2050	562.8	585.7	2207.0	2280.0	7.880	13.17	69.0	1.66	1.04
SSP585 W-T	2050	562.8	592.7	2207.0	2278.3	7.875	13.32	68.1	1.64	1.03
SSP245 Winter	2050	506.9	554.8	2192.0	2278.3	7.905	12.46	75.8	1.92	1.15
SSP585 Summer	2100	1135.2	1986.9	2330.6	2271.8	7.394	41.31	26.9	0.65	0.41
SSP585 Winter	2100	1135.2	2306.3	2360.4	2271.8	7.316	48.26	21.8	0.52	0.33
SSP585 W-A-T	2100	1135.2	1993.1	2360.4	2280.0	7.372	42.44	22.6	0.54	0.34
SSP585 W-T	2100	1135.2	2097.0	2360.4	2271.8	7.349	44.74	21.3	0.51	0.32
SSP245 Winter	2100	602.8	753.9	2217.7	2271.8	7.782	16.51	60.9	1.47	0.92

1879 Figures

1880

1881

1882

1883

1884

1885

1886

1887

1888

1889

1890

1891

1892

1893

1894

1895

1896

1897

1898

1899

1900

1901

1902

1903

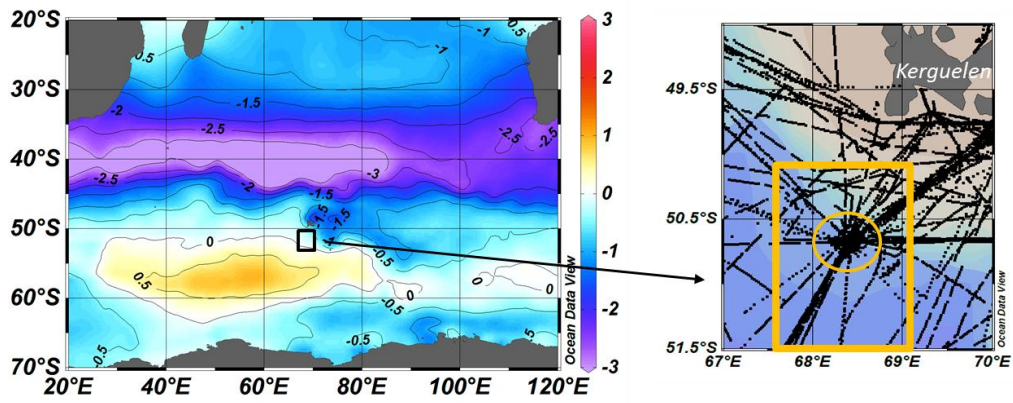


Figure 1: Left: Annual air-sea CO₂ flux (molC.m⁻².yr⁻¹) in the South Indian Ocean for year 2020 from the FFNN model (negative flux for ocean sink, positive flux for ocean source). The black box identified the location of the study south-west of Kerguelen Islands. Right: Track of cruises with underway fCO₂ data south-west of Kerguelen Islands. The station at 50°40'S-68°25'E occupied in 1985, 1992-1993 and 1998-2021 is indicated by a yellow circle. The yellow square is the region selected to calculate the mean values from the underway surface observations and from the FFNN model. Figures produced with ODV (Schlitzer, 2018).

1904
1905
1906
1907
1908
1909

1910

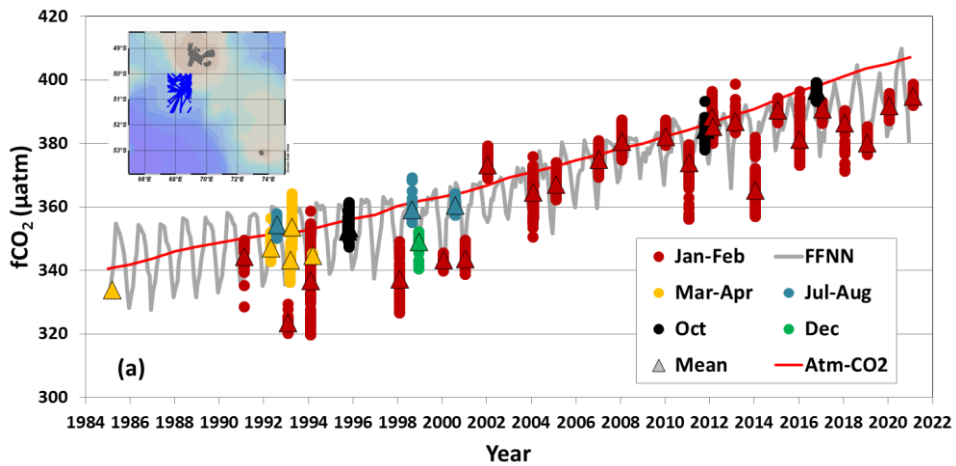
1911

1912

1913

1914

1915



1916

1917

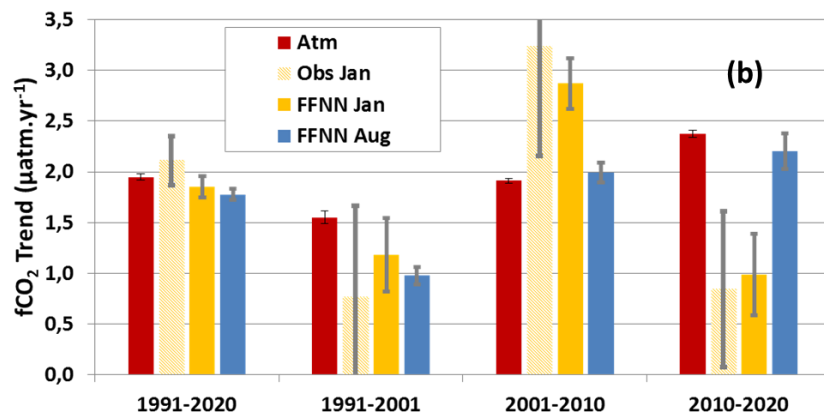
1918

1919

1920

1921

1922



1923

1924

1925

1926

1927

1928

1929

1930

1931

1932

Figure 2: (a): Time-series of sea surface $f\text{CO}_2$ observations (μatm) south-west of Kerguelen Islands in 1985-2021 (insert map shows the location of observations selected around station OISO-KERFIX at $50^{\circ}40'S-68^{\circ}25'E$). The color dots correspond to 5 periods of the year (January-February, March-April, July-August, October and December) and triangles show the average for each month. The monthly sea surface $f\text{CO}_2$ from the FFNN model is presented for the period 1985-2020 (grey line) and the atmospheric $f\text{CO}_2$ is represented by the red line. In March 1985 there was no underway $f\text{CO}_2$ observation and the triangle corresponds to $f\text{CO}_2$ calculated with A_T and C_T measured in the mixed-layer. (b): Trends of atmospheric and oceanic $f\text{CO}_2$ ($\mu\text{atm.yr}^{-1}$) in summer and winter over four different periods based on observations (January) and the FFNN model (January and August).

1933
1934
1935
1936
1937
1938
1939
1940
1941
1942
1943
1944
1945
1946
1947
1948
1949

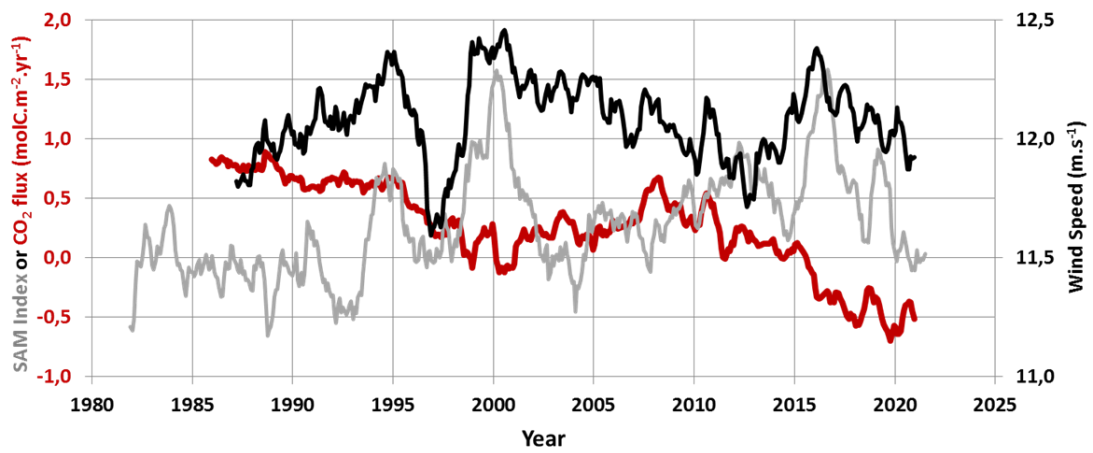


Figure 3: Time series of the SAM index in the Southern Ocean (in grey), wind-speed (in black, m.s⁻¹) and air-sea CO₂ flux (molC.m⁻².yr⁻¹) from the FFNN model (in red) at location 50.5°S-68.5°E. A positive (negative) flux represents a CO₂ source (sink). Wind-speed and SAM are presented for 24-months running mean based on monthly values. Note the positive SAM (> 0.5) in 1998-2002 and 2010-2019. SAM data from Marshall (2003), <http://www.nerc-bas.ac.uk/icd/gjma/sam.html>, last access 14/8/2021. Wind speed data from ERA5 (Hersbach et al., 2020).

1950
1951
1952
1953
1954
1955
1956
1957
1958
1959
1960
1961
1962
1963
1964
1965
1966
1967
1968
1969
1970
1971
1972
1973
1974
1975
1976
1977
1978
1979
1980
1981

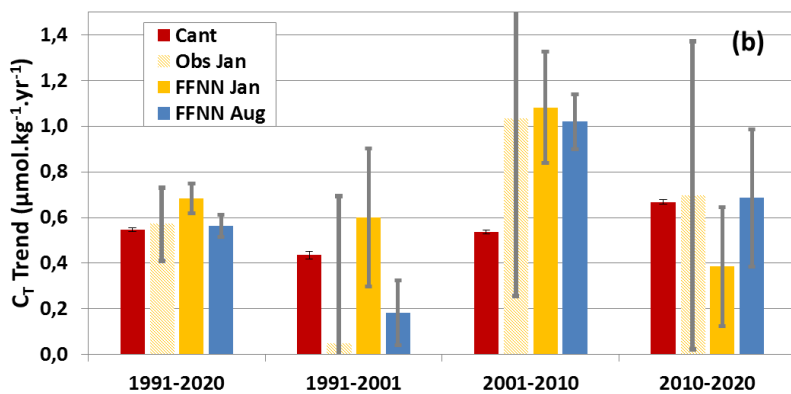
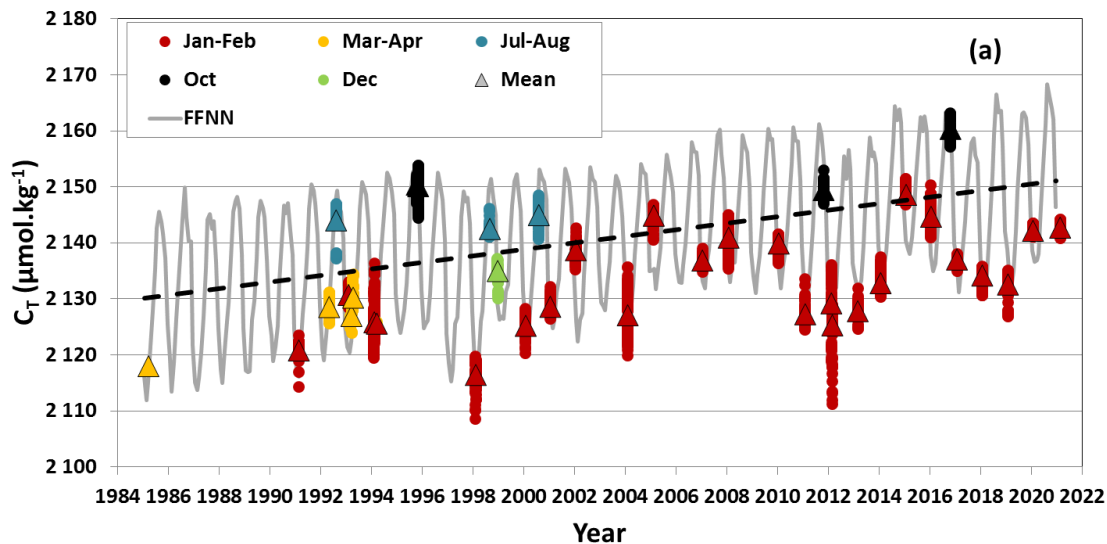


Figure 4: (a): Time-series of surface C_T ($\mu\text{mol.kg}^{-1}$) around station OISO/KERFIX at $50^{\circ}40'S-68^{\circ}25'E$ calculated from $f\text{CO}_2$ data (Figure 2) using the A_T/S relation (see Sect 2.2.5). The color dots correspond to 5 periods of the year (January-February, March-April, July-August, October and December) and triangles show the average for each month. The monthly sea surface C_T from the FFNN model is presented for the period 1985-2020 (grey line). The annual C_T trend of $+0.58 \pm 0.05 \mu\text{mol.kg}^{-1}.\text{yr}^{-1}$ (dashed line) is derived from the FFNN monthly data. In March 1985 the triangle corresponds to the observed C_T in the mixed-layer. (b): Trends of sea surface C_T ($\mu\text{mol.kg}^{-1}.\text{yr}^{-1}$) in summer and winter over four different periods based on observations (for January) and the FFNN model (for January and August). The trend for C_{ant} ($\mu\text{mol.kg}^{-1}.\text{yr}^{-1}$) is also shown (red bars) based on estimates in the Winter Water.

1982
1983
1984
1985
1986
1987
1988
1989
1990
1991
1992
1993
1994
1995
1996
1997
1998
1999
2000
2001
2002

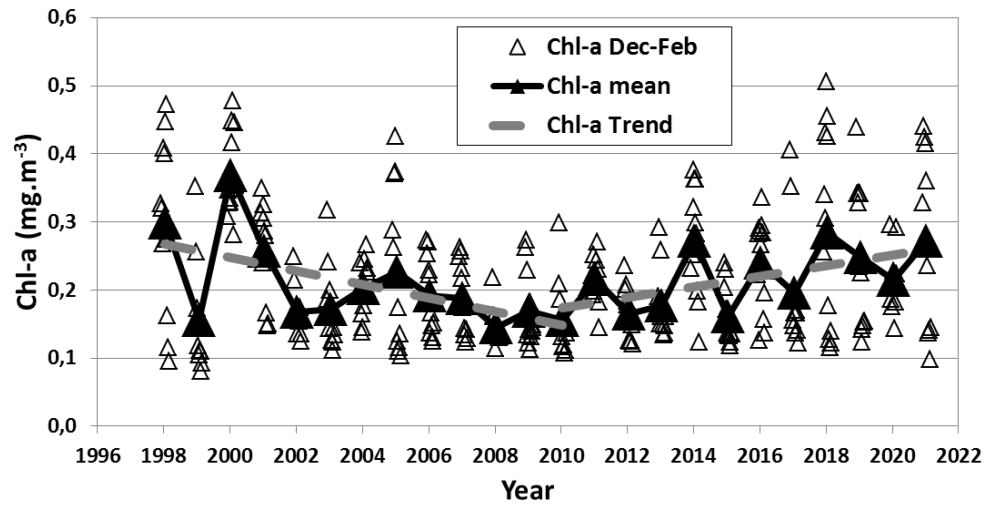


Figure 5: Time-series (1998-2021) of sea surface Chl-a (mg.m⁻³) in summer (December-February) from weekly satellite data (SeaWIFS and MODIS, open triangles) and associated mean (black triangles). The trends in 1998-2010 and 2010-2021 of respectively -0.0099 ± 0.0041 and $+0.0078 \pm 0.0032$ mg.m⁻³.yr⁻¹ (dashed grey) indicate a decrease or increase of the primary production. The full Chl-a record is shown in Supp. Mat. Figure S7.

2003
2004
2005
2006
2007
2008
2009
2010
2011
2012
2013
2014
2015
2016
2017
2018
2019
2020
2021
2022
2023
2024
2025
2026
2027
2028

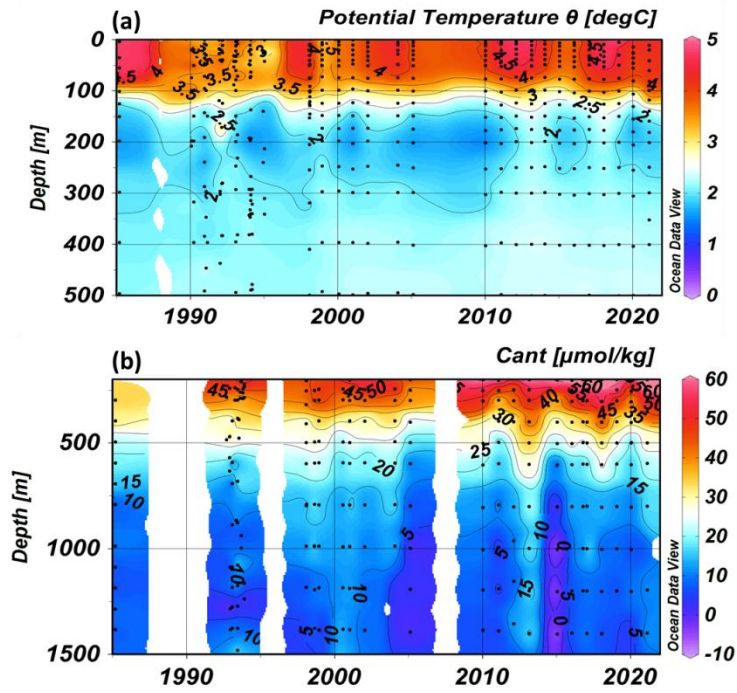


Figure 6: Hovmoller section (Depth-Time) of (a) potential temperature ($^{\circ}\text{C}$) and (b) anthropogenic CO₂ (C_{ant} , $\mu\text{mol}\cdot\text{kg}^{-1}$) over 1985-2021 at station OISO-KERFIX ($50^{\circ}40'S$ - $68^{\circ}25'E$). The section for temperature is presented in the layer 0-500m and for summer to highlight the temperature minimum around 200m (winter water, WW). The section for C_{ant} is limited below 200m. Section produced with ODV (Schlitzer, 2018).

2029
 2030
 2031
 2032
 2033
 2034
 2035
 2036
 2037
 2038
 2039
 2040
 2041
 2042
 2043
 2044
 2045
 2046
 2047
 2048
 2049
 2050
 2051
 2052
 2053
 2054
 2055
 2056
 2057
 2058
 2059

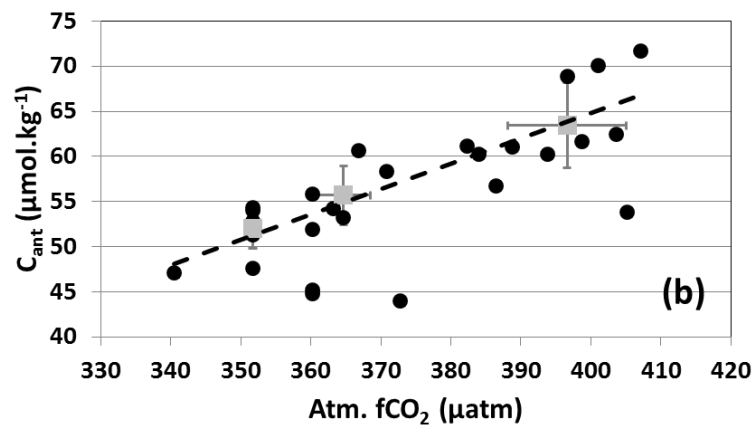
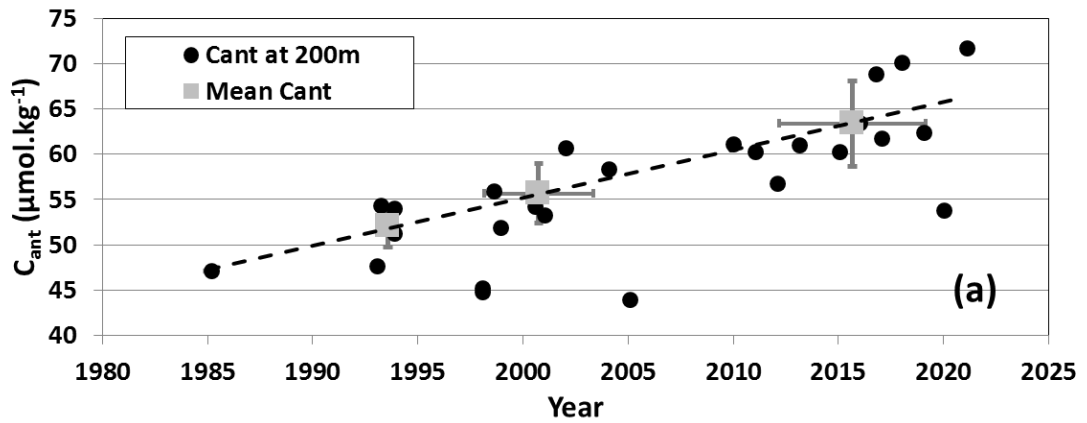


Figure 7: (a): Time-series of anthropogenic CO₂ (C_{ant} $\mu\text{mol.kg}^{-1}$) estimated in the winter water layer (WW around 200m, see figure 6) from 1985 to 2021 at station OISO-KERFIX (50°40'S-68°25'E). Black dots are the individual data in the WW and the grey squares the average for the 1990s, 2000s and 2010s (anomalies in 1998, 2005 and 2020 discarded). The C_{ant} trend of $+0.53 \pm 0.01 \mu\text{mol.kg}^{-1}.\text{yr}^{-1}$ is represented (dashed line). (b): same data for C_{ant} versus atmospheric $f\text{CO}_2$ (the slope is $+0.263 \pm 0.042 \mu\text{mol.kg}^{-1}.\mu\text{atm}^{-1}$).

2060
 2061
 2062
 2063
 2064
 2065
 2066
 2067
 2068
 2069
 2070
 2071
 2072
 2073
 2074
 2075
 2076
 2077
 2078
 2079
 2080
 2081
 2082
 2083
 2084
 2085
 2086
 2087
 2088
 2089

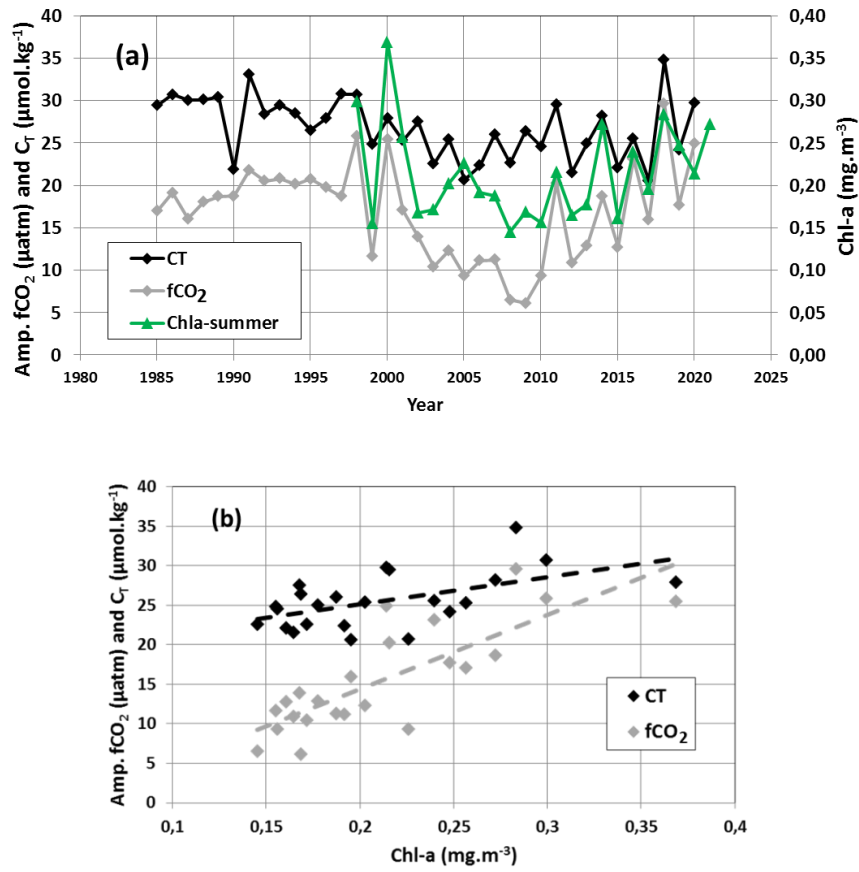


Figure 8: (a): Time-series of the seasonal amplitude (August minus January) for surface C_T (black, $\mu mol.kg^{-1}$) and fCO_2 (grey, μatm) from the FFNN model at station OISO-KERFIX ($50^{\circ}40'S-68^{\circ}25'E$). Also shown are the mean surface Chl-a (green, $mg.m^{-3}$) in summer from 1998 to 2021. (b): Seasonal amplitude of fCO_2 and C_T versus summer Chl-a over 1998-2020. The dashed lines indicate that the seasonal amplitude (August-January) increases when Chl-a is higher.

2090
 2091
 2092
 2093
 2094
 2095
 2096
 2097
 2098
 2099
 2100
 2101
 2102
 2103
 2104
 2105
 2106
 2107
 2108
 2109
 2110
 2111
 2112
 2113
 2114
 2115
 2116
 2117
 2118
 2119
 2120
 2121

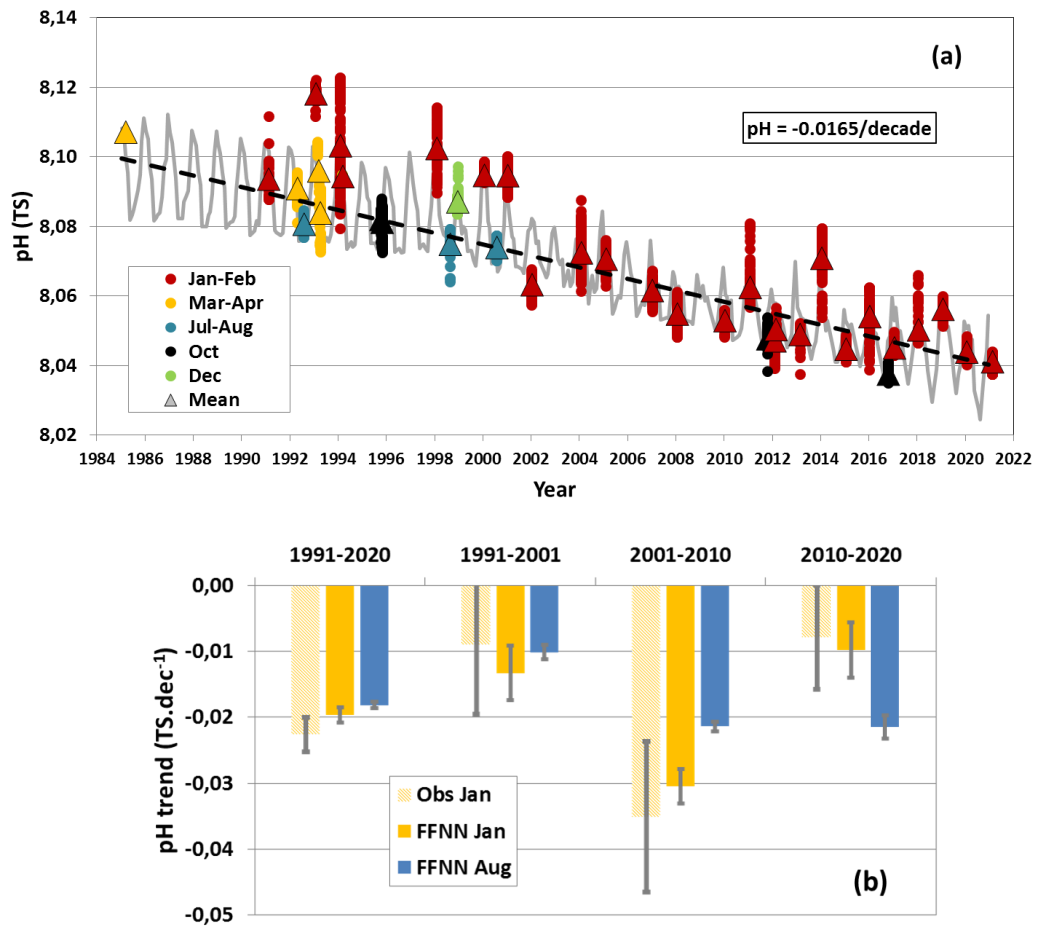


Figure 9: (a): Time-series of surface pH (Total Scale, TS) around station OISO-KERFIX (50°40'S-68°25'E) calculated from fCO₂ data (Figure 2) using the A_T/S relation (see Sect.2.2.5). The color dots correspond to 5 periods of the year (January-February, March-April, July-August, October and December) and triangles show the average for each month. The monthly sea surface pH from the FFNN model is presented for the period 1985-2020 (grey line). The annual pH trend in 1985-2020 of $-0.0165 \pm 0.0004.\text{decade}^{-1}$ (dashed line) is derived from the FFNN monthly data (the same figure for [H⁺] concentrations is presented in Supp. Mat. Figure S13). (b): Trends of pH (TS.decade⁻¹) in summer and winter four over different periods based on observations (January) and the FFNN model (January and August).

2122
 2123
 2124
 2125
 2126
 2127
 2128
 2129
 2130
 2131
 2132
 2133
 2134
 2135
 2136
 2137
 2138
 2139
 2140
 2141
 2142
 2143
 2144
 2145
 2146
 2147
 2148
 2149
 2150
 2151
 2152
 2153

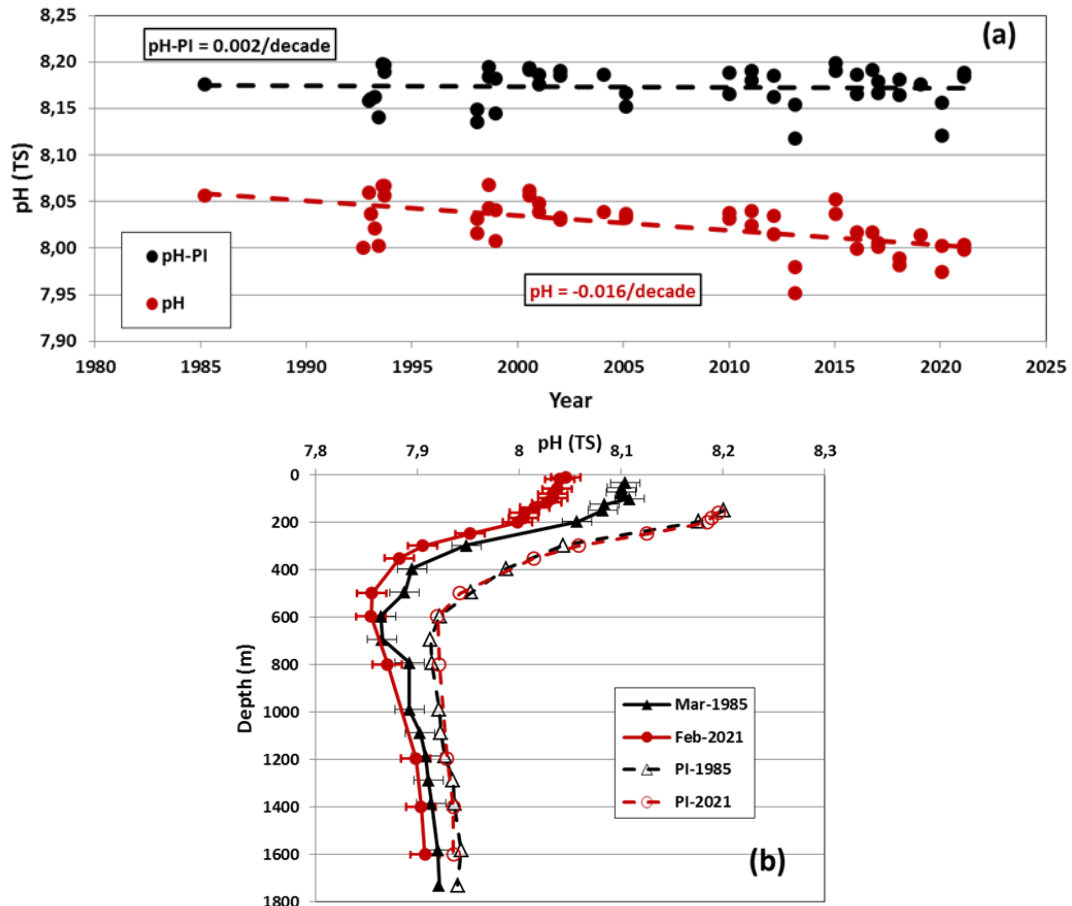


Figure 10: (a): Time-series of pH (red dots) and pre-industrial pH (pH-PI, black dots) estimated in the Winter Water layer (WW around 200m, see figure 6) over 1985-2021 at station OISO-KERFIX (50°40'S-68°25'E). pH-PI for each sample was calculated after subtracting C_{ant} to C_T . The pH trend from the present days is $-0.0161 \pm 0.0033 \cdot \text{decade}^{-1}$ (red dashed line). No trend is observed for pH-PI (black dashed). The mean pH-PI in the WW is 8.173 ± 0.020 ($n=45$). (b): Profiles of pH and pH-PI evaluated from March 1985 (black symbols) and February 2021 data (red symbols). The profiles for pH-PI are shown below 150m only as C_{ant} estimates are not available in the surface layer. Note that the pH-PI profiles are the same either using the 1985 or 2021 data.

2154
 2155
 2156
 2157
 2158
 2159
 2160
 2161
 2162
 2163
 2164
 2165
 2166
 2167
 2168
 2169
 2170
 2171
 2172
 2173
 2174
 2175
 2176
 2177
 2178
 2179
 2180
 2181
 2182
 2183

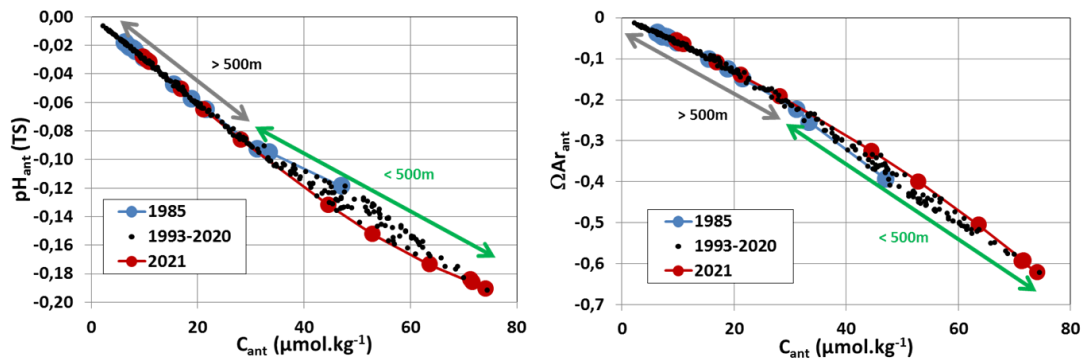


Figure 11: Anthropogenic pH (pH_{ant}) and anthropogenic Ω_{ar} ($\Omega_{ar_{ant}}$) versus anthropogenic CO_2 concentrations (C_{ant} , $\mu\text{mol.kg}^{-1}$) at station OISO-KERFIX ($50^{\circ}40'S-68^{\circ}25'E$). The data are selected in the layer 150-1600m for the periods 1985 (blue), 1993-2020 (black) and 2021 (red). The green arrow identifies the data in the layer 150-500m (for $C_{ant} > 30 \mu\text{mol.kg}^{-1}$). Below 500m (brown arrow) no change of C_{ant} was observed from 1985 to 2021 and thus for pH_{ant} and $\Omega_{ar_{ant}}$.

2184

2185

2186

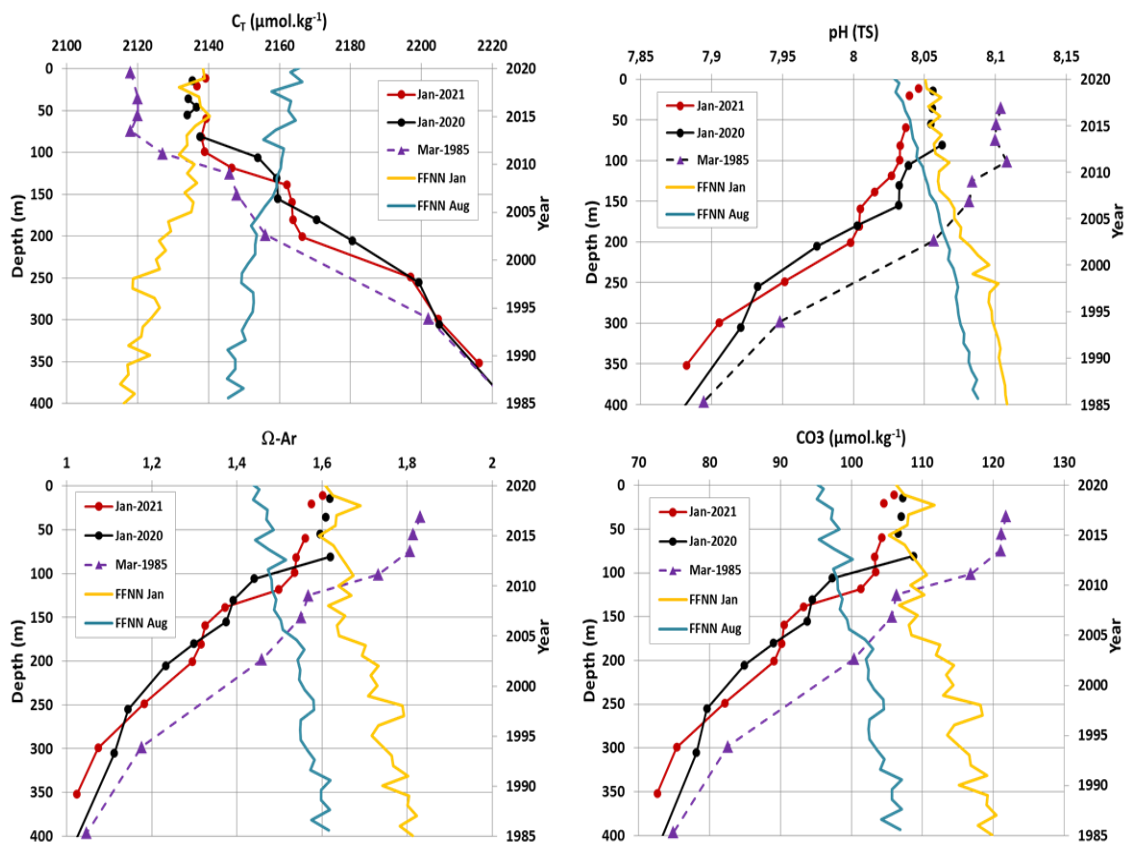
2187

2188

2189

2190

2191



2192

2193

2194

2195

2196

2197

2198

2199

2200

Figure 12: Profiles (0-400m left axis) of observed and calculated properties (C_T , pH, Ω -Ar, $[CO_3^{2-}]$) at station OISO-KERFIX ($50^{\circ}40'S$ - $68^{\circ}25'E$) in March 1985, January 2020 and January 2021 along with surface time-series in 1985-2020 (right axis) of the same properties in January (yellow line) and August (blue line) from the FFNN model. The FFNN values in January 2020 are coherent with January 2020 or January 2021 observations in the mixed-layer and in January 1985 are close to the observations in March 1985. Note that the differences of properties between 2020-21 and 1985 have a similar magnitude as the seasonal amplitude (illustrated by the FFNN values for January and August).

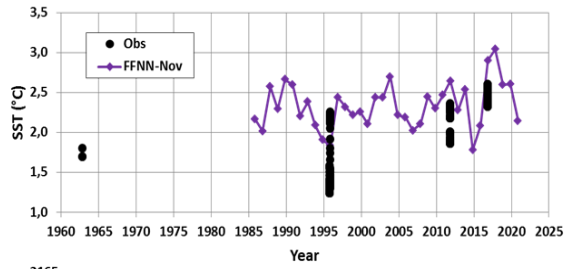
2207

2208

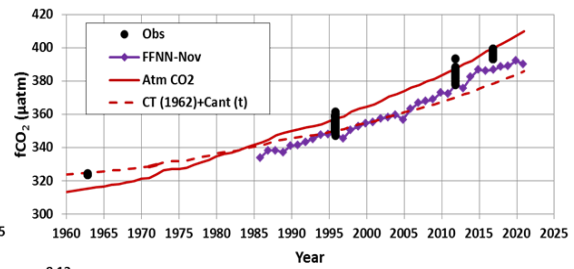
2209

2210

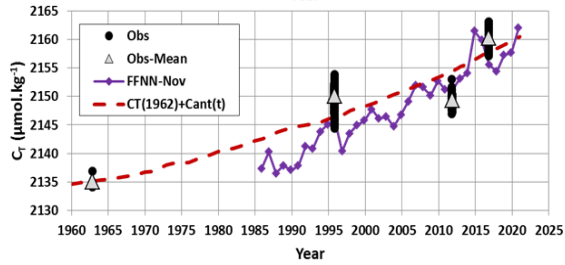
2211



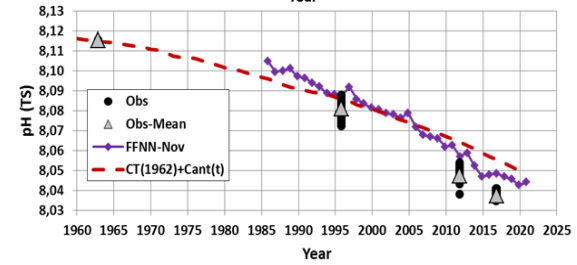
2212



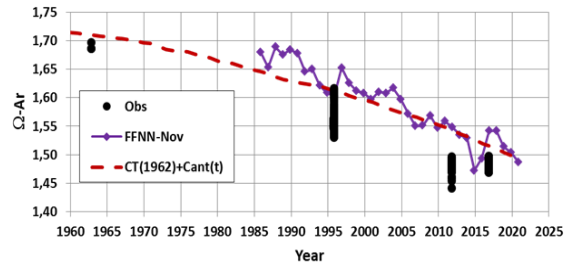
2213



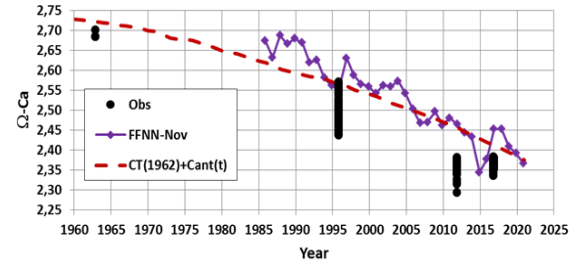
2214



2215



2216



2217

2218

2219

2220 Figure 13: Observed (black dots) sea surface temperature (°C), fCO_2 (μatm), C_T ($\mu mol.kg^{-1}$), pH (TS), $\Omega-ar$ and $\Omega-ca$ around
 2221 station OISO-KERFIX at $50^{\circ}40'S-68^{\circ}25'E$ for October-November. Also shown are the results for the FFNN model for
 2222 November in 1985-2020 (Purple). The C_T concentrations, pH, $\Omega-ar$ and $\Omega-ca$ were calculated from fCO_2 data using the A_T/S
 2223 relation (Eq. 1). The red line is the atmospheric fCO_2 and red dashed-lines in each plot are the evolution of properties since
 2224 1960 corrected for C_{ant} where fCO_2 , pH, $\Omega-ar$ and $\Omega-ca$ were recalculated using C_T+C_{ant} , A_T constant at $2290 \mu mol.kg^{-1}$ and
 2225 SST at $2^{\circ}C$. Grey triangles identify the mean values for C_T and pH.

2226

2227

2228

2229

2230

2231

2232

2233

2234

2235

2236
 2237
 2238
 2239
 2240
 2241
 2242
 2243
 2244
 2245
 2246
 2247
 2248
 2249
 2250
 2251
 2252
 2253
 2254
 2255
 2256
 2257
 2258
 2259
 2260
 2261
 2262
 2263
 2264
 2265
 2266

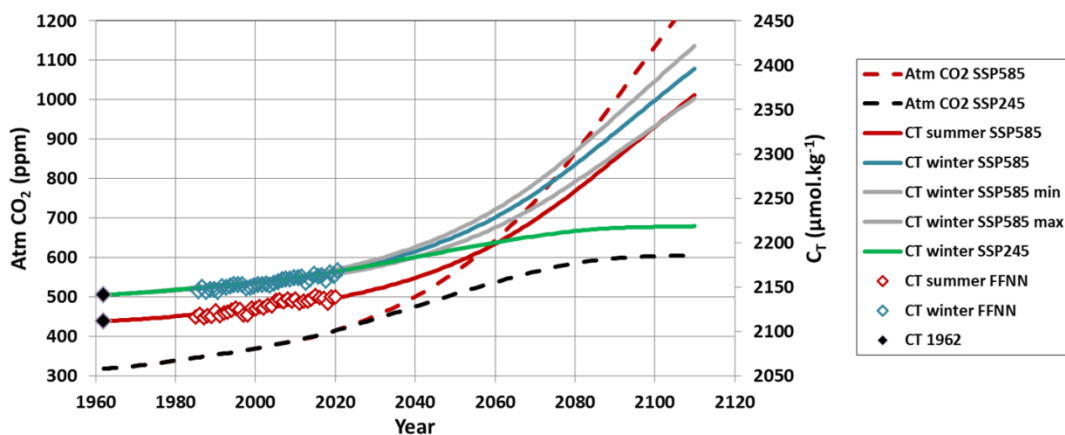


Figure 14: Evolution of atmospheric CO₂ (ppm) and sea surface C_T (μmol.kg⁻¹) between 1960 and 2110 evaluated for 2 scenarios (SSP2-4.5 black dashed and SSP5-8.5 red dashed), for summer (red line for SSP5-8.5) and winter (blue line for SSP5-8.5 and green line for SSP2-4.5). Grey lines are the high and low C_T for winter SSP5-8.5 based on the error in the C_{ant}/fCO₂ relationship (figure 7b). Also shown are the results for the FFNN model in 1985-2020 for summer (red diamonds) and winter (blue diamonds) and C_T in 1962 (black diamonds). The C_T values for different seasons and scenarios were used to calculate the carbonate properties in the future (Figure 15).

2267

2268

2269

2270

2271

2272

2273

2274

2275

2276

2277

2278

2279

2280

2281

2282

2283

2284 Figure 15: Evolution of sea surface $f\text{CO}_2$ (μatm), pH (TS), $[\text{CO}_3^{2-}]$ ($\mu\text{mol.kg}^{-1}$), $[\text{H}^+]$ (nmol.kg^{-1}), $\Omega\text{-Ar}$ and $\Omega\text{-Ca}$ between
 2285 1960 and 2110 evaluated for the SSP5-8.5 scenario for winter (blue line) and summer (red line) taking into account both A_T
 2286 and SST future trends. For winter the results are also presented using the SSP2-4.5 scenario (grey lines). Also shown are the
 2287 results for the FFNN model in 1985-2020 for summer (red diamonds) and winter (blue diamonds). Atmospheric $f\text{CO}_2$ is also
 2288 shown for SSP5-8.5 (red dashed) and SSP2-4.5 (grey dashed). Values in 2020, 2050 and 2100 for different sensitivity tests
 2289 are listed in Table 3.

2290

